FORSKNINGENS HUS
AALBORG HOSPITAL SCIENCE AND INNOVATION CENTER

Master Thesis

*Medicine with Industrial Specialisation*

# An Evaluation of Two Novel Detection Methods for Characterisation of Microparticles in Plasma

by

Sarah Nejlund

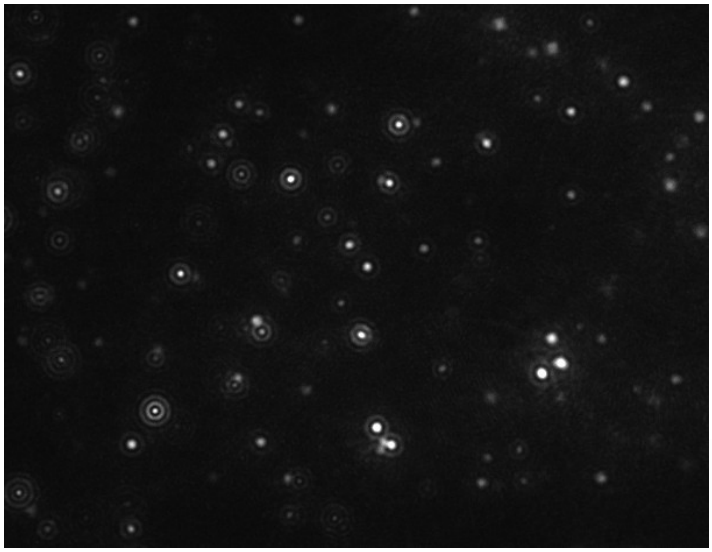

AALBORG UNIVERSITY DENMARK

1st of September 2011 — 1st of June 2012

**Title:** An evaluation of two novel detection methods for characterisation of microparticles in plasma

**Theme:** Master project

**Project Period:** September 1st 2011 to June 1st 2012

**Project Group:** 958 Biomedicine

**Group members:**

Sarah Nejlund

**Main supervisors:**
Shona Pedersen, Master of Science, Ph.D.
Egon Toft, Cand.Med., Dr. Med., Specialist in cardiovascular medicine

**Clinical supervisors:**
Søren Risom Kristensen, Professor, MD, DMSc
Morten Mørk, Specialist registrar, Ph.D. student

**Numbers Printed:** 6
**Pages:** 89
**Appendix:** 1

**Finished:** June 1st 2012

## Abstract

**Introduction:** Microparticles (MPs) are phospholipid-rich vesicles shed from a variety of eukaryotic cells. Several types of MPs exist: membrane vesicles, exosomes, exosome-like vesicles and apoptotic bodies and they can be released from the cells undergoing activation, apoptosis, and several stress induced activations. MPs express proteins in and on the surface, which are indications of which cell the MP originates from. The major cellular source of MPs has been shown to be platelets. MPs can in theory possess various functions depending on their cellular origin. The major known and described functions of MPs are the involvement in coagulation, inflammation and in the vascular system, but MPs have also been shown to act as intracellular mediators and have the potential to transfer part of their components to a target cell. The clearance of MPs from the circulation is poorly understood, but it has been proposed that MPs are mainly cleared by phagocytosis. MPs are present in both healthy individuals and in various pathologies. Elevated levels of MPs have been shown in numerous types of diseases, such as cardiovascular diseases, cancer, and infectious diseases. Despite increasing interest in MPs, the isolation, detection, and characterisation of MPs are hampered by both limitations in the available technology and the biological complexity of body fluids. The need for new methods for the characterisation of MPs is therefore crucial.

**Aim:** The aim of this project is to evaluate the potential of two novel detection methods for the characterisation of MPs, namely Nanoparticle Tracking Analysis (NTA) and Dynamic Light Scattering (DLS).

**Methods:** NTA and DLS were evaluated by investigating the reproducibility and accuracy of measurements by the use of microbeads in sizes 50 nm, 100 nm, and 200 nm. Dilution of plasma samples were investigated to find suitable dilutions of plasma samples for measurements of MPs. Different pre-analytical parameters were investigated to evaluate the potential of NTA and DLS for usage in clinical experiments. The effect of freezing was investigated by comparing fresh samples with the same samples that have been frozen for 1, 7, 15, and 40 days at -80°C. The influence of centrifugation on the particle size distribution and the concentration of MPs were investigated by comparing three different centrifugation methods. Centrifugation A, a centrifugation at 3220g for 20 minutes at 20°C, Centrifugation B, a double-step centrifugation, in which blood samples were centrifuged twice at 2500g for 15 minutes at room temperature, and finally Centrifugation C, a two-step centrifugation, in which blood samples were first centrifuged at 2500g for 15 minutes at room temperature, and the resultant platelet-poor-plasma was then ultracentrifuged at 13000g for 2 minutes at room temperature. Finally, the potentials of NTA and DLS for measurement and differentiation of healthy plasma samples and pathological samples were investigated.

**Results:** Both NTA and DLS showed relative reproducibility and accuracy for measurement of microbeads and MPs in plasma samples. The most suitable dilution of plasma samples in buffer for measurement on NTA was found to be 2 µL of plasma sample in 1000 µL DPBS for both healthy and diseased plasma samples. Freezing did not affect the particle size distributions of measured MPs, but the concentration of MPs was found to be higher for the fresh sample when measuring the samples with NTA. The DLS results were inconclusive for the fresh-frozen experiment. Centrifugation showed to have little or no effect on the particle size distribution and concentration of MPs in plasma samples for measurements with both methods. The clinical potential of both NTA and DLS was proven when both methods were able to differentiate between healthy plasma samples and pathological plasma samples.

**Conclusion:** Both methods exhibit relative reproducibility and they can be used as complementary methods for the detection and characterisation of MPs in plasma.

## Acknowledgement

I wish to express my sincere thanks to the Department of Clinical Biochemistry, Aalborg Hospital, for its collaboration in the project and for providing methods and materials for experiments. Special thanks go to Ph.D. student Alice Østergaard for critical reading of this manuscript, helpful suggestions and editorial assis-

tance, and helpful discussions. Bioanalysts, Jette Christensen, Annette Andreasen, and Rikke Bülow are gratefully thanked for their technical assistance in collection of blood samples from donors. The generous participation of the blood donors in the study is gratefully acknowledged.

## Additional notes

This project was conducted in collaboration with the Department of Clinical Biochemistry at Aalborg Hospital with Biochemist, Ph.D. Shona Pedersen as main supervisor and proposer of the project. The project was chosen for oral presentation at the first congress with main focus on MPs arranged by the International Society of Extracellular Vesicles in Gothenburg in April 2012. A poster was made for the congress, see Appendix A.1.

# Table of Content

# Part 1: Introduction

## 1.1 Introduction

Microparticles (MPs) are submicron vesicles released by numerous types of cells [Davizon & López, 2009]. The MP timeline had its beginning in 1946, where Chargaff and West [Chargaff & West, 1946] described 'precipitable factors'. They discovered thromboplastic factors in platelet-poor-plasma (PPP) that contributes to the clotting properties by high-speed centrifugation of normal blood. These precipitable factors had the potential to generate thrombin. [Chargaff & West, 1946] However, this potential was not appreciated by the scientific community, and another 20 years had to pass before a new description of MPs occurred. Peter Wolf [Wolf, 1967] found coagulant material in minute particulate form, originating from platelets, but still distinguishable from platelets. It was discovered that this coagulant material possessed no coagulant properties and was therefore called 'platelet-dust' [Wolf, 1967].

George and colleagues [George *et al.*, 1982] were the first to describe and detect MPs in both plasma and serum. He discovered a ten-fold greater concentration in serum compared to plasma, by the use of an immunoelectrophoretic assay targeting the human platelet membrane glycoprotein complexes. MPs have been investigated since then, and during the past two decades, the understanding of their formation, composition and function along with their clinical potential have slowly emerged [Davizon & López, 2009; Flaumenhaft, 2006; Freyssinet, 2003; VanWijk *et al.*, 2003].

Cells are known to secrete many types of MPs, and the types and composition depend on the cell type, the cellular microenvironment, or the pathophysiological conditions of the cell. Up till now, several types of MPs have been identified [Bucciarelli *et al.*, 2011; Burnier et al., 2009; Furie & Furie, 2006]. MPs have been found to originate from various types of cells. Platelet-derived MPs have been shown to be the most abundant MPs in the circulation, constituting approximately 70% to 90% of all circulating MPs. This was established by the findings that > 90 % were positive for platelet-specific surface markers. The remaining 10 % to 30 % consist mostly of leukocyte- and erythrocyte-derived MPs. [Davizon & López, 2009; Flaumenhaft, 2006; Horstman & Ahn, 1999] An increased concentration of MPs has been related to several pathophysiological conditions, and overproduction of MPs resulting from several normal physiological functions has also been found [Burnier et al., 2009].

## 1.2 Definition of Microparticles

MPs are generally defined as small circulating particles that are irregular in shape and have diameters ranging from 0.05 µm to 1µm [Bucciarelli *et al.*, 2011; Davizon & López, 2009; Habib *et al.*, 2008; Leroyer *et al.*, 2008].

MPs are released from several different cell types (e.g. platelets, red blood cells, monocytes, and lymphocytes) by either vesiculation or exocytosis after cell activation, apoptosis, or other mechanisms causing activation or stress of the parental cell [Burnier *et al.*, 2009; Davizon & López, 2009; Shet *et al.*, 2003; VanWijk *et al.*, 2003]. This definition is very broad and includes all types of MPs without taking the origin into account.

Common for all MPs is that they are surrounded by a membrane composed of phospholipids. An important characteristic of MPs is the exposure of the negatively charged phosphatidylserine, a procoagulant aminophospholipid, in their outer membrane leaflet along with other phospholipids. [Bucciarelli *et al.*, 2011; Davizon & López, 2009; Habib *et al.*, 2008; Leroyer *et al.*, 2008; Shet *et al.*, 2003]

On the surface of MPs different proteins may be found. These proteins may differ from MP to MP, and the receptors are indications of which cell the MP originates from. The composition of the different lipids and proteins depend, off cause, on the parental cell, but also on the mechanistic way of their release. Figure 1 illustrates the general MP shed from stimulated cells. Examples of harboured membrane proteins and cytoplasmic components are included in the figure. [Bucciarelli *et al.*, 2011; Burnier *et al.*, 2009; Furie & Furie, 2008; Hugel *et al.*, 2005; Perez-Pujol *et al.*, 2007; VanWijk *et al.*, 2003]

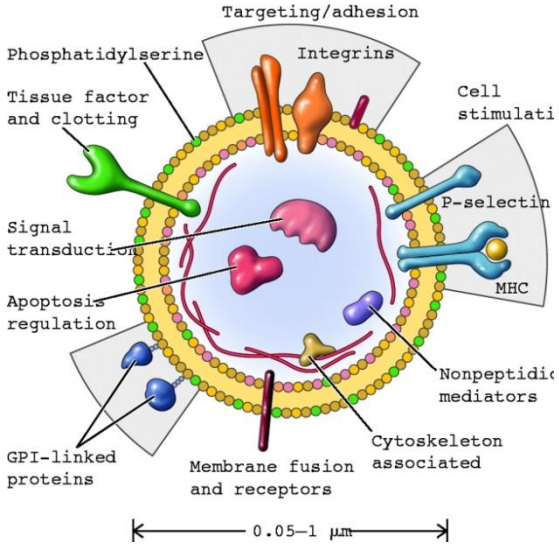


**Figure 1: Illustration of the general MP shed from a stimulated cell. The membrane is composed of phospholipids randomly distributed in the inner and outer leaflets. The general MP is illustrated with several different kinds of membrane proteins, such as tissue factor and integrins. The cytoplasm of the general MP contains elements from the cell of origin, such as RNA molecules. [Hugel *et al.*, 2005]**

## 1.3 Composition of Microparticles

The composition of phospholipids in MPs isolated from plasma has been investigated by the use of horizontal, one-dimensional high-performance thin-layer chromatography (HPTLC). Minor quantities of membrane phospholipids were separated, and the MPs appeared to compose of ~60 % phosphatidylcholine, ~20 % sphingomyelin, ~10 % phosphatidylethanolamine, and relatively small amounts of other phospholipids. [Weerheim *et al.*, 2002] The composition of the MPs further determines the function of the MPs, such as cytoplasmic RNA and specific proteins.

## 1.4 Types of Microparticles

There is a lack of consensus of nomenclature of MPs in the literature, but according to Abcam® several different types of MPs exist such as microvesicles, exosomes, exosome-like vesicles, and apoptotic bodies [Abcam®, 2011], and they are defined based on their way of release from the cell.

Microvesicles are released by membrane blebbing and may therefore contain surface receptors from its cell of origin. The size of microvesicles lies within 100 nm to 1 µm [Abcam®, 2011; Dragovic *et al.*, 2011]. In figure 2, the microvesicle is illustrated with surface receptors CD40 and CD62 which is expressed on antigen presenting cells and platelets, respectively. Integrins illustrate that the microvesicles can be derived from several different cells. [Abcam®, 2011; del Conde *et al.*, 2005; Falati *et al.*, 2003; Freyssinet, 2003; Furie & Furie, 2008]

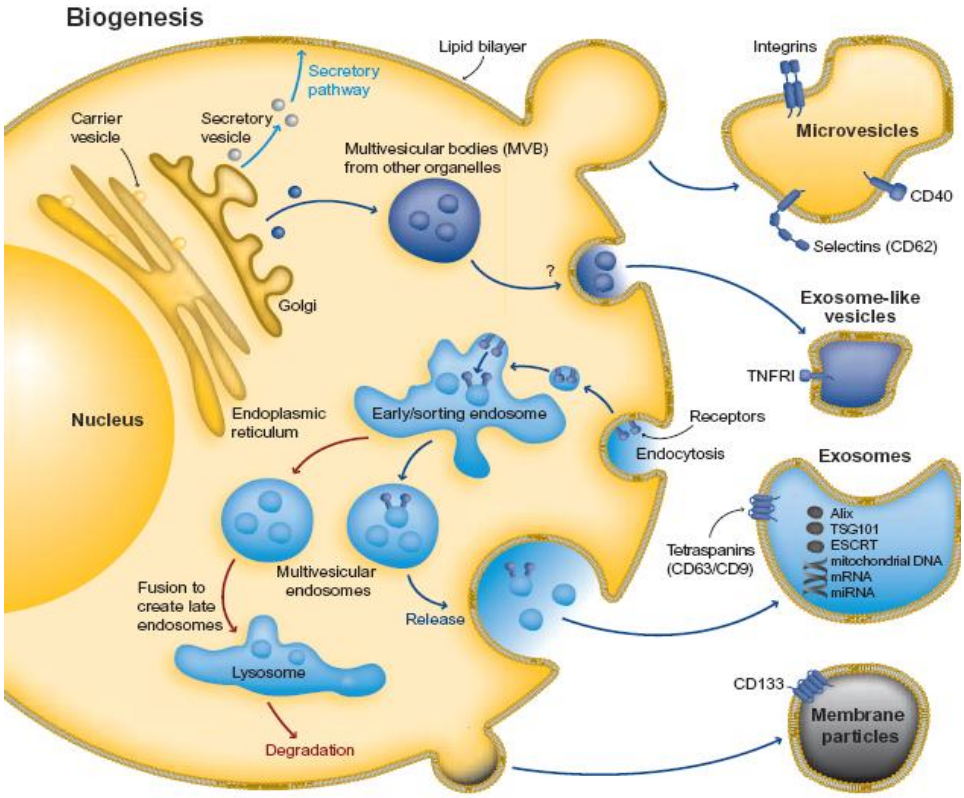


**Figure 2: Illustration of the different types of MPs. Microvesicles are vesicles shed from the membrane of the cell and they express on their surface membrane proteins from their cell of origin. Exosome-like vesicles are shed into the extracellular space by exocytosis from multivesicular bodies. They often express tumour necrosis factor 1 on their surface. Exosomes are also released into the extracellular space by exocytosis. Their formation is through endocytosis and they often contain components of the cytoplasm. Membrane particles, also known as apoptotic bodies, are released from cells undergoing apoptosis. [Abcam®, 2011]**

Exosomes are cup-shaped membrane vesicles originating from exocytosis of multivesicular bodies [Bucciarelli *et al.*, 2011]. Multivesicular bodies are endosomes formed by inward budding of the cell membrane, as illustrated in figure 2 [Abcam®, 2011]. Exosomes have proven to be involved in the transfer of material such as mRNA from one cell to another. [Blanchard *et al.*, 2002]

Exosome-like vesicles are small irregular vesicles released from multivesicular bodies, though the pathway of exosome-like vesicle release is still not known [Abcam®, 2011]. These small vesicles has diameters ranging from 20 nm to 50 nm, and they are often recognised by their expression of tumour necrosis factor receptor type 1 (TNFR1), see figure 2 [Abcam®, 2011].

Apoptotic bodies are small membrane particle released from cells undergoing apoptosis. The size of apoptotic bodies can vary from 500 nm to as high as 3 µm in diameter. The function of apoptotic bodies is still not known [Abcam®, 2011; Dragovic *et al.*, 2011].

In the remainder of this project the term 'MPs' will be used as the general nomenclature for all types of MPs.

## 1.5 Origin of Microparticles

MPs derived from several types of cells have been investigated for their composition of surface proteins, making it possible to determine cell of origin. In the following, a few examples will be described.

T cells have been shown to release exosomes from endosomes in culture medium by exocytosis, the so-called multivesicular bodies [Blanchard *et al.*, 2002]. These exosomes are small in diameter, ranging from 50 nm to 100 nm, and they bear several T cell specific proteins on their surfaces. It was shown by different pro-

tein analysis methods that these exosomes express the T cell receptor β/CD3/ζ complex on their surface along with proteins such as CD2, CD63, MHC class I and II, and different chemokine receptors, all indicating endocytic formation of the MPs/exosomes. [Blanchard *et al.*, 2002]

Platelets are the major source of MPs, and it has been shown that platelets can be stimulated in several different ways to release MPs, e.g. by C5b-9 complement activation, thrombin plus collagen, and the calcium ionophore A23187 [Burnier *et al.*, 2009; Sims *et al.*, 1989]. MPs released by platelets have been shown to express the plasma membrane glycoproteins GPIb, IIb, and IIIa, and membrane receptors targeting coagulation factor Va, providing these MPs with a possible procoagulant potential. Platelet-derived MPs can therefore be characterised by their expression of these proteins and their procoagulant potential. [Sims *et al.*, 1989]

Falati and colleagues [Falati *et al.*, 2003] investigated pathways of accumulation of tissue factor (TF) in a developing thrombus and found indication of localisation of PSGL-1-bearing MPs in thrombi that express P-selectin through P-selectin-PSGL-1 interaction, but not in thrombi lacking P-selectin. Furthermore, Falati demonstrated the presence of TF-positive MPs in platelet-poor-plasma derived from monocytes, indicated by bearing PSGL-1 (CD162), CD11b, and CD14. [del Conde *et al.*, 2005; Falati *et al.*, 2003]

## 1.6 Formation of Microparticles

The knowledge about the formation of MPs has emerged in recent years through *in vitro* studies. Little about the *in vivo* formation of MPs is known, but several speculations and suggestions based on *in vitro* studies and the common knowledge about the behaviour of cells have been discussed. [Burnier *et al.*, 2009; VanWijk *et al.*, 2003]

The most recent suggested mechanism of the formation of MPs from the cell membrane involves budding of the surface membrane, loss of membrane asymmetry, and three enzymes known as flippase, floppase, and scramblase [Biró *et al.*, 2005; Davizon & López, 2009; Leroyer *et al.*, 2008]. The cell membranes of resting cells are asymmetric in the composition and distribution of phospholipids in the inner and outer leaflets. The outer leaflet is rich in the cholinephospholipids phosphatidylcholine and sphingomyelin, whereas the inner leaflet is rich in the aminophospholipids phosphatidylserine and phosphatidylethanolamine. [Burnier *et al.*, 2009; Freikman *et al.*, 2008; Horstman & Ahn, 1999; VanWijk *et al.*, 2003; Zwaal *et al.*, 1992] This asymmetry of the resting cells is maintained by three enzymes: flippase, an aminophospholipid translocase that translocates phosphatidylserine and phosphatidylethanolamine from the outer leaflet to the inner; floppase, a phospholipid translocase that transports phospholipids from the inner leaflet to the outer; and scramblase, which is responsible for the asymmetric redistribution (scrambling) of phospholipids in the plasma membrane, which is illustrated in figure 3A. [Burnier *et al.*, 2009; Davizon & López, 2009; Hugel *et al.*, 2005] The floppase enzyme is always active, whereas flippase and scramblase need inhibition and activation, respectively, before microvesiculation can occur [Davizon & López, 2009]. The budding of the cell membrane results in alterations in the asymmetry of the phospholipids, and once flippase is inhibited and floppase and scramblase are activated, phosphatidylserine and other phospholipids are flip-flopped to the outer/inner membrane leaflet and scrambled, as illustrated in figure 3B. This reorganisation of the cytoskeleton and membrane blebbing can result in the formation of MPs, a process known as vesiculation. [Bucciarelli *et al.*, 2011; Burnier *et al.*, 2009; Freikman *et al.*, 2008; Horstman & Ahn, 1999; Leroyer *et al.*, 2008]

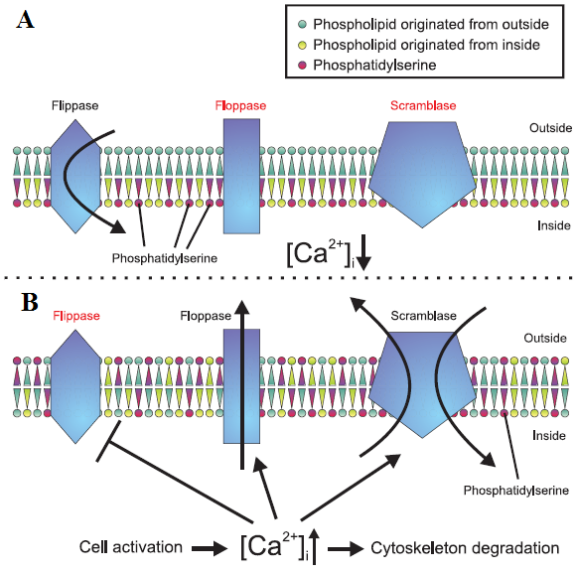


**Figure 3: Illustration of the asymmetric distribution of phospholipids in the cell membrane by three key enzymes: flippase, floppase and scramblase. (A) An illustration of the membrane of a resting cell. The flippase is active, whereas the floppase and scramblase are inactive. (B) An illustration of the process in which the formation of MPs occurs. The asymmetric appearance of the resting cell membrane is lost after the activation of floppase and scramblase and the inhibition of flippase. This process occurs during cell activation which is followed by an increase in the intracellular concentration of $Ca^{2+}$. [Burnier *et al.*, 2009]**

As previous mentioned several mechanisms can trigger the externalisation of phosphatidylserine to the other membrane leaflet and microvesiculation of cells, including cell activation, apoptosis, high shear stress, oxidative stress, and other less described mechanisms. The main mechanism of membrane vesiculation is through cell activation and apoptosis. [Bucciarelli *et al.*, 2011; Davizon & López, 2009; Freikman *et al.*, 2008; Hugel *et al.*, 2005; Leroyer *et al.*, 2008; VanWijk *et al.*, 2003].
In figure 4, a simplified illustration of the mechanism of membrane vesiculation after cell activation is shown.

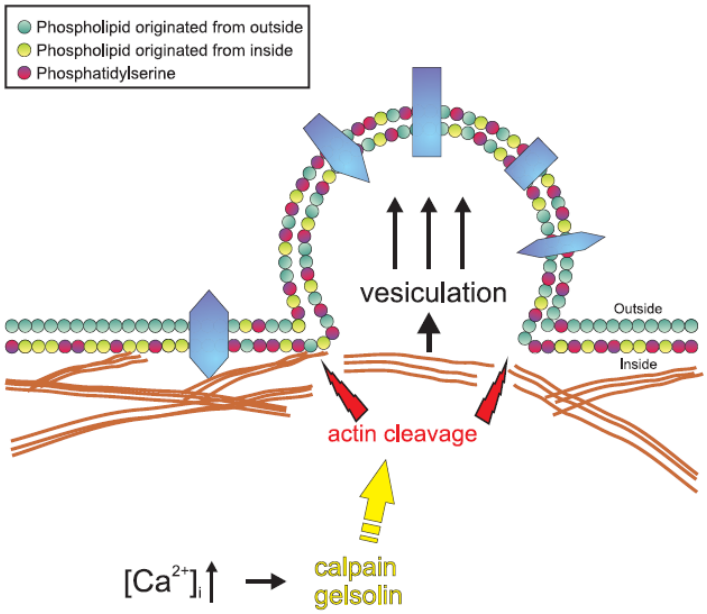


**Figure 4: Illustration of the vesiculation of MPs from the cell membrane. After an influx of $Ca^{2+}$, calpain and gelsolin is activated. The actin-binding proteins are then hydrolysed and the actin filaments are cleaved from the cell membrane, resulting in a subsequent vesiculation. [Burnier *et al.*, 2009]**

Cell activation followed by a significant $Ca^{2+}$-influx in the cytosol is the best described mechanism for the formation of MPs. $Ca^{2+}$-influx leads to reorganisation of the cytoskeleton, change in the shape of the cell, and exocytosis of multivesicular bodies. This reorganisation of the cytoskeleton is followed by a stimulation of scramblase and floppase activity and inhibition of flippase. The increase in cytosolic $Ca^{2+}$-concentration is followed by an activation of the $Ca^{2+}$-dependent protease calpain. [Biró *et al.*, 2005; Flaumenhaft, 2006; Hugel *et al.*, 2005; VanWijk *et al.*, 2003] Activation of calpain and in platelets gelsolin leads to the hydrolysis of the actin-binding protein. Actin-filaments are not associated with any membrane glycoprotein prior to cell activation, but become associated with myosin and the glycoprotein IIb-IIIa complex when the cell is activated. [Fox *et al.*, 1990; Fox *et al.*, 1991] The hydrolysis of the actin-binding protein further leads to cleavage of the attachment of membrane proteins, and thus decreased association of actin with membrane glycoproteins and subsequent vesiculation due to membrane disruption. The involvement of calpain in vesiculation of MPs were first described by Fox and colleagues who proved that the shedding of MPs must be correlated with the activation of calpain, since inhibition of calpain led to inhibition of shedding of MPs. [Davizon & López, 2009; Flaumenhaft, 2006; Fox *et al.*, 1990; Fox *et al.*, 1991]
Bassé and colleagues [Bassé *et al.*, 1994] found results supporting these findings. By activating platelets with the calcium ionophore A23187 and inhibiting calpain with calpeptin, the vesiculation of MPs was strongly inhibited as well [Bassé *et al.*, 1994; Leroyer *et al.*, 2008].
In platelets, gelsolin interferes with the hydrolysis of the actin-binding protein and is involved in the cleavage of the actin capping proteins. Gelsolin stays attached to one of the actin-filament ends after disassociation with the membrane glycoproteins, which traps $Ca^{2+}$ in the complex. This prevents reannealing, and thus enables the end attached to gelsolin to be extended by monomers. These will then be released as vesicles. [Burnier *et al.*, 2009; McLaughlin *et al.*, 1993]

The removal of intracellular $Ca^{2+}$ re-establishes the translocase activity, given that intracellular calpain is inactivated, which is illustrated in figure 3A. This re-establishment results in translocation of phosphatidylserine from the outer leaflet of the cell membrane back into the inner leaflet, and the cell returns to a resting state with normal asymmetry in its membrane. [Zwaal *et al.*, 1992]
The possibility of other mechanisms of MP formation beside the calpain-dependent vesiculation was evident, when it was proved, that MPs were formed in the presence of calpain inhibitors such as calpeptin. It has been shown that platelets release MPs in response to C5b-9 complement activation by cytoplasmic increase of $Ca^{2+}$ concentration, and this mechanism do not require metabolic energy or calpain-mediated proteolysis of the cytoskeletal proteins [Flaumenhaft, 2006; Wiedmer *et al.*, 1990]. Activation of platelets by C5b-9 normally leads to vesiculation of membrane vesicles, indicating that C5b-9 may play a role in the blebbing and vesiculation of the plasma membrane. The role of calpain in this mechanism seems not to play a role, since inhibition of calpain along with stimulation of platelets by C5b-9 still cause membrane vesiculation. [Wiedmer *et al.*, 1990]
Apoptosis also leads to the formation and vesiculation of MPs. The executive phase of apoptosis is characterised by changes in cell morphology due to contraction of the membrane and release of MPs, as illustrated in figure 5. MPs formed during apoptosis may differ from MPs formed during cell activation in their size, the composition of phospholipids and proteins on the surface, and the physiological function. The contraction of the cell membrane is caused by the generation of actin-myosin cytoskeletal structures, which then is thought to lead to release of MPs. This release is dependent on activation of the Rho-associated kinase I (ROCK I), which play a role in the stabilisation of actin-filaments, phosphorylation of myosin light chains, and coupling of actin-myosin filaments to the plasma membrane, thus promoting generation of the actin-myosin force that

leads to the cell contraction. ROCK I is activated by caspases, which cleaves the kinase and enabling it to activate the actin-myosin force. [Coleman *et al.*, 2001; Mause & Weber, 2010; VanWijk *et al.*, 2003]

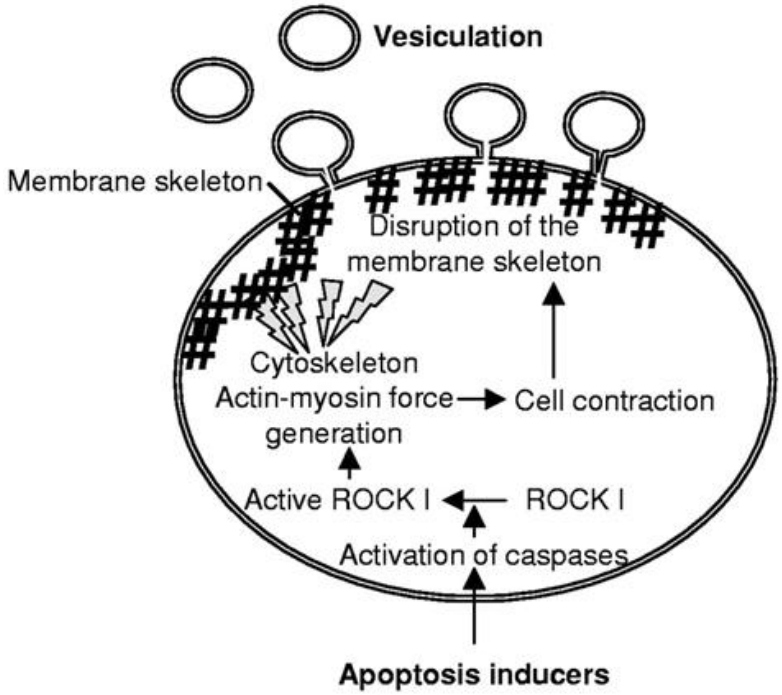


**Figure 5: Illustration of the formation of MPs during apoptosis. When a cell is induced to undergo apoptosis, activation of caspases occurs. These caspases further activates the Rho-associated kinase I (ROCK I), leading to generation of the actin-myosin force. Generation of this force leads to a contraction of the cell, and thus disruption of the membrane skeleton, resulting in the vesiculation of MPs. [Modified from VanWijk *et al.*, 2003]**

As previously mentioned MPs can be formed during conditions of high shear and oxidative stress.
High shear stress is often present during episodes of vasospasm of the arteries and in diseases such as atherosclerosis. Miyazaki and colleagues [Miyazaki *et al.*, 1996] investigated the effect of high shear stress on the production of MPs from platelets. The high shear stress was induced by a viscometer up to that of a known pathological level and the amount of formed MPs was measured by flow cytometry. It was found that high shear stress in fact does induce the formation of MPs, and this formation is connected to $Ca^{2+}$ influx to the cytoplasm of the cell and to the activation of calpain. [Burnier *et al.*, 2009; Miyazaki *et al.*, 1996]
Furthermore, von Willebrand factor has proven to play an important role in the formation of MPs during high shear stress. Von Willebrand factor normally interacts with glycoprotein complex Ib. This opens the calcium channels, leading to increase in cytosolic calcium, which followed by binding of von Willebrand factor to the glycoprotein complex IIb/IIIa leads to membrane vesiculation. [Burnier *et al.*, 2009; Furie & Furie, 2008; Miyazaki *et al.*, 1996; Reininger *et al.*, 2006]
Oxidative stress can be caused by various environmental factors and pathological conditions, such as ultraviolet or radioactive radiation, inflammation or hypoxia. Oxidative stress has been associated with the aminophospholipid re-organisation that occurs during cell activation, especially in red blood cells. Freikman and colleagues [Freikman *et al.*, 2008] have shown that MPs can be released due to oxidative stress from red blood cells, and thus provide evidence of MP release in several pathological conditions and due to environmental factors.
As previous described, MPs can be derived from several types of cells and the most abundant type of MPs in the circulation are platelet-derived MPs. Most platelet-derived MPs are released during activation or apoptosis of platelets [Burnier *et al.*, 2009], but it has been shown that platelet-derived MPs also derive directly

from megakaryocytes during megakaryopoiesis [Flaumenhaft *et al.*, 2009]. By investigating MPs derived from both active platelets and megakaryocytes, Flaumenhaft and colleagues have demonstrated that both types of MPs are present in the circulation [Flaumenhaft *et al.*, 2009]. Platelet-derived MPs express on their surface markers originating from platelets, e.g. CD62P and lysosome-associated membrane protein-1, whereas megakaryocyte-derived MPs do not express these markers. Instead, they contain full-length filamin A, which otherwise normally is cleaved during platelet formation. Thus, megakaryocytes play a role in the production of platelet-derived MPs. [Flaumenhaft *et al.*, 2009]

Furthermore, it has also been postulated that MPs can arise from lipid rafts. Lipid rafts are specialised membrane microdomains that amongst other things organise centers assembling signalling molecules and influence the membrane fluidity [Biró *et al.*, 2005; Korade & Kenworth, 2008]. del Conde and colleagues [del Conde *et al.*, 2005] has found MPs to arise from lipid raft rich regions of the cells by looking at the surface markers. They found MPs to be rich in TF and P-selectin glycoprotein ligand 1, which is localised in the lipid rafts, whereas proteins excluded from the lipid rafts were only found in relatively devoid amounts, which is similar to several enveloped viruses. Enveloped viruses infect cells by fusing with their target cell membrane, and del Conde and colleagues [del Conde *et al.*, 2005] therefore postulated a possibility of fusion between MPs bearing TF and activated platelets. Their investigation showed that MPs indeed fuse with activated platelets when transferring their complement of membrane proteins. [del Conde *et al.*, 2005] This was further confirmed by Biró and colleagues [Biró *et al.*, 2005] who investigated the cholesterol content and phospholipid composition of MPs and found that MPs seems to have a higher cholesterol content compared to platelet membrane fractions and the phospholipid composition is intermediate when compared to platelet membranes indicative of implication of lipid rafts in MP formation [Biró *et al.*, 2005].

## 1.7 Function of Microparticles

Hypothetically, MPs should be able to possess various functions depending on their origin. These functions could be normal physiological functions as well as pathophysiological functions. The majority of the literature reports the main function of circulating MPs to be in coagulation. Due to the exposure of phosphatidylserine in the outer membrane leaflet and in some MPs TF, a coagulant potential of MPs have been proposed. [Bucciarelli *et al.*, 2011; Hugel *et al.*, 2005; Leroyer *et al.*, 2008; VanWijk *et al.*, 2003] Phosphatidylserine has the potential to promote the assembly of the tenase complexes of the coagulation cascade. This can lead to activation of the coagulation cascade and thus the formation of thrombin. In theory, all negatively charged phospholipids have the potential to act as a catalytic surface for the assembly of the tenase complexes, but phosphatidylserine display the highest procoagulant activity. Furthermore, phosphatidylserine can maintain this catalytic surface despite the overall charge of the lipid surface or ionic strength. [Freyssinet, 2003; Simak *et al.*, 2004; Zwaal *et al.*, 1992]

An anticoagulant function of MPs has also been investigated. MPs derived from tumour cells express, as well as all MPs, phosphatidylserine in their surface membrane and membrane protein alike their parental cell [Davizon & López, 2009]. The first descriptions of shedding of MPs by tumour cells were in 1981, where Dvorak and colleagues [Dvorak *et al.*, 1981] found three different tumour cell lines to release procoagulant activity both in tissue culture and *in vivo*. This released procoagulant activity was found to be associated with vesicles derived from the tumour cells, which provides the first evidence of MPs to possess function in coagulation [Dvorak *et al.*, 1981].

Tans and colleagues [Tans *et al.*, 1999] compared procoagulant and anticoagulant potentials of both platelets and platelet-derived MPs. Their results showed that ~25 % of the anticoagulant effect previously connected to platelets and their function in inactivation of factor Va (activated factor V) through activated protein C was associated with the released MPs. Thus, platelet-derived MPs display anticoagulant and procoagulant functions. [Tans *et al.*, 1991]

TF is well known to play a major role in the initiation of the coagulation cascade. Recently, some investigators have described findings of circulating TF. Circulating TF have been linked to MPs, which further support the potential of MPs as procoagulant participants. The role of MPs expressing TF during the development of a thrombus has been investigated by Gross and colleagues [Gross *et al.*, 2005]. The time of accumulation of MPs in the thrombus was compared with the time of accumulation of leukocytes in the thrombus. The TF-positive MPs rapidly, within 60 seconds, accumulated in the developing thrombus, whereas the leukocytes were not observed until after two to three minutes. Gross and colleagues postulate if this rapid accumulation is due to the small size of MPs, and thus their ability to access platelets inside the thrombus. [Gross *et al.*, 2005]

Another potential function of MPs involves response to inflammation, in which MPs have been shown to be biologically active and stimulate the inflammatory response. When an inflammation is developing, endothelial cells express specific adhesion molecules which attract leukocytes to the site. Ligands for these adhesion molecules are expressed both on leukocytes and some leukocytes-derived MPs, thus MPs are attracted as well. The binding of leukocytes and MPs to the ligands result in the release of cytokines and growth factors into the intima by the endothelial cells. The migration and proliferation of vascular smooth muscle cells results in the formation of a plaque. [Leroyer *et al.*, 2008; VanWijk *et al.*, 2003] Furthermore, Messer and colleagues [Messer *et al.*, 2009] provide evidence that MPs have the potential to participate in the control of humoral B cell responses in rheumatoid arthritis and osteoarthritis. They investigated the ability of MPs to induce synthesis and release of different cytokines, such as B cell-activating factor (BAFF) and secretory leukocyte protease inhibitor in rheumatoid arthritis and osteoarthritis. Their data showed indications of MPs were able to induce release of especially BAFF from activated fibroblast-like synoviocytes. BAFF is released in response to stimulation of innate immune receptors, and it was proved that MPs have the potential to cause the release of BAFF and must therefore also possess potential proinflammatory abilities. [Messer *et al.*, 2009]

A vascular function of MPs has also been proposed. It is well known that diminished vascular function is involved in many cardiovascular diseases. Often the diminished function is due to endothelial dysfunction and it has been shown that MPs may be involved in this process. In patients with acute myocardial infarction, it has been reported that MPs reduced the vascular endothelial-dependent relaxation in arteries by affecting the endothelial nitric oxide transduction pathway. [Boulanger *et al.*, 2001; VanWijk *et al.*, 2003]

On the other hand, MPs have also been shown to possess potential functions of benefit for the vascular system. Platelet-derived MPs have been shown to be able to transfer arachidonic acid to endothelial cells, resulting in the production of prostacyclins, which induces vasodilation of the arteries. [VanWijk *et al.*, 2003]

Figure 6 briefly summarises the highlights of the role of MPs in coagulation, inflammation and in the vascular system [VanWijk *et al.*, 2003].

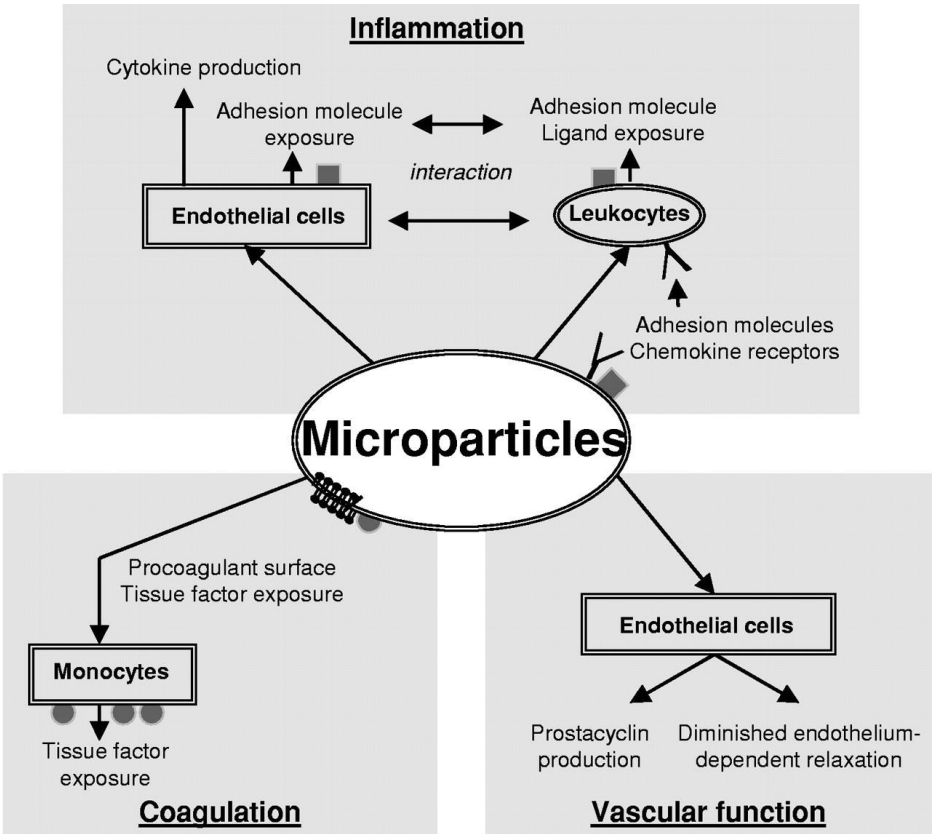


**Figure 6: Schematic illustration of the main functions of MPs. Due to the expression of phosphatidylserine in the outer leaflet and the possible expression of tissue factor in the membrane, MPs may play a role in coagulation. Furthermore, MPs released from endothelial cells have the potential to release cytokines and interact with leukocytes and thus play a role in inflammation. And finally, some MPs may possess a vascular function. These MPs may be platelet-derived MPs, which is able to transfer arachidonic acid to endothelial cells, resulting in the production of prostacyclins. Prostacyclins have the ability to induce vasodilation of the arteries. [VanWijk *et al.*, 2003]**

Finally, MPs have been shown to be able to transfer parts of their components to target cells, including transfer of proteins, RNA, receptors and others. MPs may act as intercellular mediators in two ways. They may act as circulating signalling molecules that affect cellular properties and responses, or they may act as mediators of signals by directly transfer components to a recipient cell, affecting cell activation or phenotypic modifications. [Mause & Weber, 2010]

The two functions apply both circulating MPs and MPs in the extracellular fluid, thus the MPs may not only affect the cells surrounding their cell of origin, but they may also affect cells at notable distances from the cell of origin. [Mause & Weber, 2010]

Evidence of transfer of components from MPs to cells has been provided by Rozmyslowicz and colleagues, who investigated how HIV can infect cell types that do not express virus co-receptors, such as endothelial cells and cardiomyocytes. It was found that MPs expressing CXCR4 could transfer this receptor to CXCR4-null mice, and thus make them susceptible to HIV infection. [Rozmyslowicz *et al.*, 2003]

In figure 7, the known transfer mechanisms of MPs are illustrated. Mediators released by MPs are delivered to recipient cells during interactions between the MPs and the recipient cell, which can elicit several different responses. MPs have also the potential to transfer different membrane components, receptors and cytosolic components, such as RNA, by fusion with the recipient cell. [Mause & Weber, 2010]

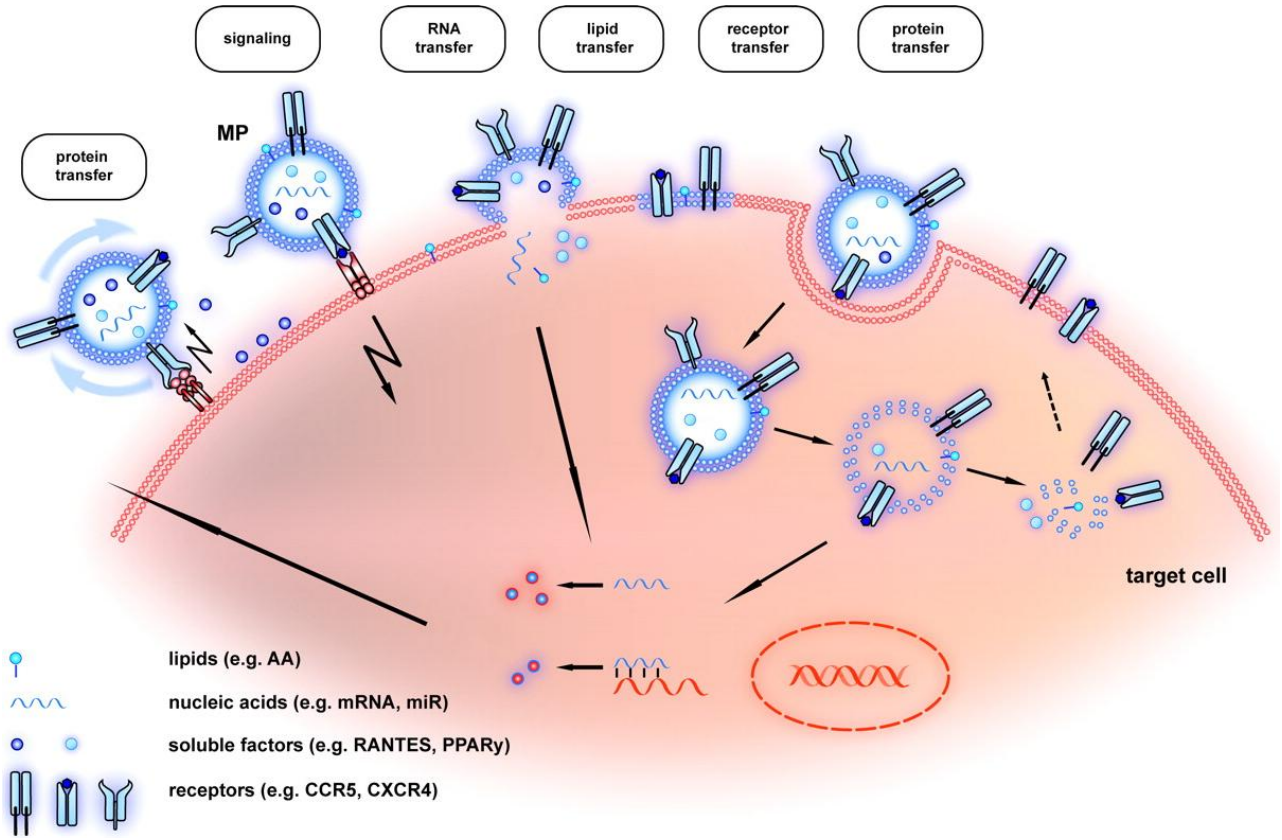


**Figure 7: Illustration of the different transfer mechanism of MPs. MPs may release soluble mediators that can be delivered to target cells and induce specific responses in the target cell. MPs may also transfer membrane proteins to the target cell, such as receptors or cytosolic components, by membrane fusion or by internalisation.**

## 1.8 Clearance of Microparticles

Only few descriptions of the life span of MPs, the kinetics of their clearance, the organs involved in their clearance and the mechanisms of the clearance of MPs can be found in the literature [Flaumenhaft, 2006].

The life span of MPs has been investigated by Rand and colleagues [Rand *et al.*, 2006]. They labelled platelets with a biotin and then stimulated the platelets by A23187 to release MPs. Rabbits were injected with either biotin-labelled, unstimulated platelets or the platelet-derived MPs. Blood samples were collected after 10, 30, and 60 minutes, and the MPs were analysed by flow cytometry. It was discovered that the MPs were cleared from the circulation within 10 minutes of injection, and they did not return to the circulation within the following 50 minutes. This indicates that there must be a continuous production and clearance of MPs from the circulation. [Rand *et al.*, 2006]

MPs can be cleared in two ways: (1) Resident macrophages in the tissue ingest the MPs, and (2) macrophages in the liver and spleen ingest MPs in the circulation [Davizon & López, 2009]. The phagocytotic removal of MPs can further occur in two ways: (1) recognition of altered-self (clearance of cell fragments) by the direct mechanisms such as phosphatidylserine exposure and by the indirect mechanisms such as opsonisation proteins (e.g. protein S, thrombospondin, and phospholipase $A_2$), and (2) innate recognition of non-self (clearance of both cell fragments and foreign bodies). [Davizon & López, 2009; Flaumenhaft, 2006; Fourcade *et al.*, 1995; Wu *et al.*, 2006]

Removal of MPs through the liver has been investigated in a rat model [Willekens *et al.*, 2005]. MPs were derived from red blood cells from a donor rat. The haemoglobin in the MPs were then labelled with a chromate, and finally injected into a recipient rat. Approximately 85 % of the MPs were cleared from the circulation within five minutes, whereas the remainder was removed much more slowly, as if a plateau was reach.

Liver tissue was removed from the recipient rat and investigated for uptake of the chromate. More than 90 % of the radioactivity was found in the Kupffer cells, indicating that MPs derived from red blood cells are removed from the circulation by these cells in rats. Willekens and colleagues [Willekens *et al.*, 2005] postulate that this mechanism occurs in humans as well, since the removal of haemoglobin from red blood cells in humans follows the same pathway. [Willekens *et al.*, 2005]

## 1.9 Microparticle Involvement in Disease

Different levels and concentration of MPs have been reported in several different pathological states, and the majority of these described diseases have a common outcome: thrombosis. Thrombosis is associated with vascular damage and the activation of the coagulation cascade and as it has been stated previously, MPs potentially play a role in coagulation through their expression of TF and phosphatidylserine in the outer leaflet. Amongst the investigated diseases are Castaman's syndrome and Scott's syndrome, venous thromboembolism, paroxysmal nocturnal haemoglobinuria, heparin-induced thrombocytopenia, thrombotic thrombocytopenic purpura, sickle cell disease, diabetes mellitus, cancer and HIV infections. [Burnier *et al.*, 2009; Davizon & López, 2009; Freyssinet, 2003; Habib *et al.*, 2008; Leroyer *et al.*, 2008; Simak *et al.*, 2004; Tomer *et al.*, 2001] Table 1 lists some of the diseases in which the MP levels have been shown to differ from the levels found in healthy individuals. [Bucciarelli *et al.*, 2011]

This is merely few of the diseases in which MPs have been shown to be elevated, and it seem as MPs can be used in diagnostics and prognostics of diseases [Simak *et al.*, 2004]. In order to do so, MPs need to be determined in concentration, size, origin and surface expression.

Despite increasing scientific and clinical interest in MPs, the isolation, detection and characterisation of MPs are hampered by both limitations in the technology available for their measurement and the biological complexity of body fluids. Several of the methods used today can be time-consuming and present with results that can be difficult to interpret, especially in heterogeneous samples containing a wide range of particle sixes, such as body fluids. [Carr *et al.*, 2009; Furie & Furie, 2006]

The most widely used method for determination of the concentration of MPs in a liquid is flow cytometry. From the above mentioned references, a total of 21 references out of 24 have used flow cytometry to investigate the MP content in the diseases samples, illustrating the diverse use of flow cytometry. The classical flow cytometer has been developed in recent years and the limitations seen in the classical flow cytometer have been diminished. Changes in the flow speed, a lower noise and an improvement in the electronic capabilities have resulted in a better sensitivity and thus more accurate measurements. Flow cytometry is the optimal method of choice when measuring antigens on cell surfaces with the use of fluorescence, but obtainment of a correct size of even platelets with diameters of 1 µm to 2 µm is difficult. Thus, the major limitation of flow cytometry is the high detection limit. MPs are often detected near the electronic noise and cellular debris in the first quarter in the logarithmic scale of the light scatter. Furthermore, flow cytometry cannot detect very small MPs (less than 300 nm in diameter), and in some diseases these small MPs predominate. Investigators choose to ignore this limitation, and therefore many of the results in the literature should be handled with great caution. [Furie & Furie, 2006; Burnier *et al.*, 2009; Horstman & Ahn, 1999; Perez-Pujol *et al.*, 2007]

The need of new methods for the characterisation of MPs is therefore crucial. This project aims to evaluate two novel detection methods for the characterisation of MPs, namely Nanoparticle Tracking Analysis (NTA) and Dynamic Light Scattering (DLS).

**Table 1: List of some pathological conditions, their manifestations and the MP level detected in plasma unless otherwise is noted.**

| Pathological condition | Disease manifestations | Microparticle level in plasma compared to normal levels | Reference |
|---|---|---|---|
| Castaman's syndrome | Life-long bleeding disorder associated with prolonged bleeding time | Lower | [Castaman *et al.*, 1996] [Castaman *et al.*, 1997] |
| Scott's syndrome | Isolated defect in platelets in the inducible procoagulant activity; translocation of phosphatidylserine to the outer leaflet is impaired | Lower | [Sims *et al.*, 1989] [Zwaal *et al.*, 2004] |
| Venous thromboembolism | Thrombosis formation due to endothelial damage, blood stasis, and hypercoagulability | Higher | [Bucciarelli *et al.*, 2011] [Chirinos *et al.*, 2005] |
| Paroxysmal nocturnal haemoglobinuria | Stem cell disorder associated with increased incidence of thrombosis; cell surface complement inhibitors are partially or completely deleted from the plasma membrane | Higher | [Hugel *et al.*, 1999] [Simak *et al.*, 2004] [Wiedmer *et al.*, 1993] |
| Heparin-induced thrombocytopenia | Moderate thrombocytopenia due to complication of heparin use; results in thrombosis | Higher (in serum) | [Hughes *et al.*, 2000] [Warkentin *et al.*, 1994] |
| Thrombotic thrombocytopenic purpura | Thrombocytopenia with endothelial injury leading platelet activation and formation of thrombi in microvasculature | Higher | [Jimenez *et al.*, 2001] [Kelton *et al.*, 1992] |
| Sickle cell disease | Mutated red blood cells; vascular occlusion, acute chest syndrome, stroke, and aplasia are all linked to sickle cell disease | Higher | [Shet *et al.*, 2003] [Simak *et al.*, 2004] [Wun *et al.*, 1997] [Wun *et al.*, 1998] |
| Diabetes mellitus | Impairment of the production of insulin; vascular complications, such as atherosclerosis, are often seen | Higher | [Leroyer *et al.*, 2008] [Nomura *et al.*, 1995] [Sabatier *et al.*, 2002] |
| Cancer | Cancer is associated with venous thromboembolism, and TF plays a central role in the tumour growth and angiogenesis of the tumour | Higher | [Tesselaar *et al.*, 2007] [Toth *et al.*, 2008] |
| HIV | Infects cells through CD4, CXCR4, and CCR5; primary targets include lymphocytes, macrophages, megakaryocytes, and dendritic cells | Higher | [Mack *et al.*, 2000] [Rozmyslowicz *et al.*, 2003] |

# Part 2: Experimental strategy

## 2.1 Aim of Project

The discussed limitations in the technology used to characterise MPs today is very problematic. Despite the development of new technologies with new technical possibilities, evidence of their clinical potential is inadequate. The overall aim of this project is therefore to evaluate the potential of two novel detection methods for the characterisation of MPs, namely Nanoparticle Tracking Analysis (NTA) and Dynamic Light Scattering (DLS), including an assessment and comparison of pre-analytical parameters such as centrifugation, freezing, and dilution of plasma samples.

## 2.2 Experimental Strategy

The hypothesis of this project is based on five separate experiments. These experiments focus on the variations of results in between different runs and the pre-analytical parameters. The five separate hypotheses are given in the explanations of each experiment.
The general experiment strategy of this project is illustrated below in figure 8.

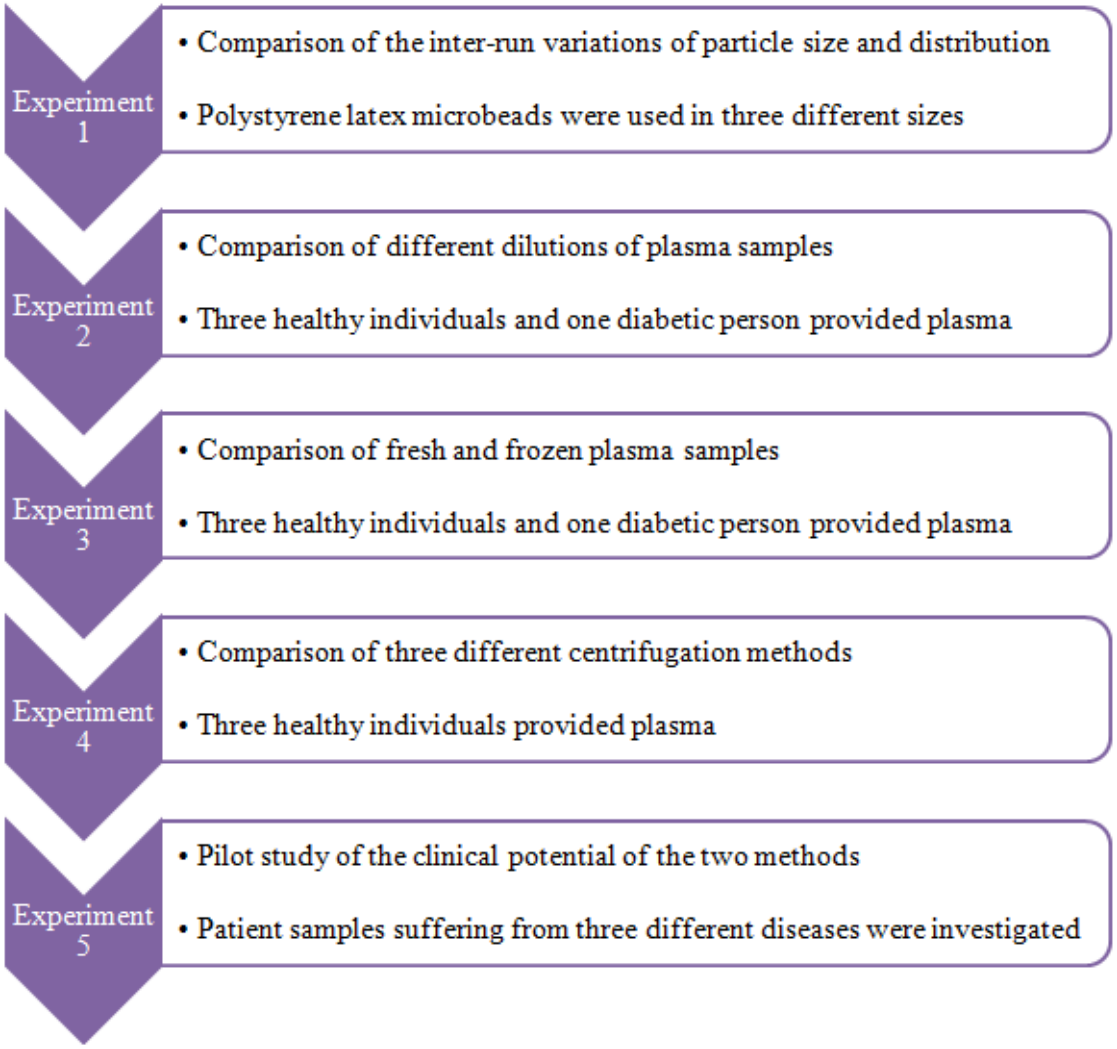


**Figure 8: Schematic overview of the experimental strategy.**

Results obtained from one experiment forms the basis of the subsequent experiment. Therefore, the project has been divided into different parts in which each experimental setup will be clarified and a presentation of the obtained results and a short discussion is given.

### 2.2.1 The Five Experimental Parts of the Project:

Experiment 1:

The comparison of the inter-run variations of particle size and distribution is conducted in order to investigate the methods capability to reproduce a result. Polystyrene latex microbeads will be used diluted in Dulbecco's Phosphate Buffered Saline (DPBS), and different ratios will be tested on both methods. The aim is to show that both methods display reproducibility and can measure the size and concentration with accuracy.

Experiment 2:

The comparison of different dilutions of plasma in a buffer is conducted in order to determine means of viscosity of plasma sample. Plasma samples will be prepared as suggested by Lacroix and colleagues [Lacroix *et al.*, 2012].The prepared plasma from three healthy individuals and one diabetic patient will be diluted in DPBS in different ratios. On the NTA device, the following dilutions will be tested: 1 µL plasma sample in 1000 µL DPBS, 2 µL plasma sample in 1000 µL, 3 µL plasma sample in 1000 µL DPBS, 4 µL plasma sample in 1000 µL DPBS, and finally 5 µL plasma sample in 1000 µL DPBS. On the DLS device, no dilutions will be tested, since it is known from the inventors of the device that this device only can test pure plasma samples. The aim is to find the maximum limit of detection of tracks by NTA. Furthermore, it will provide a basis for expected intensity measured by the DLS device of healthy samples.

Experiment 3:

The comparison of fresh and frozen samples is conducted in order to investigate the influence of freezing on the size and distribution of detected MPs. Plasma samples from three healthy individuals and one diabetic patient is tested as freshly obtained samples (Day 0), then frozen for 1, 7, 15, and 40 days. Based on the results obtained in the experiment of the dilution of plasma samples in DPBS, the plasma samples will be tested on the NTA device diluted as so. The aim is to show that there is no difference in the measured particle size or distribution between fresh and frozen samples.

Experiment 4:

The comparison of three different centrifugation methods is conducted in order to investigate the influence of centrifugation on the formation of MPs. The three centrifugation methods, which in this project are named Centrifugation A, B, and C, and they are as follows: Centrifugation A is a single-step centrifugation used in the hospital routine laboratory, Centrifugation B is a double-step centrifugation recently proposed on the last SSC meeting, and finally Centrifugation C is a two-step centrifugation which has been proposed several years ago [Lacroix *et al.*, 2012]. The aim is to show that there is no difference in the measured particle sizes, concentration or distribution however the plasma samples are centrifuged.

Experiment 5:

In order to test the clinical potential of the two methods, patients samples suffering from three different diseases where collected. The patients were suffering from atrial fibrillation (AF), ischemic heart disease (IHD), and multiple myeloma (MM), respectively. The pre-analytical preparations of the samples were based on the results obtained in the previous experiments. The samples were compared to healthy control sample. The aim is to investigate if there is a significant difference in the concentration of MPs in healthy individuals compared to diseases individuals. Furthermore, the clinical potential of the two methods will be evident.

# Part 3: Methods

## 3.1 Introduction

Nanoparticle tracking analysis (NTA) is a newly developed laser-illuminated optical microscope-based method for the characterisation of MPs. Its primary advantage is its ability to detect, visualise in real-time and directly analyse MPs in a liquid. The NTA software tracks the Brownian motions of MPs and calculates their diameter. [Carr *et al.*, 2009; Dragovic *et al.*, 2011]

Dynamic light scattering (DLS) is a laser-light based method used to determine size of proteins and now also MPs, and it is a widely used and excepted technology. The DLS software detects the Doppler shift of the laser-light as it is scattered from the moving MP and calculate their radius.

## 3.2 Nanoparticle tracking analysis

Nanoparticle tracking analysis (NTA) is newly developed and was first commercialised in 2006. NTA is an optimal method for detection of MPs in a liquid based on laser-illuminated optical microscopy. The primary advantage of this method is its ability to detect, visualise in real-time, and directly analyse particles as they move in the liquid. All particles in liquid moves by Brownian motion, and this principle is also applicable for NTA. As the particles moves by Brownian motion, a two-dimensional video is taken. This video is analysed by the NTA software on a frame-by-frame basis. The average speed and distance of movement of the particles is established and this information is used to calculate the diameter of each particle and thus a size distribution and concentration will also be evident. Since each particle in measured both simultaneously and individually, it is possible to measure both the particle size and the relative light scattering intensity, which provides a more precise result of liquid containing mixtures of different particle sizes, such as biological fluids. [Carr *et al.*, 2009; Dragovic *et al.*, 2011]

The device used to obtain the aim of this project was a NanoSight LM10-HS (NanoSight Ltd., Amesbury, United Kingdom), which is illustrated in figure 8.

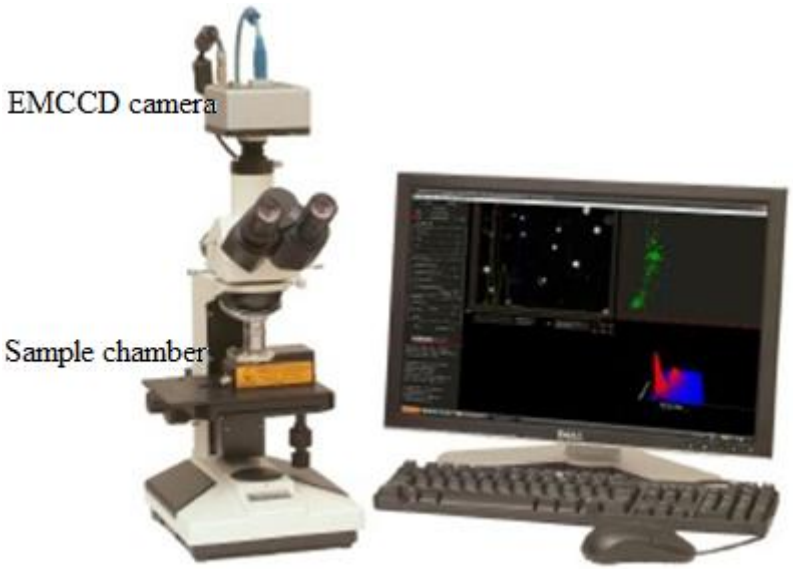


**Figure 8: Illustration of NanoSight LM10-HS device. The microscope has an electron multiplying charged-couple device (EMCCD) camera positioned on top, and the sample chamber is positioned under the lens. The computer shows the NTA 2.1 software as it is analysing a sample.**

Positioned on top of the microscope is an electron multiplying charged-couple device (EMCCD) camera. This camera is extremely sensitive and makes the device capable of detecting very small MPs, such as viruses with diameters below 50 nm and low refractive indexes. Cellular particles and thus the MPs of interest have a low refractive index. The EMCCD camera has a frame rate of 30 frames per second and typically this

video is 60 seconds in duration. The video field of view is ~100 µm x ~80 µm. [Carr *et al.*, 2009; Dragovic *et al.*, 2011]
The NanoSight LM10-HS is equipped with a x20 magnification microscope objective just above the sample chamber, which is highlighted in figure 9. [Carr *et al.*, 2009; Dragovic *et al.*, 2011]

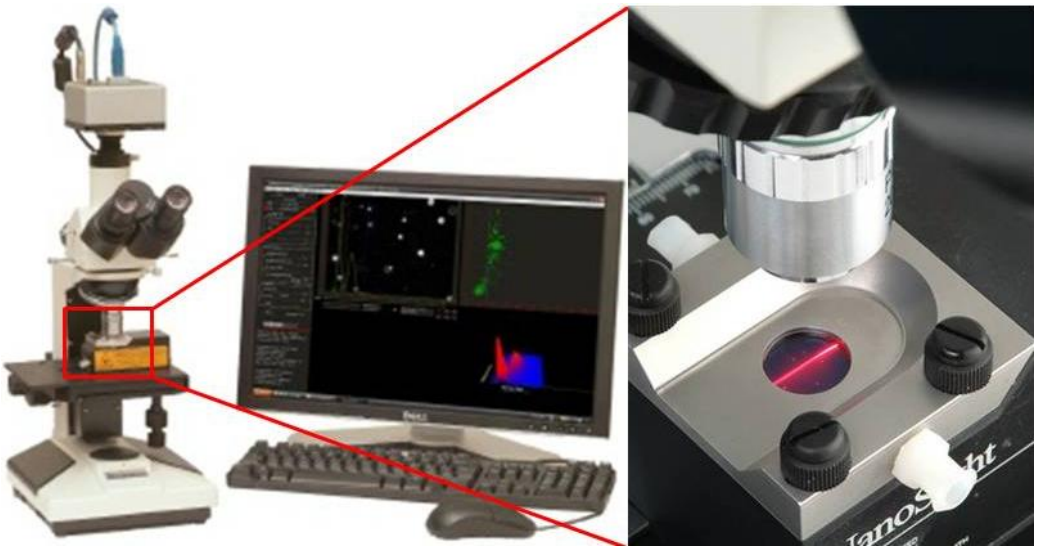

**Figure 9: Illustration of the NanoSight LM10-HS microscope with the sample chamber highlighted to the right. In the sample chamber, the finely focused laser beam can be seen. [Downloaded and modified from NanoSight Ltd. webpage: www.nanosight.com]**

The sample chamber is equipped with an inlet where the sample is injected with a sterile syringe, and an outlet where the sample can be ejected through. The sample chamber is ~500 µm deep and can contain ~0.25 mL of sample. As figure 9 illustrates, a laser beam passes through the sample chamber. The NanoSight LM10-HS system uses a finely focused 405 nm laser beam, which is introduced into the sample chamber through a glass prism-edged optical flat. The refractive index of the glass prism is as such that the laser beam is refracted just above the glass flat and into the liquid above it. This low angle refraction results in a thin laser beam that illuminates MPs through the sample. The EMCCD camera collects the light scattered from each MP as it refracts the light in the field of view. Figure 10 graphically illustrates how the laser beam is refracted in the glass prism at a low angle into the liquid containing the MPs. [Carr *et al.*, 2009; Dragovic *et al.*, 2011]

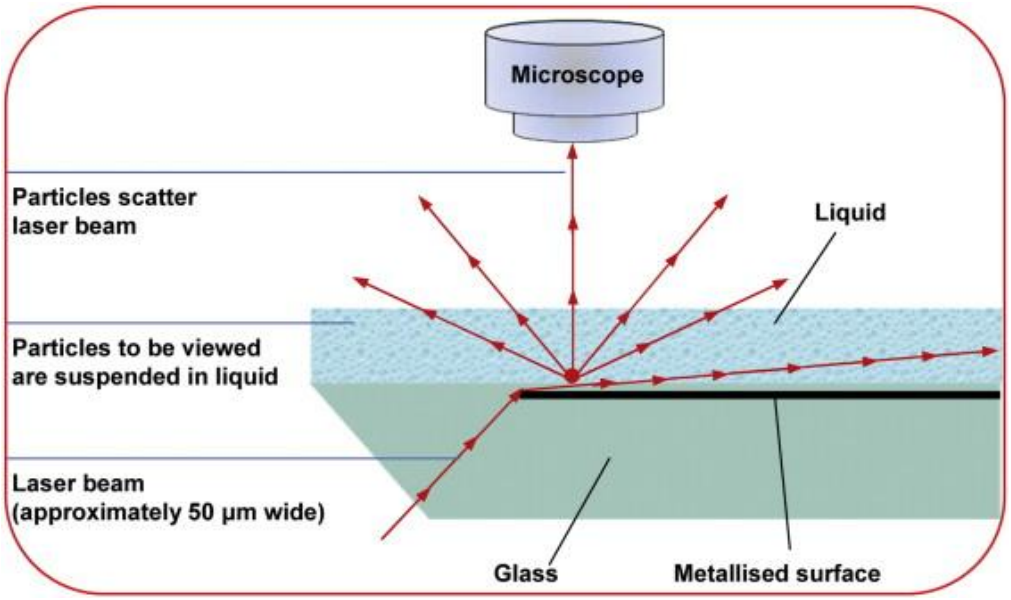


**Figure 10: Graphical illustration of the principle of the NanoSight LM10-HS (NanoSight Ltd., Amesbury, United Kingdom). The laser beam passes through the glass prism and is refracted in a low angle as it reaches the metallic flat. The MPs scatter the laser light as they passes the laser beam, and this scattered light is collected by the microscope and the EMCCD camera positioned on top. [Dragovic *et al.*, 2011]**

As mentioned earlier, MPs move by Brownian motion in liquid. This movement can be observed in the captured video, and it is used by the NTA software to determine the size and distribution of the MPs. The NTA software identifies the center of each moving particles and follow it frame by frame throughout the length of the video. The mean square displacement in the two dimensions of the video is calculated. This equals the diffusion coefficient, $D_t$, which is accommodated by use of the following equation (Equation 1) [Carr *et al.*, 2009; Filipe *et al.*, 2010]:

$$D_t = \frac{\overline{(x,y)}^2}{4} \qquad \textit{Equation 1}$$

This diffusion coefficient along with a known sample temperature, $T$ and the viscosity of the sample, η, is then used to calculate the particle diameter (the sphere hydrodynamic diameter; $d_h$) of each MP. The two-dimensional Stokes-Einstein equation (Equation 2) is used since the particles are tracked in two dimensions although they move in three dimensions in the liquid. [Carr *et al.*, 2009; Dragovic *et al.*, 2011; Filipe *et al.*, 2010]

$$D_t = \frac{TK_B}{3\pi\eta d_h} \leftrightarrow d_h = \frac{TK_B}{3\pi\eta D_t} \qquad \textit{Equation 2}$$

where $K_B$ is Boltzmann's constant.
Several different parameters can be changed both during the video capture, such as camera gain and camera shutter, and during the analysis of the video, such as filter settings, removal of background noise, and the minimum expected particle size. This allows the user to track particles of interest and optimise the results. [Dragovic *et al.*, 2011]
NTA requires concentrations in the range of $10^7$-$10^9$ particles/mL [Filipe *et al.*, 2010]. Dragovic and colleagues [Dragovic *et al.*, 2011] have provided evidence for the detection limits of NanoSight. MPs as small as ~50 nm could be measured, and it is therefore much more sensitive than flow cytometry that has a limit of ~300 nm. One major disadvantage of NTA is its limitation in measuring MPs above 1 µm in diameter. These large particles moves very slowly in a liquid and thus move under a slow Brownian motion, hampering the

analysis of them. Therefore, the analysis of MPs with sizes above ~500 nm should perhaps be analysed using flow cytometry. Some non-biological MPs, such as colloidal gold, have high refractive indexes and the diameter of these MPs can be obtained to as low as 10 nm in diameter. [Carr *et al.*, 2009; Dragovic *et al.*, 2011]

Besides being an optimal method for detection and analysis of MPs in liquids, Dragovic and colleagues [Dragovic *et al.*, 2011] have shown that NTA can differentiate between MPs derived from different types of cells by the use of fluorescence. By labelling the MPs with specific antibody-conjugated quantum dots, the phenotype of the MPs could be determined. [Dragovic *et al.*, 2011]

Numerous scientific papers using NTA have been published in several different research areas, including drug delivery, nanotoxicity, and viruses. Carr and colleagues [Carr *et al.*, 2009] have assembled a table with some of the different applications of NTA, which is given in table 2.

**Table 2: Few applications in which NTA has been used (from Carr *et al.*, 2009).**

| Application | Sample type | Reference |
|---|---|---|
| **Drug delivery** | Coated nanocapsules drug delivery<br>Non-viral siRNA delivery<br>Non-viral lipopolyamine vectors<br>Anticancer conjugates | [Nassar *et al.*, 2009]<br>[Soltan *et al.*, 2009]<br>[Ghonaim *et al.*, 2009]<br>[Miller *et al.*, 2009] |
| **Nanotoxicity** | Genotoxicity of cobalt nanoparticles | [Colognato *et al.*, 2008] |
| **Synthesis** | Thiol-sillicate nanoparticles<br>Poly(acrylic acid) with n-vinyl pyrrolidone<br>Carbon nanotubes | [Neville *et al.*, 2009]<br>[Zhunuspayev *et al.*, 2008]<br>[Trushkevych *et al.*, 2008] |
| **Metals** | Magnetic nanoparticles | [Kendall & Kosseva, 2006 |

## 3.3 Dynamic light scattering

Dynamic light scattering (DLS) is postulated to be a suitable method for the detection of MPs. This technology is frequently used in proteomic studies as a non-invasive tool for determination of size and protein-protein interactions. Earlier versions of DLS were not able to detect MPs in a suspension containing platelets, thus the platelets had to be separated from the sample. The development of a new and improved version of DLS, the ThromboLUX device (LightIntegra Technology Inc, Vancouver, Canada), provides the possibility of investigating small sample sizes with very complex compositions, such as plasma containing platelets. [Maurer-Spurej *et al.*, 2006; Xu *et al.*, 2010]

The ThromboLUX device is composed of several different components. The major difference between earlier developed DLS devices and ThromboLUX is the improvement of the sample holder. The sample holder is composed of one movable part and one immovable part. Each of these parts have Peltier elements, which a mostly known as components of a normal thermal cycler (PCR machines) for cooling and heating, and four magnets, that pulls the two parts together. The movable parts allow the use of different sizes of sample capillaries with diameters ranging from 1.7 mm to 3.5 mm. A small V-shaped notch in which the sample capillary inserts provides efficient surface for great temperature control. In the midsection of the sample holder, a complete slit through allows the light to pass from the fiber directing the light into the sample to the fiber detecting the scattered light. The sample holder is illustrated in figure 11. [Maurer-Spurej *et al.*, 2006]

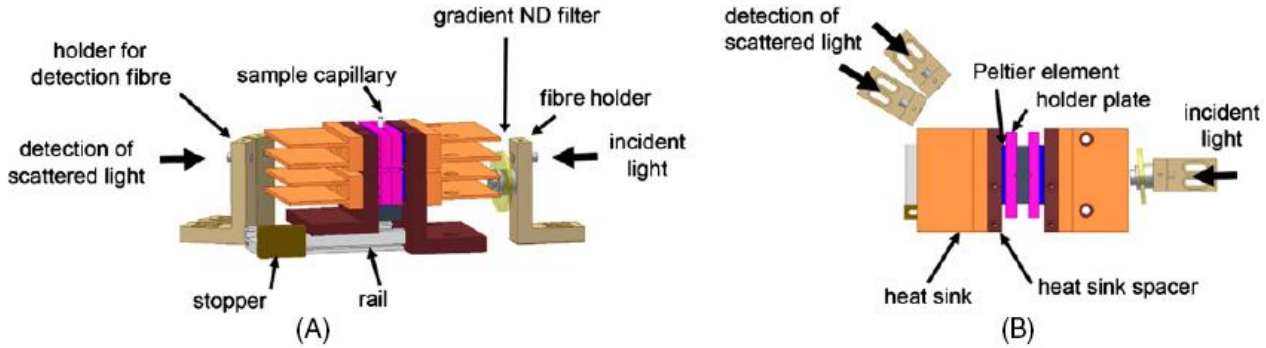


**Figure 11: Schematic illustration of the ThromboLUX sample holder. (A) A front view of the sample holder, closed with a sample capillary tightly anchored in between the Peltier elements and the four magnets. Furthermore, the optical fiber directing light into the sample is shown to the right and the fiber detecting the scattered light is shown to the left. (B) A top view of sample holder with the Peltier elements separated and no sample capillary in between them. [Maurer-Spurej *et al.*, 2006]**

The sample holder is accessible through a sliding door in the cover of the ThromboLUX. Through this sliding door, sample capillaries are both loading and unloaded. The ThromboLUX device is illustrated in figure 12 with an illustration of the sliding door in the inset.

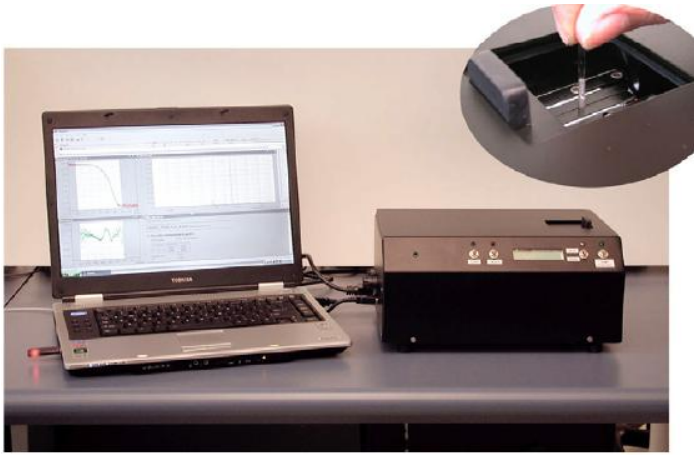

**Figure 12: Photograph of the ThromboLUX device and the laptop for data analysis. The inset illustrates the sliding door and sample holder. [Maurer-Spurej *et al.*, 2006]**

Other compartments of the ThromboLUX device include a thermocontroller, a diode laser with a wavelength of 635 nm, a single photon counting module, a correlator and a power supply, which is illustrated in figure 13. [Maurer-Spurej *et al.*, 2006; Xu *et al.*, 2010]

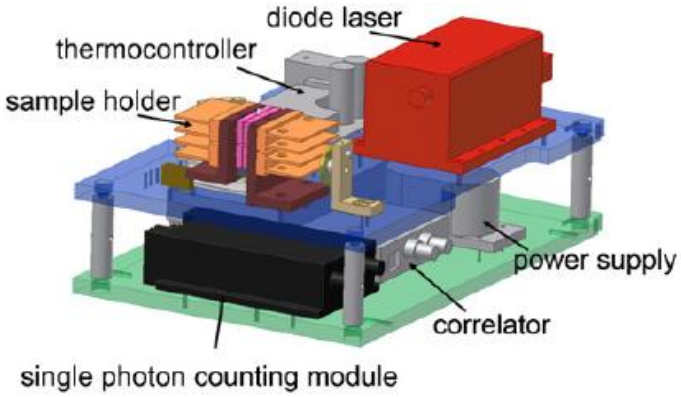


**Figure 13: Schematic illustration of the ThromboLUX device without the cover, fibers and cables. The sample holder is illustrated in the front with the thermocontroller next to it. The diode laser contains a 635 nm laser, and the correlator is used to transform the collected measurements into the computer system. [Maurer-Spurej *et al.*, 2006]**

Similar to NTA, DLS uses the Brownian motion of MPs to determine the size of the measured MPs, but DLS also uses the Doppler shift of the scattered light from the moving MPs. Doppler shift occurs when the laser light is scattered from the MPs as they pass through the laser light. The Doppler shift is defined as the frequent change in scattered light compared to unscattered light. Large particles which are moving slowly have a small Doppler shift, and small particles which are moving fast have large Doppler shift. DLS also uses the two dimensional Stokes-Einstein equation for the calculation of particle size. NTA determines the diffusion coefficient by the mean square displacement, whereas DLS determines the diffusion coefficient by measuring the Doppler shift. The calculated diffusion coefficient is then used to calculate the hydrodynamic radius ($R_H$) by the use of the following equation [Maurer-Spurej *et al.*, 2006; Xu *et al.*, 2010]:

$$D_t = \frac{TK_B}{6\pi\eta R_H} \leftrightarrow R_H = \frac{TK_B}{3\pi\eta D_t} \qquad \textbf{\textit{Equation 3}}$$

It has been evident that this requires efficient and accurate temperature control. This is obtained with the development of ThromboLUX using Peltier elements in direct contact with the sample capillary. [Maurer-Spurej *et al.*, 2006; Xu *et al.*, 2010]

DLS can measure samples with a relatively high amount of MPs. The optimal concentration of MPs for DLS is $10^8$-$10^{12}$ particles/mL, which is a significantly higher concentration compared to NTA, which is very sensitive to both too high and too low concentrations of MPs. [Filipe *et al.*, 2010]

DLS is not only used to detect MPs and determine the size of round particle, but it has a broad range of applications. These applications are wide spread and cover several areas of medicine, biology and material science. ThromboLUX was firstly developed to analyse platelets in a plasma sample and determine the quality of platelets. [Maurer-Spurej *et al.*, 2006]

# Part 4: Experiment 1

# Inter-run variation experiment

## 4.1 Aim of Experiment

The aim is to show that both methods display reproducibility and can measure the size and concentration with accuracy.

## 4.2 Materials

NTA measurements were conducted by the use of a NanoSight LM10-HS device (NanoSight Ltd., Amesbury, United Kingdom), and the used software was NTA 2.1 analytical software (NanoSight Ltd., Amesbury, United Kingdom). DLS measurements were conducted by the use of a prototype of a ThromboLUX device (Light Integra Technology, Vancouver, Canada), and the analysis software were FLEX02-12BD (measurement software) and CorrelatorComms 1.141 (analysis software). Polystyrene latex microbeads with sizes 50 nm, 100 nm, and 200 nm were purchased from Thermo Scientific (Fremont, USA). Dulbecco's phosphate buffered saline (DPBS) without $Ca^{2+}$ and $Mg^{+}$ (Lonza, Verviers, Belgium) was used to dilute microbeads into appropriate concentrations.

## 4.3 Methods

### 4.3.1 Nanoparticle Tracking Analysis

All experiments with microbeads were conducted as described in the protocol in appendix A.2. Several different concentrations of microbeads were tested, because the start concentrations of the microbeads were not given on the purchased containers. Preparation of microbeads was conducted by diluting the microbeads in DPBS into monodisperse dilutions. Starting with very high concentrations of microbeads, the concentration was systematically lowered until a suitable concentration was reached.

The suitable concentrations was prepared as follows: 1 µL of 50 nm microbeads was diluted in 35,000 µL DPBS, 1 µL of 100 nm microbeads was diluted in 25,000 µL DPBS, and 1 µL of 200 nm microbeads was diluted in 10,000 µL DPBS, according to protocol in appendix A.2. A total of 1000 µL of each dilution was used for each measurement, which was prepared in 1.5 mL microtubes. Experiments with 50 nm microbeads were repeated six times, five times for 100 nm microbeads, and four times for 200 nm microbeads.

Prior to measurement of microbeads, the sample chamber was washed and a blank sample was run to locate the thumbprint. The blank sample was injected into the sample chamber by the use of 1 mL sterile syringes (Becton Dickinson, Madrid, Spain) until it reached the tip of the sample chamber output. The thumbprint was located along with the preferred measuring area and the appropriate camera and parameter settings were found, according to protocol in appendix A.2. A video of the blank sample was taken. Then the blank sample was removed from the sample chamber, which was rewashed. After each run the chamber was washed in 70 % EtOH.

The samples were measured in the 'single shutter and gain mode' for 60 seconds. The temperature of each run was measured by a temperature measuring device specifically developed to the sample chamber. The NTA 2.1 Analytical Software was used for capturing and analysing the data.

### 4.3.2 Dynamic Light Scattering

All experiments with microbeads were conducted as described in the protocol in appendix A.2. Several different concentrations of microbeads were tested, because the start concentrations of the microbeads were not given on the purchased containers. Preparation of microbeads was conducted by diluting the microbeads in DPBS into monodisperse dilutions. Starting with very high concentrations of microbeads, the concentration was systematically lowered until a suitable concentration was reached. The suitable concentrations was prepared as follows: 4 µL of 50 nm microbeads was diluted in 10 µL DPBS, 1 µL of 100 nm microbeads was diluted in 5 µL DPBS, and 1 µL of 200 nm microbeads was diluted in 10 µL DPBS, according to point 2 in protocol B. A total of 40 µL of each dilution was used to each measurement, which was prepared in 1.5 mL

microtubes. Experiments concerning 50 nm and 100 nm microbeads were repeated five times, whereas experiments with 200 nm microbeads were repeated three times. Prior to measurement of microbeads, the intensity settings were checked by the use of a blank sample only composed of DPBS. The blank sample was loaded into the sample holder in a disposable plastic capillary (Drummond Scientific Company, Pennsylvania, USA), according to protocol in appendix A.2. The blank sample was measured, and when a satisfactory intensity was observed, the blank sample was removed from the sample chamber.
The samples were measured for 240 seconds, and all experiments were conducted at room temperature. The CorrelatorComms software was used to analyse data obtained by the FLEX02-12BD software. The mean particle sizes were read directly from the resultant graph.

### 4.3.3 Statistical Analysis

The mode particle size, the value of the highest point of the peak, and standard deviation (SD) values obtained by both the NTA software and DLS software were used to describe the results. Mean results were calculated for each size. Based on the measured mode particle sizes, a SD was found, and by the use of Equation 4, coefficient variation (CV %) for each size was calculated:

$$CV\ \% = \frac{\sigma}{\mu} \times 100 \qquad \textbf{\textit{Equation 4}}$$

where σ is the standard deviation and μ is the mean particle size. All statistics were evaluated using Microsoft Excel.

## 4.4 Results

### 4.4.1 Nanoparticle Tracking Analysis

In order to investigate the accuracy and capability to reproduce a result, polystyrene latex microbeads were analysed by NTA. Microbeads of 50 nm, 100nm, and 200 nm in diameter were used. NTA requires concentrations in the range of $10^7$-$10^9$ particles/mL [Filipe *et al.*, 2010]. Six repeats with 50 nm microbeads were conducted. Illustrated in figure 14 are the results from the six individual runs.

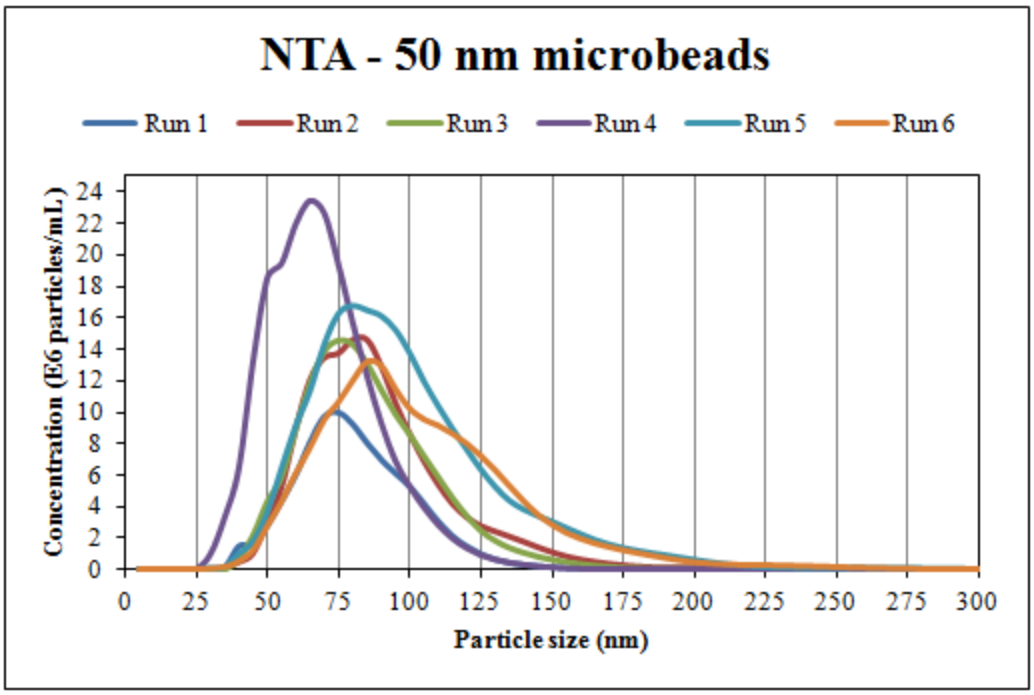


**Figure 14: Illustration of six runs with 50 nm microbeads. The x-axis show particle size in nm, and the y-axis show the concentration of MPs per mL. A comparison of graphs shows that NTA is capable of finding approximately the same size for every run although the concentration is not the same. See raw data in appendix A.3.**

A comparison of the mode of each graph, which is where each graph peaks, and their corresponding standard deviations shows, that there are only minor differences between each run due to the large confidence intervals (CIs). The large CIs can also be used as an indication of the broad distribution of the particle sizes. Table 3 list the mode of each run, the corresponding SD values and the CI values for each run obtained by the NTA 2.1 Analytical Software.

**Table 3: Table of mean particle size, mode and standard deviation of 50 nm monodisperse polystyrene microbeads from NTA measurements. The high mode may be due to the detection limit of NTA of ~50 nm.**

| Run | Mean particle size | Mode | Standard deviation |
|---|---|---|---|
| **1** | 80 | 73 | ± 20 |
| **2** | 88 | 83 | ± 25 |
| **3** | 85 | 75 | ± 23 |
| **4** | 69 | 66 | ± 19 |
| **5** | 98 | 80 | ± 33 |
| **6** | 103 | 87 | ± 34 |

None of the mean particle sizes the six runs lies near the certified mean diameter given by the manufacturer (46 nm ± 2 nm), which is approximately 50 nm for microbeads, and since the CIs overlap greatly there is no difference between the six runs. The broad CIs indicate a broad range of particle sizes.

Five repeats with 100 nm microbeads were conducted. In figure 15 are the results from the five runs illustrated.

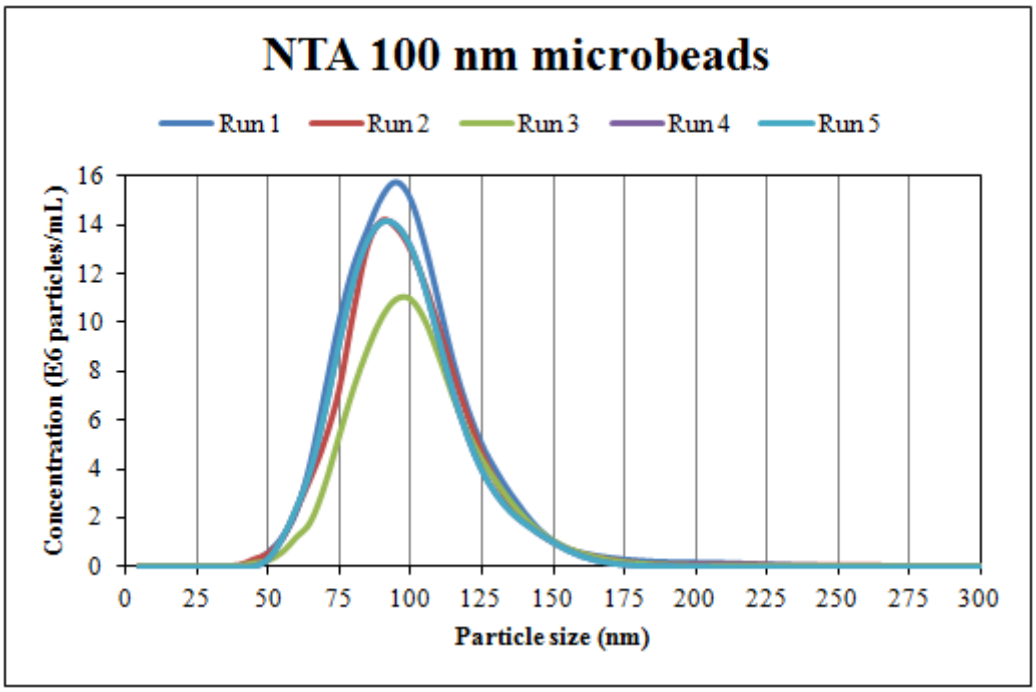


**Figure 15: Illustration of five runs with 100 nm microbeads. The x-axis shows particle size in nm, and the y-axis shows concentration of $10^6$ of MPs per mL. A comparison of the graphs shows that NTA is capable of finding approximately the same size for every run although the concentration is not the same. See raw data in appendix A.3.**

Figure 15 illustrates that the mode of each runs is approximately the same, but there is a differences in the measured concentrations. The particle size distributions are the same for all five runs. A comparison mode and its corresponding SDs are given in table 4. The table lists the mode particle sizes, the corresponding SD values and the CI values for each run obtained by the NTA 2.1 Analytical Software.

**Table 4: List of mean particle size, mode and standard deviation of 100 nm monodisperse polystyrene microbeads from NTA measurements. The means and modes are found close to the expected values.**

| Run | Mean particle size | Mode | Standard deviation |
|---|---|---|---|
| **1** | 98 | 95 | ± 23 |
| **2** | 98 | 91 | ± 21 |
| **3** | 101 | 98 | ± 21 |
| **4** | 96 | 92 | ± 21 |
| **5** | 96 | 92 | ± 21 |

Both the means and modes of the five runs are close to the certified mean diameter given by the manufacturer (102 nm ± 3 nm), though a few still fall outside. The broad CIs is indicative of a broad range of MP sizes in the samples.

Four repeats with 200 nm microbeads were conducted. Illustrated in figure 16 are the results from the four runs.

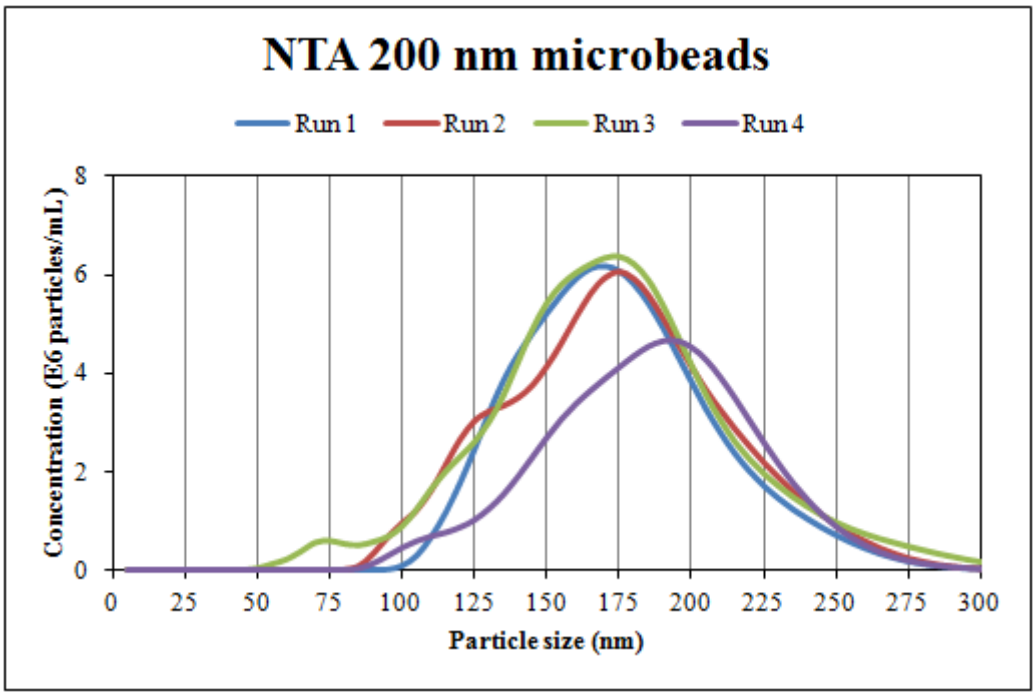


**Figure 16: Illustration of four runs with 200 nm microbeads. The x-axis shows particle size in nm, and the y-axis shows concentration of $10^6$ of MPs per mL. A comparison of the graphs shows that NTA is capable of finding approximately the same size for every run although the concentration is not the same. See raw data in appendix A.3.**

Figure 16 illustrates that NTA measures 200 nm microbeads to have a size of ~175 nm, except for run 4, which displays a diameter close to 200 nm. The particle size distributions of runs 1, 2, and 3 are almost the same, whereas run 4 differs slightly. Table 5 provides a comparison of the mean particle sizes, modes and the calculated SDs from the NTA 2.1 Analysis Software.

**Table 5: List of mean particle size, mode and standard deviation of 200 nm monodisperse polystyrene microbeads from NTA measurements. The means and modes are not found close to the expected values.**

| Run | Mean particle size | Mode | Standard deviation |
|---|---|---|---|
| **1** | 175 | 169 | ± 37 |
| **2** | 174 | 175 | ± 37 |
| **3** | 172 | 174 | ± 42 |
| **4** | 185 | 193 | ± 35 |

When comparing to the certified mean diameter and CI provided by the manufacturer (203 ± 5 nm) a major difference is found. The CIs overlap for all four runs, thus no difference between these run can be found.

Figure 17 illustrates mean results of the measurements on the three different sizes. The means are found by the use of the results shown above. The mean diameter is used as an indication of precision and accuracy of the method.

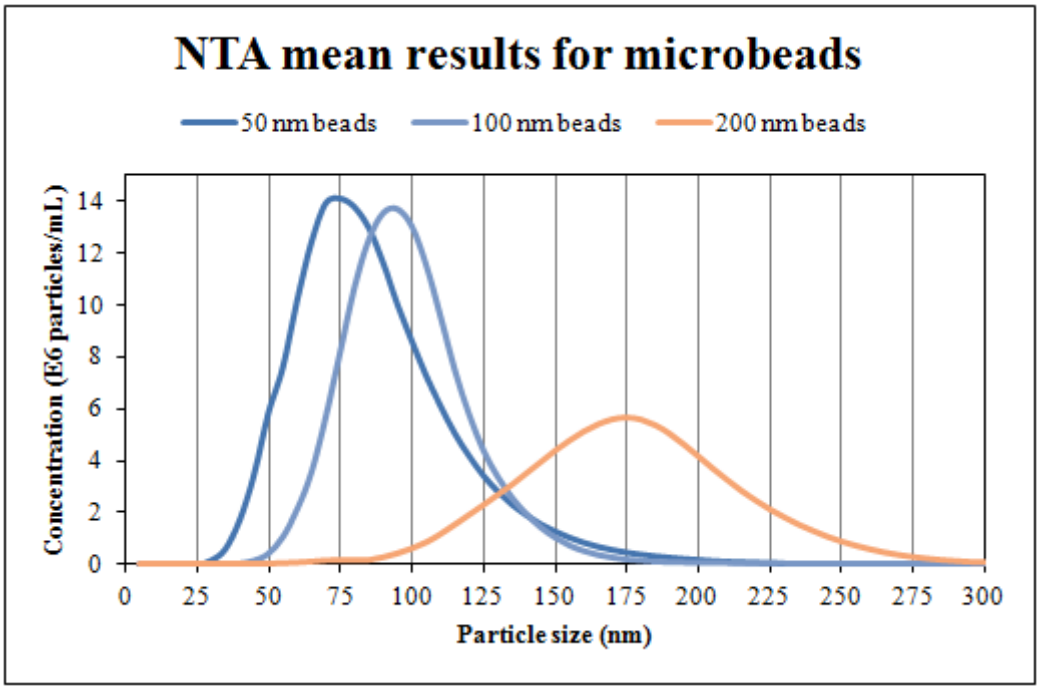


**Figure 17: Illustration of the mean results based on measurements of 50, 100, and 200 nm microbeads. The x-axis shows particle size in nm, and the y-axis shows concentration of $10^6$ of MPs per mL. The mean diameter measured for 50 nm microbeads is found to be 75 nm, the mean diameter measured for 100 nm microbeads is found to be 98, and the mean diameter measured for 200 nm microbeads is found to be 179 nm. See raw data in appendix A.3.**

The mean diameters of microbeads of sizes 50 nm, 100 nm, and 200 nm were measured by NTA to be 77.5, 92, and 178.75 nm, respectively. Coefficient variations based on the measured mean diameters and mean SDs have been calculated for each size to clarify the capability of NTA to reproduce a result.
For 50 nm microbeads the CV % was calculated to be 8.81 %, for 100 nm microbeads the CV % was 2.74 %, and for 200 nm microbeads the CV % was 11.09 %.

### 4.4.2 Dynamic Light Scattering

In order to investigate the accuracy and capability to reproduce a result, polystyrene latex microbeads were analysed by DLS. Microbeads of 50 nm, 100nm, and 200 nm were used. The microbeads were diluted in DPBS in concentrations suitable for measurement on DLS. DLS requires concentrations in the range of $10^{8}$-$10^{12}$ particles/mL [Filipe *et al.*, 2010].

Five repeats with 50 nm microbeads were conducted. Illustrated in figure 18 are the results from the five runs.

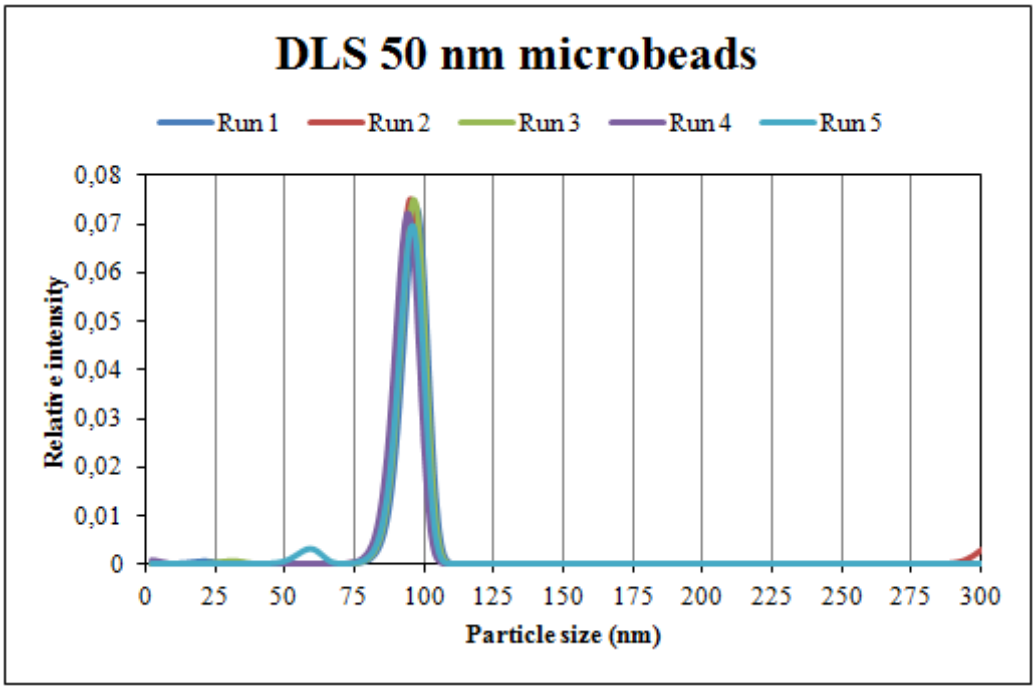


**Figure 18: Illustration of five runs with 50 nm microbeads. The x-axis shows particle size in nm, and the y-axis shows relative intensity of light. A comparison of the graphs shows that DLS is capable of finding the same size for every run. However, the size measured is far from the expected 50 nm. See raw data in appendix A.3.**

Figure 18 illustrates that DLS measures 50 nm microbeads to have a size much higher than the expected size. The particle size distributions are for all five runs almost the same. All of the modes were read directly from the graphs to be 95 nm. When the data is transformed from the CorrelatorComms Software into the data analysis program, it seems as if the data is changed. In figure 19 is a screen shot of one result obtained in the CorrelatorComms from measurement on 50 nm microbeads shown.

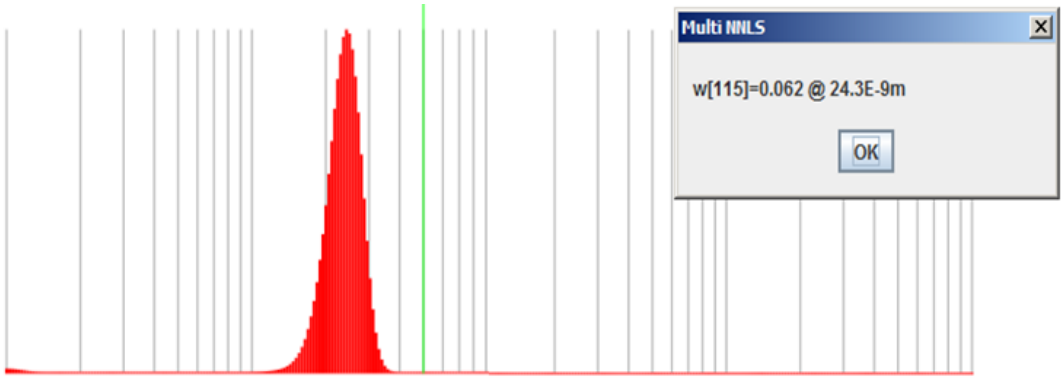


**Figure 19: Illustration of a screen shot of a result obtained using CorrelatorComms Software to analyse measurement of 50 nm microbeads. The box on the right of the figure displays a value describing the result. 0.062 is indicative of the relative intensity measured for the sample, and 24.9E-9m is the mean radius of the measured particle sizes.**

The first value, 0.062, indicates the relative intensity and the second value, 24.3E-9m, is the mean radius measured for the particles in the sample. Compared to the results obtained in the data analysis program, where the mode was measured to be 95 nm, the measured diameter in the CorrelatorComms is 48.6 nm, which is very close to the certified mean diameter provided by the manufacturer (46 nm ± 2 nm).

Five repeats with 100 nm microbeads were conducted, which is illustrated in figure 20.

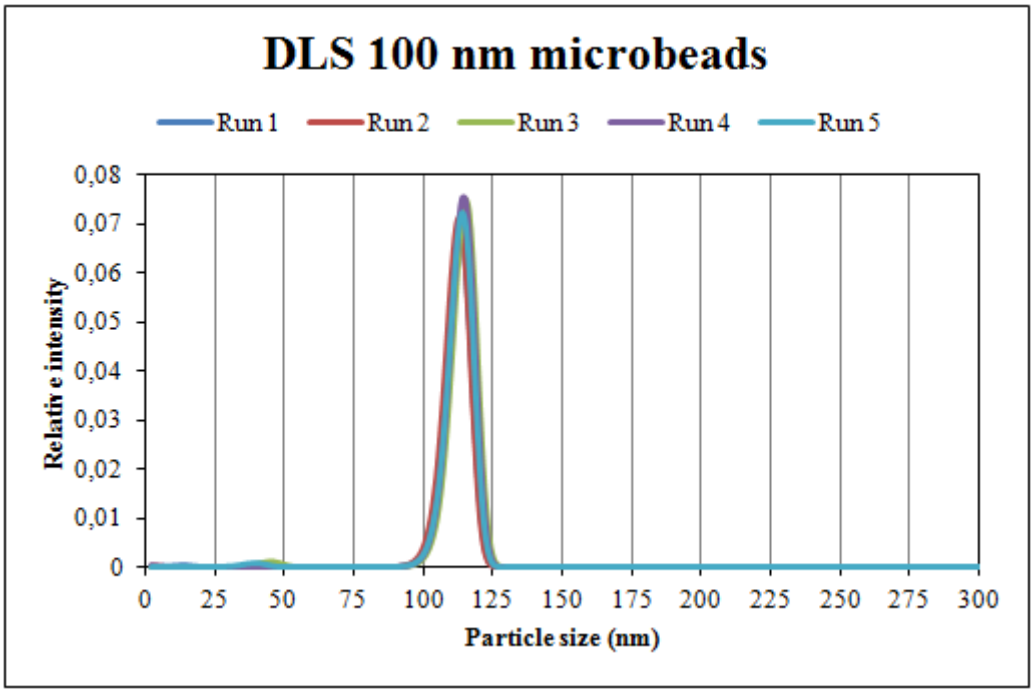


**Figure 20: Illustration of five runs with 100 nm microbeads. The x-axis shows particle size in nm, and the y-axis shows relative intensity of light. A comparison of the graphs shows that DLS is capable of finding the same size for every run. Furthermore, the measured sizes are close to the expected diameters. See raw data in appendix A.3.**

Figure 20 illustrates that DLS measures 100 nm microbeads to have a size near the expected size. The particle size distributions are for all five repeats almost the same. All of the modes were read directly from the graphs to be 113 nm. Again, the data changes as it is transformed from the CorrelatorComms Software into the data analysis program. In figure 21 is a screen shot of one result obtained in the CorrelatorComms from measurement on 100 nm microbeads shown.

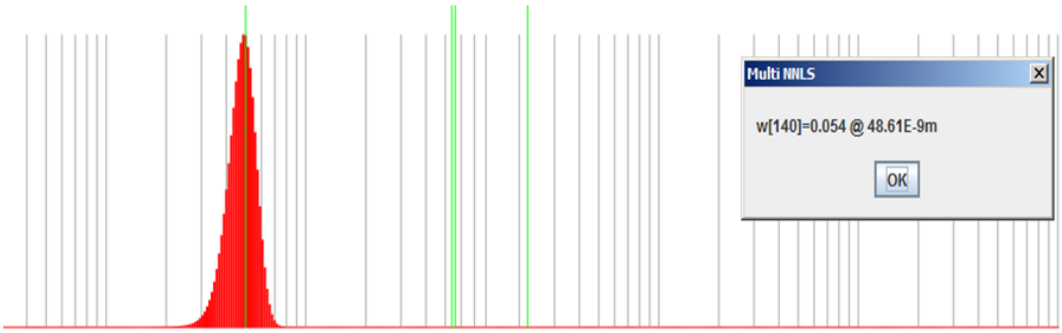


**Figure 21: Illustration of a screen shot of a result obtained using CorrelatorComms Software to analyse measurement of 100 nm microbeads. The box on the right of the figure displays a value describing the result. 0.054 is indicative of the relative intensity measured for the sample, and 48.61E-9m is the mean radius of the measured particle sizes.**

The relative intensity was 0.054 and the mean radius was determined to be 48.61E-9m. Compared to the results obtained in the data analysis program, where the mode was measured to be 113 nm, the measured diameter in the CorrelatorComms was 97.22 nm, which is very close to the certified mean diameter provided by the manufacturer (102 nm ± 3 nm).

Four repeats with 200 nm microbeads were conducted. Illustrated in figure 22 are the results from the four runs.

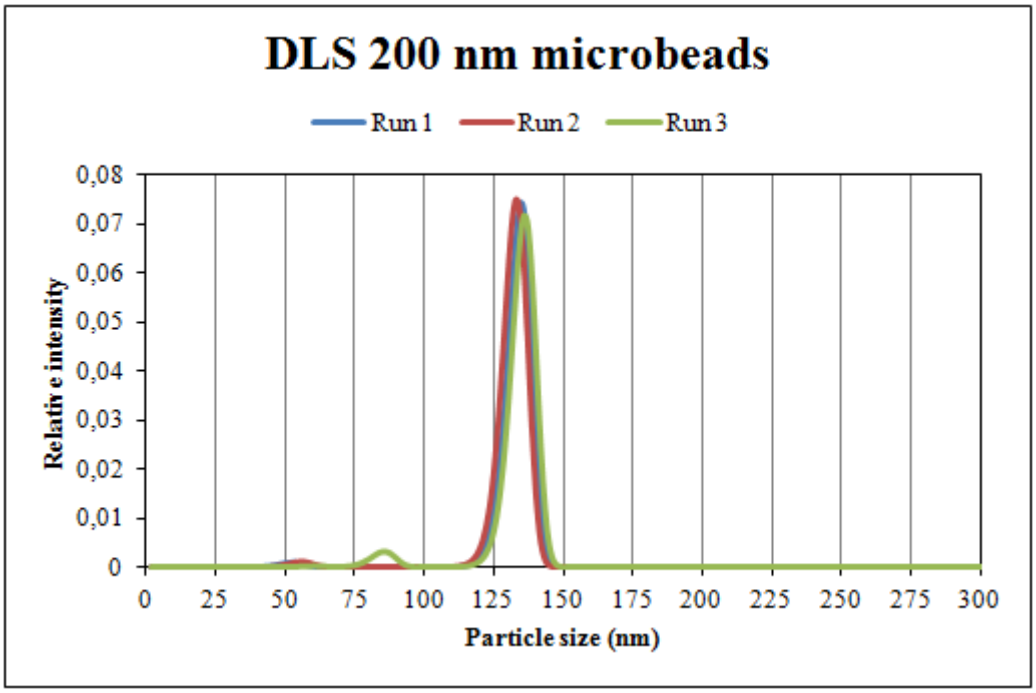


**Figure 22: Illustration of four runs with 200 nm microbeads. The x-axis shows particle size in nm, and the y-axis shows relative intensity of light. A comparison of the graphs shows that DLS is capable of finding the same size for every run. However, the size measured is far from the expected 200 nm. See raw data in appendix A.3.**

The DLS measures 200 nm microbeads diameters that are far from the expected diameter. Again, the particle size distributions are for all five runs almost the same. All of the modes were read directly from the graph to be 134 nm. Again, the data changes as it is transformed from the CorrelatorComms Software into the data analysis program. In figure 23 is a screen shot of one result obtained in the CorrelatorComms from measurement on 200 nm microbeads.

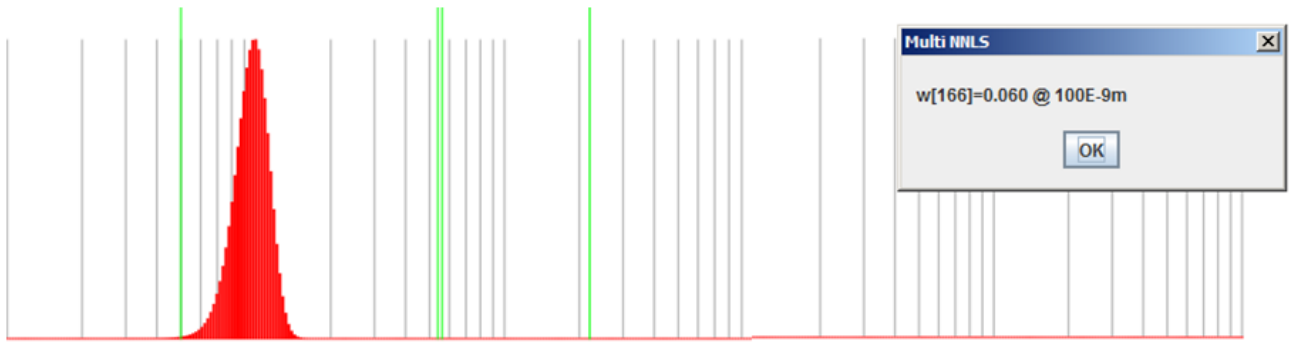


**Figure 23: Illustration of a screen shot of a result obtained using CorrelatorComms Software to analyse measurement of 100 nm microbeads. The box on the right of the figure displays a value describing the result. 0.060 is indicative of the relative intensity measured for the sample, and 100E-9m is the mean radius of the measured particle sizes.**

The relative intensity was 0.060 and the mean radius was determined to be 100E-9m. Compared to the results obtained in the data analysis program, where the mode was measured to 134 nm, the measured diameter in the CorrelatorComms is 200 nm, which is very close to the certified mean diameter provided by the manufacturer (203 nm ± 5 nm).

Figure 24 illustrates the mean results of the measurements on the three different sizes. The means are found by the use of the results shown above. The mean diameter is used as an indication of precision and accuracy of the method.

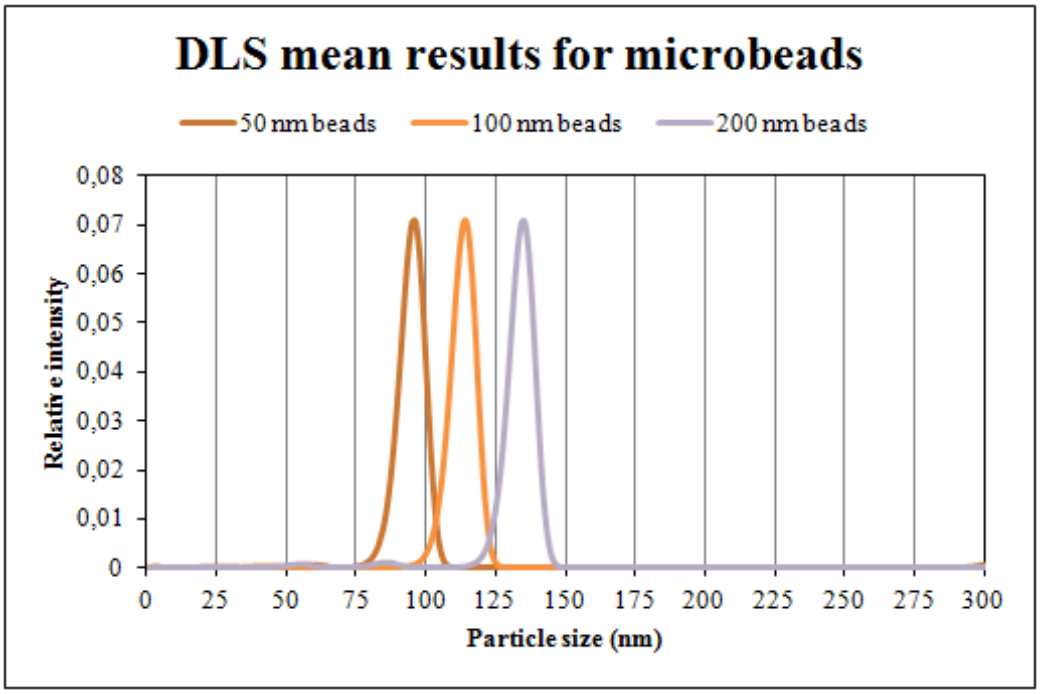


**Figure 24: Illustration of the mean results based on measurements of 50, 100, and 200 nm microbeads based on the results found after the transformation of data into Microsoft Excel. The x-axis shows particle size in nm, and the y-axis shows relative intensity of light. The mean diameters are read directly from the graphs, and for 50 nm microbeads is found to be 95 nm, the mean diameter for 100 nm microbeads is found to be 113, and the mean diameter for 200 nm microbeads is found to be 134 nm. See raw data in appendix A.3.**

The mean diameters of the three microbead sizes were measured to be 95, 113, and 134. The CV % of all three measured sizes was below 2 %. The CV % for the 50 nm microbead measurements were calculated to be 1.59 %, for the 100 nm microbead measurements the CV % were calculated to be 0.74 %, and the CV % for the 200 nm microbead measurements was calculated to be 1.13 %.

## 4.5 Discussion

The inter-run variation experiment was conducted in order to determine the precision and accuracy of both NTA and DLS.

The experiment showed that NTA is capable of reproducing a result, although great variation between the measured size and concentrations was found for all experiments. The results obtained for the 50 nm microbeads showed that NTA measures the size to be higher than that provided by the manufacturer. The mean measured particle size for 50 nm microbeads was found to be 77.5 nm. This may be due to the detection limit of NTA of ~50 nm. On the other hand, the result is still reproducible, since the calculated CV % was only 8.81 %. This means that when measuring 50 nm microbeads on the NTA, it can be expected than the mean diameter size will be found to be ~77.5 nm with a variation of ~9 %. In contrast, the measurements on 100

nm microbeads showed that NTA is both capable of reproducing a result and shows great accuracy when measuring particles with sizes close to 100 nm. The mean diameter was measure to be 92 with a variation of only 2.74 %. The 200 nm microbeads were measured to have a mean diameter of 178.75, thus NTA measures 200 nm microbeads to have a smaller diameter than the size provided by the manufacturer. The high CIs found for all three sizes are very broad. Therefore, no conclusive difference between the different runs will be found.

The investigation of the reproducibility and accuracy of measurements by NTA have been conducted by other researches. Filipe and colleagues [Filipe *et al.*, 2010] have also evaluated the accuracy and reproducibility of NTA. Microbeads in five different sizes were measured and NTA was proved to have great sizing accuracy and relatively narrow distributions. Comparing this to the results obtained in the present study, similarities are found. The mean particle sizes were found close to the particle size provided by the manufacturer, except for the 50 nm microbeads. Furthermore, Dragovic and colleagues [Dragovic *et al.*, 2011] determined the capability of NTA to measure particle size and concentration. It was found that NTA can both resolve and accurately measure different particle sizes, such as the above presented experiment have proven. In addition, NTA was proven by Dragovic and colleagues [Dragovic *et al.*, 2011] to be able to measure different particle sizes in the same dilution. 100 nm microbeads and 300 nm microbeads were mixed in the same sample and measured. Thus, NTA is capable of differentiating between different particle sizes in a solution, such as a biological sample.

The experiment with the DLS device showed that DLS is capable of detecting correct particle sizes, but a difficulty was experienced when transforming data from the DLS analysis software to Microsoft Excel for statistical analysis and comparison of repeats. The lack of capability to detect the correct particle size is probably due to the fact that the device and analysis software are prototypes and the further development will overcome this limitation in the future. The DLS analysis software measured 50 nm microbeads to have a diameter of ~48 nm, whereas the transformed data shows a mean diameter of 95 nm, but this incorrect size was consistent for all measurements, since a extremely low CV % was calculated to by only 1.59 %. Therefore, DLS is considered to be capable of reproducing a result with less than 2% variation in between runs. The same was found for measurements on 100 nm microbeads and 200 nm microbeads. The mean diameter sizes for 100 nm and 200 nm microbeads were by the DLS analysis software found to be 97.22 and 200 nm, respectively, whereas the transformed data display mean diameters of 113 and 134 nm, respectively.

Filipe and colleagues [Filipe *et al.*, 2010] also investigated the ability of a DLS device to measure particle sizes. For monodisperse samples, the DLS device was capable of finding all five sizes investigated, but the result appeared with broad particle size distribution, which is contrary to the results obtained in the above presented experiment, where all results were displayed with very narrow particle size distributions. Furthermore, Filipe and colleagues [Filipe *et al.*, 2010] investigated whether DLS was capable of differentiating between two different sizes in the same sample, and this was investigated in several different concentration ratios. The results showed that DLS rather measures the large particles than the smaller ones up to a concentration ratio of 150:1 with the smaller particles as the major content. This result provides evidence that DLS may not be able to differentiate between different sizes in a solution containing several different particle sizes, such as biological samples. This problem will be considered in the following experiments.

DLS therefore display great reproducibility when looking at the transformed results and great accuracy when looking at the results from the DLS analysis software. The shown inability of DLS to measure different sizes in the same solution will be problematic when investigating biological samples.

# Part 5: Experiment 2

# Dilution experiment

## 5.1 Aim of Experiment

The aim is to find the maximum limit of detection of tracks by NTA. Furthermore, it will provide a basis for expected intensity measured by the DLS device of healthy samples.

## 5.2 Materials

Blood samples were kindly provided by three healthy volunteers and one diabetic volunteer, which gave informed consent. The donors were between 27 and 42 years old (50 % women, 50 % men). The healthy volunteers were not taking any medication that might interfere with the result. Blood samples were drawn directly in the laboratory at the same time in the morning. Fasting was not mandatory. Blood samples were drawn from the antecubital vein with a 21-gauge needle and collected in three 9 mL citrate glasses containing 0.109 M citrate (Vacuette®; Greiner Bio-One, Kremsmünster, Austria). The first few millilitres were discarded to avoid artefacts, which can be generated by contact phase activation.
NTA measurements were conducted by the use of a NanoSight LM10-HS device (NanoSight Ltd., Amesbury, United Kingdom), and the used software was NTA 2.1 analytical software (NanoSight Ltd., Amesbury, United Kingdom). DLS measurements were conducted by the use of a prototype of a ThromboLUX device (Light Integra Technology, Vancouver, Canada), and the analysis software were FLEX02-12BD (measurement software) and CorrelatorComms 1.141 (analysis software). DPBS was used as diluents.

## 5.3 Methods

### 5.3.1 Sample Preparation

The blood samples were centrifuged to separate blood cells and plasma with the intention to produce platelet-free-plasma (PFP), according to the protocol in appendix A.2. The blood samples were first centrifuged at 2,500g for 15 minutes at room temperature (RT). The supernatant was transferred into a 15 mL centrifugation tube. Aspiration of plasma was stopped approximately one centimetre above the buffy coat. The resultant platelet-poor-plasma (PPP) was then centrifuged again at 2,500g for 15 minutes at RT. The resultant platelet-free-plasma (PFP) was transferred to 1.5 mL microtubes, each containing 100 µL of plasma sample. Aspiration was stopped approximately 100 µL above the bottom of the tube. One aliquot was used for the experiment, whereas the remaining aliquots were frozen and used for future experiments. Plasma samples were diluted in DPBS in 1.5 mL microtubes in five different systematic concentrations as follows: 1 µL plasma sample in 1000 µL DPBS, 2 µL plasma sample in 1000 µL DPBS, 3 µL plasma sample in 1000 µL DPBS, 4 µL plasma sample in 1000 µL DPBS, and finally 5 µL plasma sample in 1000 µL DPBS.

### 5.3.2 Nanoparticle Tracking Analysis

All experiments with plasma samples were conducted as described in the protocol in appendix A.2. Prior to measurement of plasma samples, the thumbprint was located by the use of a blank sample, and microbeads prepared as in ‘Experiment 1’ were measured to check the instrument settings. The blank sample was injected into the sample chamber by the use of 1 mL sterile syringes (Becton Dickinson, Madrid, Spain) until it reached the tip of the sample chamber output. The thumbprint was located along with the preferred measuring area and the appropriate camera and parameter settings were found, according to protocol in appendix A.2. The first plasma sample was then loaded by injecting the sample with a 1 mL sterile syringe and measured. Each syringe can contain a total of three samples, thus triplicates of each sample was conducted. The sample chamber was washed after each sample by 70 % EtOH. The samples were measured in the ‘single shutter and gain mode’ for 60 seconds. The temperature of each run was measured by a temperature measuring device specifically developed to the sample chamber. The NTA 2.1 Analytical Software was used for capturing and analysing the data.

### 5.3.3 Dynamic Light Scattering

All experiments with plasma samples were conducted as described in the protocol in appendix A.2. Prior to measurement of plasma samples, the intensity setting were checked using a blank sample and microbeads in the suitable concentrations found in 'Experiment 1', according to protocol in appendix A.2. A total of 40 µL of each dilution was used to each measurement, which was prepared in 1.5 mL microtubes. The blank sample was measured, and when a satisfactory intensity was observed, the blank sample was removed from the sample chamber. The microbeads were then measured to verify the intensity. The plasma samples were then measured in triplicates. The samples were measured for 240 seconds, and all experiments were conducted at room temperature. The CorrelatorComms software was used to analyse data obtained by the FLEX02-12BD software.

### 5.3.4 Statistical Analysis

The observed differences in MP concentration and a calculated area under curve (AUC) for each result were used to describe the results. Mean results were calculated for each sample and dilution. All statistics were evaluated using Microsoft Excel.

## 5.4 Results

### 5.4.1 Nanoparticle Tracking Analysis

In order to investigate the maximum detection limit of tracks by NTA, plasma samples in different concentrations were analysed on NTA. Both healthy plasma samples and one diseased sample were used. Figure 25 illustrates the results obtained from the NTA measurements on the healthy plasma samples.

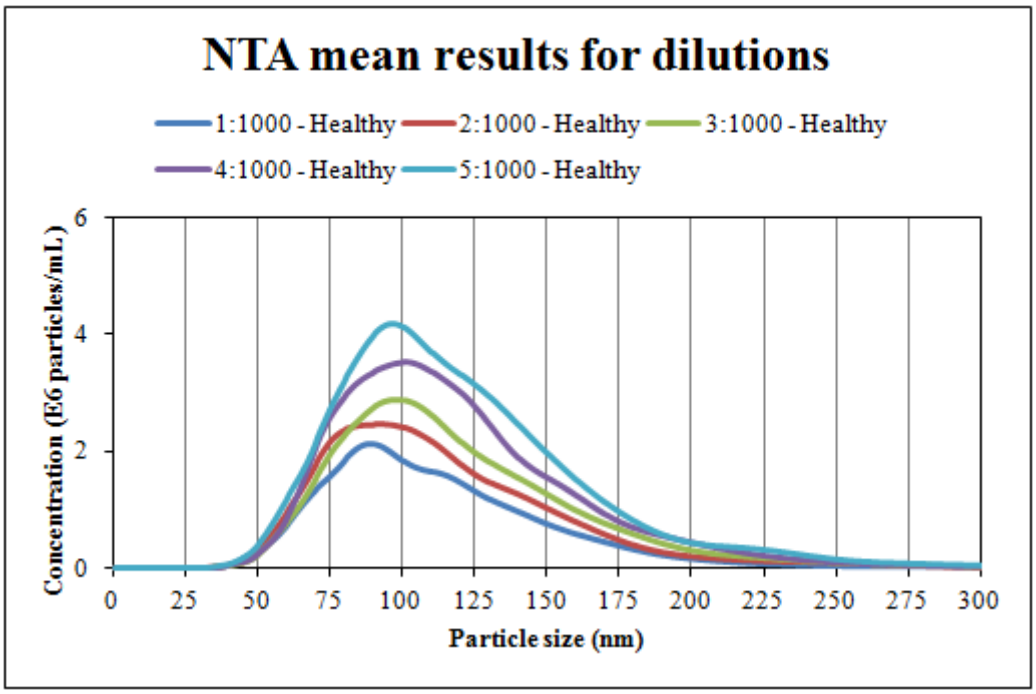


**Figure 25: Illustration of results obtained for the plasma samples from healthy donors in the dilution experiment, where concentration increases as the dilution decreased. The x-axis shows particle size in nm, and the y-axis shows concentration of $10^6$ of MPs per mL. The size distributions for the five graphs are the same, and they all peak close to 100 nm. See raw data in appendix A.4.**

The size distributions of the five dilutions are the same, and therefore the AUC can be compared. The AUC calculated for the 1:1000 dilution resulted in 163.62. When the amount of sample added to the dilution is increased to 2:1000, the AUC increases to 209.43, thus the concentration increases approximately one quar-

ter. A further increase in the amount of sample added to the dilution to a final dilution of 3:1000 resulted in an AUC of 240.49, thus the concentration does not increase one quarter every time. The AUC for the 4:1000 and 5:1000 dilutions were calculated to be 304.30 and 356.48, respectively. Based on these results, a detection limit for the NTA was not obtained. The proportional correlation between the dilutions and the AUC shows a linear tendency, as illustrated in figure 26. The more amount of plasma sample in the solution results in a larger AUC.

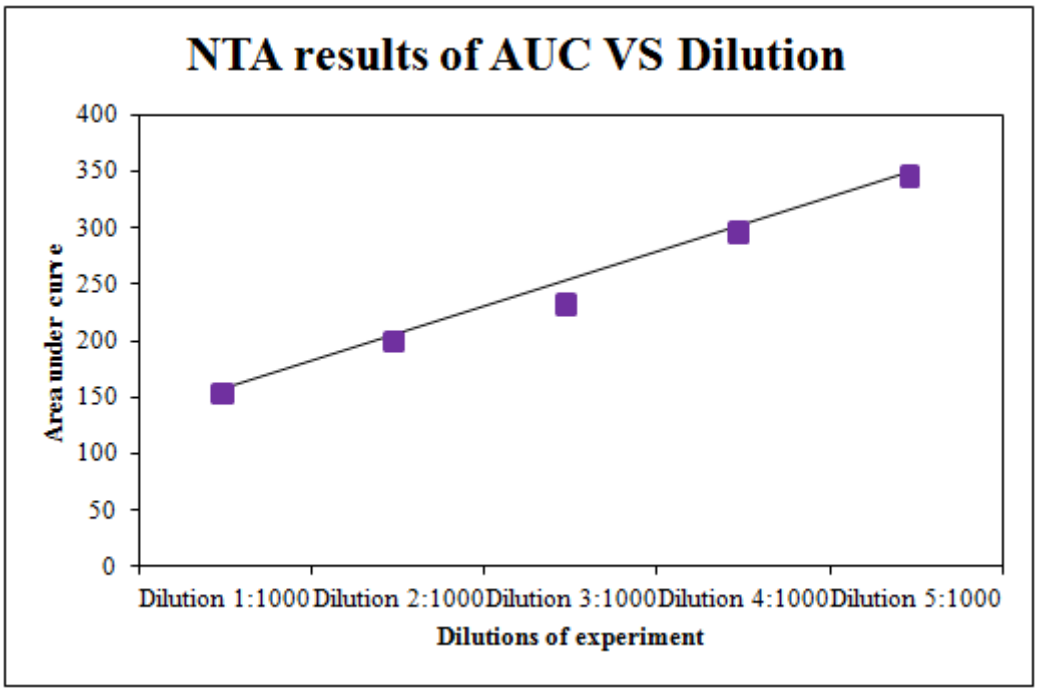


**Figure 26: Illustration of the proportional correlation between the dilutions and the calculated area under the curve (AUC) for each measurement. The x-axis shows each measured dilution. The y-axis shows the values for the AUC. See raw data in appendix A.4.**

The detection limit was found by analysis of the plasma sample collected from the diabetic patient due to the high amount of MPs in the plasma sample. Again, five dilutions were prepared, but the detection limit was found when testing the 4:1000 dilution, thus no final result could be obtained for this dilution and the 5:1000 dilution. The results obtained for the diabetic plasma sample is illustrated in figure 27. The AUC obtained for the three dilutions were 916.20, 985.27, and 1232.06, respectively. The concentration does not increase between the 1:1000 and 2:1000 dilutions, whereas the 3:1000 dilution does display an increase in concentration of MPs.
The difference in concentration between the healthy plasma samples and the diabetic plasma sample provides evidence for increased concentration of MPs in patient suffering from diabetes.

The results obtained from both the experiments on the healthy plasma samples and the diabetic plasma sample, which is shown in figures 25, 26, and 27, lays the ground for the most suitable dilution of all future experiments on plasma samples. The 2:1000 dilution has been chosen.

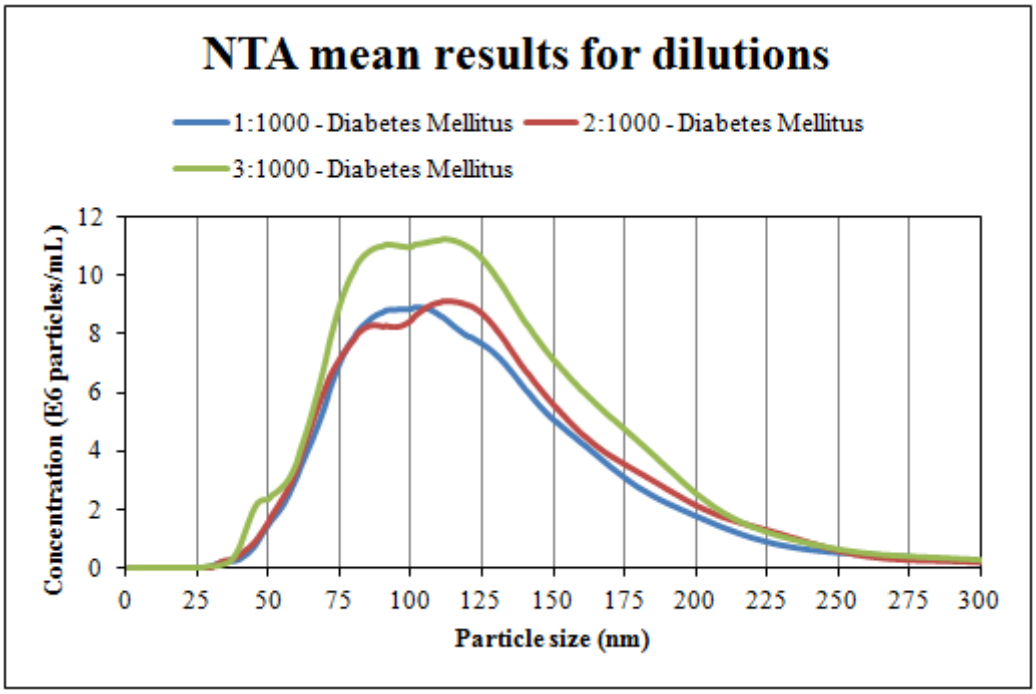


**Figure 27: Illustration of results obtained for the plasma sample from the donor suffering from diabetes in the dilution experiment, where concentration increases as the dilution decreases. The x-axis shows particle size in nm, and the y-axis shows concentration of $10^6$ of MPs per mL. The size distributions for the five graphs are the same, and they all peak close to 100 nm. The three resultant graphs display the same size distributions. See raw data in appendix A.4.**

### 5.4.2 Dynamic Light Scattering

In order to investigate the expected intensity measured by DLS, plasma samples from three different donors and a diabetic patient were analysed. Plasma sample 1 was run as a pure sample. The intensity was measured to be nearly as low as the intensity measured for the blank sample and therefore, no dilution of plasma samples is needed when measuring plasma samples on DLS. In the figure 28, the results from the measurement of the pure plasma samples are illustrated. Peaks below 0.01 in relative intensity are considered background noise.

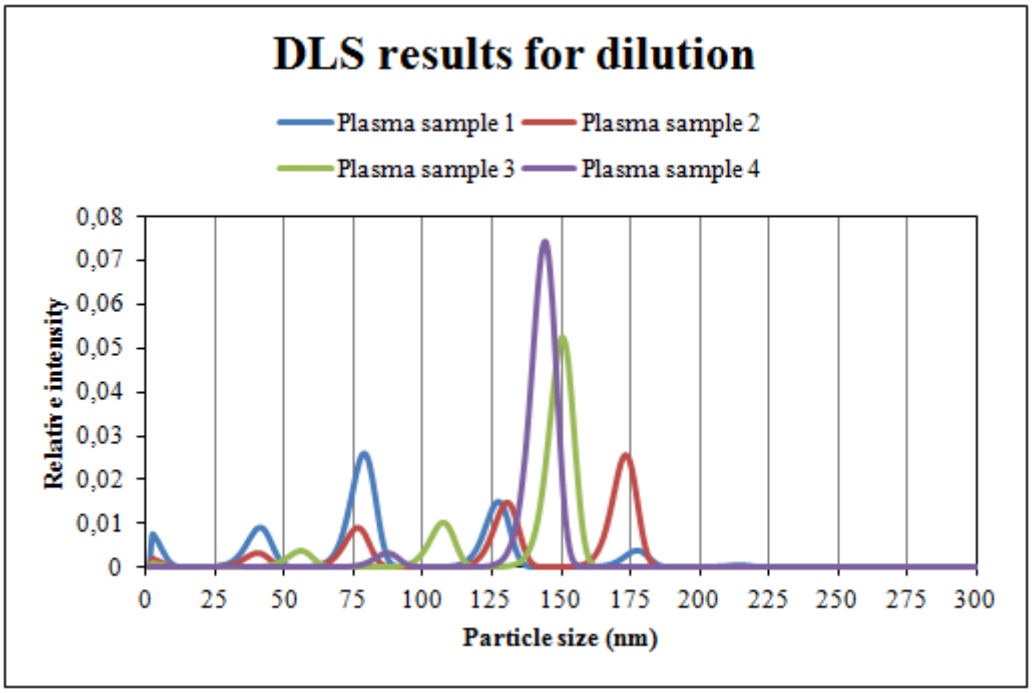


**Figure 28: Illustration of the results obtained for three plasma samples collected from healthy donors (Plasma samples 1, 2, and 3) and one plasma sample from a patient suffering from diabetes (Plasma sample 4). The x-axis shows particle size in nm, and the y-axis shows relative intensity of light. See raw data in appendix A.4.**

In figure 28, Plasma sample 2 appeared as Plasma sample 1, but with a shift in particle size, whereas Plasma sample 3 displayed a higher intensity than both Plasma sample 1 and 2. Plasma sample 4, on the other hand, displays an even higher intensity, which supports the result obtained by NTA. Future experiments on plasma samples will thus be conducted on pure plasma. Due to the variations of particle size distributions of plasma samples, the AUC was not calculated.

## 5.5 Discussion

The dilution experiment was conducted in order to determine the detection limit of NTA and the expected intensity of measurements of plasma sample by DLS.

The experiment with healthy plasma samples on the NTA device clearly shows an increase in particle concentration when the amount of added plasma sample to the DPBS solution increases, which was expected. This increase was found to be proportional as illustrated in figure 26. A linear tendency was found for the healthy samples, and therefore it was determined not to proceed with other dilutions. The diabetic sample was measured to find a suitable dilution that could be applied to all plasma samples. A high concentration of MPs was observed for all dilutions tested, and the dilution containing 4 µL of the diabetic plasma sample in 1000 µL DPBS displayed a concentration of MPs too high to be measured by NTA. Based on the results obtained on the diabetic plasma sample the suitable dilution for investigation of particle size distribution and concentration in plasma samples was determined to be 2 µL of plasma sample in 1000 µL DPBS, but this

may be varied for samples with even higher MP content, but since a linear relationship between measured particle concentration and dilution was found, the dilution can be extrapolated back to the original centration. This dilution should provide clear results for healthy plasma samples as well as diseased plasma samples. Therefore, this dilution will be used in future experiments of this project.

Furthermore, it is known from the inventors of NanoSight that a certain amount of MPs must be present in the sample for the result to of statistical value. Therefore, no lower dilutions were evaluated. The diluted sample must not contain less than $10^6$ MPs/mL, and the suitable concentrations are found the range of $10^7$-$10^9$ MPs/mL [Filipe *et al.*, 2010].

Only one other research group have investigated the effects of increasing the concentration of MPs. Dragovic and colleagues [Dragovic *et al.*, 2011] conducted their experiments on microbeads and compared the actual concentration of MPs with the measured concentration of MPs by NTA. A linear proportional correlation was also found by Dragovic and colleagues [Dragovic *et al.*, 2011], thus the results obtained in the present experiment confirms their observations.

The experiment conducted with the use of the DLS device showed from the first sample that no dilution was necessary for the measurement of the MP content. Xu and colleagues [Xu *et al.*, 2010], who wished to provide evidence of the potential of ThromboLUX to measure MPs in plasma samples, conducted their experiment on pure samples as well. Therefore, the results obtained in the present study confirm prior experiments and pure plasma samples will be used for the future experiments of this project.

# Part 6: Experiment 3

# Fresh-frozen experiment

## 6.1 Aim of Experiment

The aim is to show that there is no difference in the measured particle size or distribution between fresh and frozen samples.

## 6.2 Materials

Healthy plasma samples obtained for 'Experiment 1' were also used for this experiment. The extra aliquots from 'Experiment 1' were frozen for 1 day, 7 days, 15 days, and 40 days, and they were then re-measured. NTA measurements were conducted by the use of a NanoSight LM10-HS device (NanoSight Ltd., Amesbury, United Kingdom), and the used software was NTA 2.1 analytical software (NanoSight Ltd., Amesbury, United Kingdom). DLS measurements were conducted by the use of a prototype of a ThromboLUX device (Light Integra Technology, Vancouver, Canada), and the analysis software were FLEX02-12BD (measurement software) and CorrelatorComms 1.141 (analysis software). DPBS was used as diluents.

## 6.3 Methods

### 6.3.1 Sample Preparation

Based on the results obtained in 'Experiment 1', the plasma samples were diluted for measurement on NTA in DPBS in 1.5 mL microtubes in the following concentration: 2 µL plasma sample in 1000 µL DPBS, and for DLS measurements the plasma sample were kept pure. Frozen plasma samples were thaw in waterbath at 37°C for 3 minutes. The samples were then prepared for measurement.

### 6.3.2 Nanoparticle Tracking Analysis

All experiments with plasma samples were conducted as described in the protocol in appendix A.2. Prior to measurement of plasma samples, the thumbprint was located by the use of a blank sample, and microbeads were measured to check the instrument settings, according to protocol in appendix A.2. The blank sample was injected into the sample chamber by the use of 1 mL sterile syringes (Becton Dickinson, Madrid, Spain) until it reached the tip of the sample chamber output. The thumbprint was located along with the preferred measuring area and the appropriate camera and parameter settings were found, according to protocol in appendix A.2. The first plasma sample was then loaded by injecting the sample with a 1 mL sterile syringe and measured. Each syringe can contain a total of three samples, thus the prepared sample was tested in triplicates. The sample chamber was washed after each sample by 70 % EtOH. The samples were measured in the 'single shutter and gain mode' for 60 seconds. The temperature of each run was measured by a temperature measuring device specifically developed to the sample chamber. The NTA 2.1 Analytical Software was used for capturing and analysing the data.

### 6.3.3 Dynamic Light Scattering

All experiments with plasma samples were conducted as described in the protocol in appendix A.2. Prior to measurement of plasma samples, the intensity setting were checked using a blank sample and microbeads in the suitable concentrations found in 'Experiment 1'. The blank sample was loaded into the sample holder in a disposable plastic capillary (Drummond Scientific Company, Pennsylvania, USA), according to protocol in appendix A.2. The blank sample was measured, and when a satisfactory intensity was observed, the blank sample was removed from the sample chamber. The microbeads were measured to verify the intensity. The samples were then measured in triplicates. The samples were measured for 240 seconds, and all experiments were conducted at room temperature. The CorrelatorComms software was used to analyse data obtained by the FLEX02-12BD software.

### 6.3.4 Statistical Analysis

A calculated AUC for each result was used to describe the results. Mean results were calculated for each sample. Furthermore, the CV % for the samples is calculated by the use of Equation 4. All statistics were evaluated using Microsoft Excel.

## 6.4 Results

### 6.4.1 Nanoparticle Tracking Analysis

In order to investigate the effects of freezing on the concentration of MPs and the particle size distribution, plasma samples were measured as fresh sample and after being frozen for 1, 7, 15, and 40 days at -80°C. Only healthy plasma samples were used for this experiment. Figure 29 illustrates the mean results obtained from triplicates of the NTA measurements.

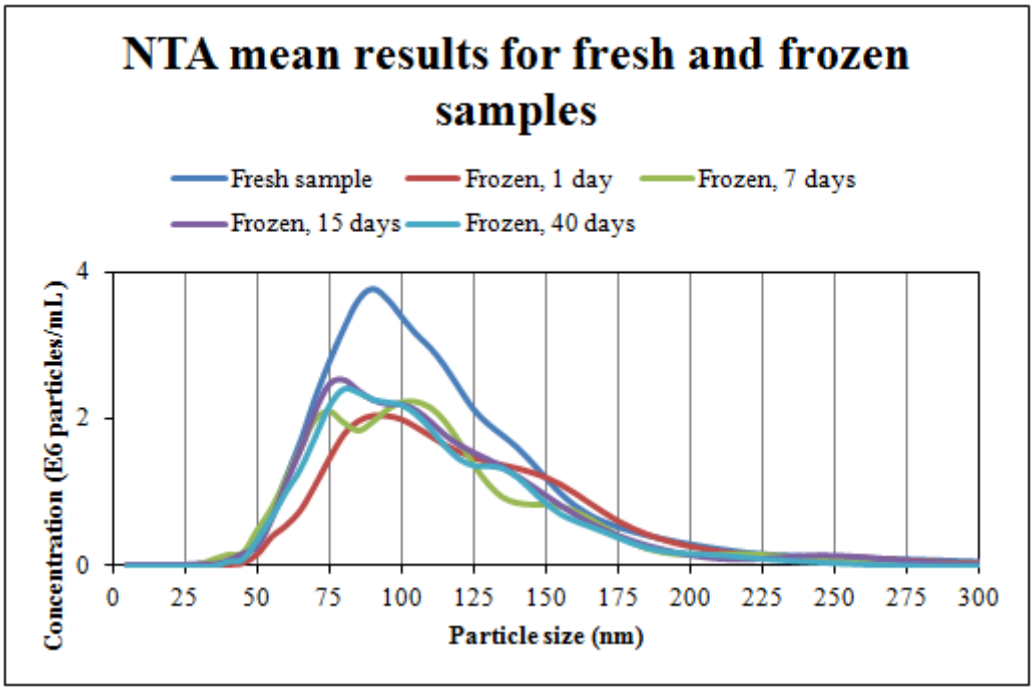


**Figure 29: Illustration of results obtained for the plasma samples from healthy donors in the fresh-frozen experiment. The x-axis shows particle size in nm, and the y-axis shows concentration of $10^6$ of MPs per mL. The size distributions for the five graphs are approximately the same, but the fresh sample display a higher concentration of MPs. See raw data in appendix A.4.**

As illustrated in figure 29, the fresh sample displays a higher concentration of MPs compared to the frozen samples. Furthermore, the fresh sample and the frozen samples display a broad particle size distribution. The concentration of MPs is not the same for the fresh sample compared to the frozen samples, but the size distributions are nearly the same. On the other hand, the different frozen times appear to display MP concentrations that are very close.

The AUC for the fresh sample was calculated to 278.61. The AUCs for the frozen samples was calculated to 186.60 for the sample frozen for one day, 189.95 for the sample frozen for seven days, 202.05 for the sample frozen for 15 days, and 189.94 for the sample frozen for 40 days. The difference between the frozen samples was described using the CV %. A mean AUC for the four graphs was calculated to be 192.14 and the standard deviation was calculated to be 6.79. The CV % was therefore calculated to be 3.54 %.

### 6.4.2 Dynamic Light Scattering

The results obtained with the DLS device are illustrated on figure 30.

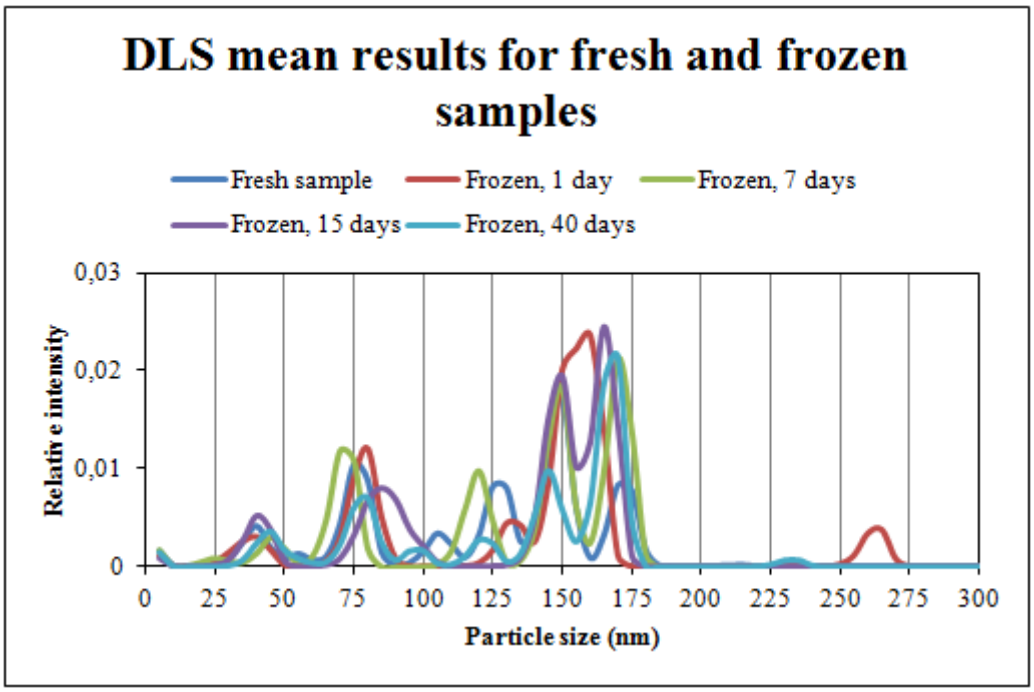


**Figure 30: Illustration of the results obtained for three plasma samples collected from healthy donors. The x-axis shows particle size in nm, and the y-axis shows relative intensity of light. Peaks below 0.01 in relative intensity are considered background noise. See raw data in appendix A.4.**

When considering that the peaks below 0.01 are background noise, only few peaks remained for analysis, see figure 30. These peaks do not display the same size distributions, and therefore the AUCs cannot be compared.

## 6.5 Discussion

The fresh-frozen experiment was conducted in order to investigate the influence of freezing on the particle size distribution and concentration in plasma samples. For the two methods to have clinical potential, storage of samples may be required, and therefore the issue of the stability of MPs during storage was investigated. Healthy plasma samples were first measured as fresh samples after being drawn from the donors in the morning. The samples were then frozen at -80°C for 1, 7, 15, and 40 days.

The NTA measurements showed that the fresh plasma samples contained a broad range of particles of different sizes. The concentration of MPs decreased after the plasma samples have been frozen, but the particle size distribution stayed the same, which may provide some evidence that no aggregation of MPs occur during freezing or thawing of the samples. Furthermore, the decrease seems to be consistent since the AUCs can be expected to only vary with 4 %. No major differences could be found when comparing the frozen samples. In addition, the separation of different particle sizes seems to be improved after freezing, although an explanation to this improved separation is unknown. The minor differences found between the frozen samples could also be due to variation in the measurements in between days. Since the NTA device has very sensitive instrument settings and the fact that it has to be adjusted by the operating person, it may result in biases in the measurements merely due to the fact that it is not measured on the same day at the same time and thus not with completely the same settings.

Sokolova and colleagues [Sokolova *et al.*, 2011] have also investigated the effects of freezing on MPs. Exosomes obtained from a human cell line was measured by NTA after freezing at -20°C. No differences between the measured particle size distributions found from the fresh sample and the frozen samples were found. This indicates that it may be possible to store plasma samples for measurement on NTA at only -20°C instead of at -80°C. Further study on this issue is needed to confirm the results obtained by Sokolova and colleagues.

The DLS data were inconsistent to interpret. There were only few peaks above the limit of measured background noise, and these displayed a great variation in particle size distributions, thus a comparison was not possible. This may be due to the limitation of DLS in measuring several particle sizes in a complex sample. No literature describing the effects of freezing on the measurement of MPs by DLS could be found, but one study has investigated the effects of freezing using other methods for the detection and characterisation of MPs.

Lacroix and colleagues [Lacroix *et al.*, 2011] have investigated the effects of both deep-freezing directly at -80°C and snap-freezing in liquid nitrogen prior to freezing at -80°C on the MP count using flow cytometry, a thrombin generation assay, and a procoagulant phospholipid-dependent clotting time assay. Although the methods differ, the results of either increase or decrease in MP count can be compared to the results obtained in the present study. Lacroix and colleagues observed that neither deep-freezing nor snap-freezing or storage of plasma sample strongly influence the analysis of MPs and MP count.

Therefore, it does not appear that freezing and storage of plasma samples at -80°C affect the particle size distribution, but the concentrations of MPs seem to be affected somehow. It is therefore suggested that all plasma samples are frozen prior to investigation on NTA and DLS devices so a common basis is obtained.

# Part 7: Experiment 4

# Centrifugation experiment

## 7.1 Aim of Experiment

The aim is to show that there is no difference in the measured particle sizes, concentration or distribution however the plasma samples are centrifuged.

## 7.2 Materials

Blood samples were kindly provided by three healthy volunteers, which gave informed consent. The donors were between 25 and 26 years old (33 % women, 67 % men). The healthy volunteers were not taking any medication that could interfere with the result. Blood samples were drawn directly in the laboratory at the same time in the morning. Fasting was not mandatory. Blood samples were drawn from the antecubital vein with a 21-gauge needle and collected in three 9 mL citrate glasses containing 0.109 M citrate (Vacuette®; Greiner Bio-One, Kremsmünster, Austria). The first few millilitres were discarded to avoid artefacts, which can be generated by contact phase activation.

NTA measurements were conducted by the use of a NanoSight LM10-HS device (NanoSight Ltd., Amesbury, United Kingdom), and the used software was NTA 2.1 analytical software (NanoSight Ltd., Amesbury, United Kingdom). DLS measurements were conducted by the use of a prototype of a ThromboLUX device (Light Integra Technology, Vancouver, Canada), and the analysis software were FLEX02-12BD (measurement software) and CorrelatorComms 1.141 (analysis software). DPBS was used as diluents.

## 7.3 Methods

### 7.3.1 Sample Preparation

The blood samples were centrifuged to separate blood cells and plasma with the intention to produce platelet-free-plasma (PFP), according to the protocol in appendix A.2. Three different centrifugation methods were investigated. Centrifugation A centrifuged at 3220g for 20 minutes at 20°C. The supernatant was transferred to 1.5 mL microtubes, each containing 100 µL of platelet-free-plasma (PFP). Aspiration was stopped approximately 1 cm above the buffy coat. In Centrifugation B, the blood samples were centrifuged twice at 2,500g for 15 minutes at room temperature (RT). Between the centrifugations, the supernatant was transferred into a 15 mL centrifugation tube. Aspiration of plasma was stopped approximately one centimetre above the buffy coat. The resultant platelet-free-plasma (PFP) was transferred to 1.5 mL microtubes, each containing 100 µL of plasma sample. Aspiration was stopped approximately 100 µL above the bottom of the tube. In Centrifugation C, the blood samples were centrifuged at 2,500g for 15 minutes at RT. The supernatant was transferred to 2 mL microtubes. Aspiration of plasma was stopped approximately one centimetre above the buffy coat. The resultant platelet-poor-plasma (PPP) was then centrifuged again at 13,000g for 2 minutes at RT. The resultant platelet-free-plasma (PFP) was transferred to 1.5 mL microtubes, each containing 100 µL of plasma sample. Aspiration was stopped approximately 100 µL above the bottom of the tube. Three aliquots from each donor were used for the experiment, whereas the remaining aliquots were frozen and used for future experiments. Based on the results from ‘Experiment 2’, plasma samples for measurement on the NTA device were diluted in DPBS in the following way: 2 µL plasma sample in 1000 µL DPBS. The plasma samples for measurement on the DLS device were kept pure.

### 7.3.2 Nanoparticle Tracking Analysis

All experiments with plasma samples were conducted as described in the protocol in appendix A.2. Prior to measurement of plasma samples, the thumbprint was located by the use of a blank sample, and microbeads were measured to check the instrument settings, according to protocol in appendix A.2. The blank sample was injected into the sample chamber by the use of 1 mL sterile syringes (Becton Dickinson, Madrid, Spain) until it reached the tip of the sample chamber output. The thumbprint was located along with the preferred measuring area and the appropriate camera and parameter settings were found, according to protocol in ap-

pendix A.2. The first plasma sample was then loaded by injecting the sample with a 1 mL sterile syringe and measured. Each syringe can contain a total of three samples, thus triplicates with the same prepared sample can be tested in triplicates. The sample chamber was washed after each sample by 70 % EtOH. The samples were measured in the 'single shutter and gain mode' for 60 seconds. The temperature of each run was measured by a temperature measuring device specifically developed to the sample chamber. The NTA 2.1 Analytical Software was used for capturing and analysing the data.

### 7.3.3 Dynamic Light Scattering

All experiments with plasma samples were conducted as described in the protocol in appendix A.2. Prior to measurement of plasma samples, the intensity setting were checked using a blank sample and microbeads in the suitable concentrations found in 'Experiment 1'. A total of 40 µL of each dilution was used to each measurement, which was prepared in 1.5 mL microtubes. The blank sample was loaded into the sample holder in a disposable plastic capillary (Drummond Scientific Company, Pennsylvania, USA), according to protocol in appendix A.2. The blank sample was measured, and when a satisfactory intensity was observed, the blank sample was removed from the sample chamber. The microbeads were then measured to verify the intensity. The samples were then measured in triplicates. The samples were measured for 240 seconds, and all experiments were conducted at room temperature. The CorrelatorComms software was used to analyse data obtained by the FLEX02-12BD software.

### 7.3.4 Statistical Analysis

A calculated the AUC for each result was used to describe the results. Mean results were calculated for each sample and dilution. The CV % was calculated for each result by the use of Equation 4. All statistics were evaluated using Microsoft Excel.

## 7.4 Results

### 7.4.1 Nanoparticle Tracking Analysis

In order to investigate the influence of centrifugation on the particle size distribution and concentration of MPs, three different centrifugation methods have been compared. In figure 31, the results obtained by the NTA device is illustrated.

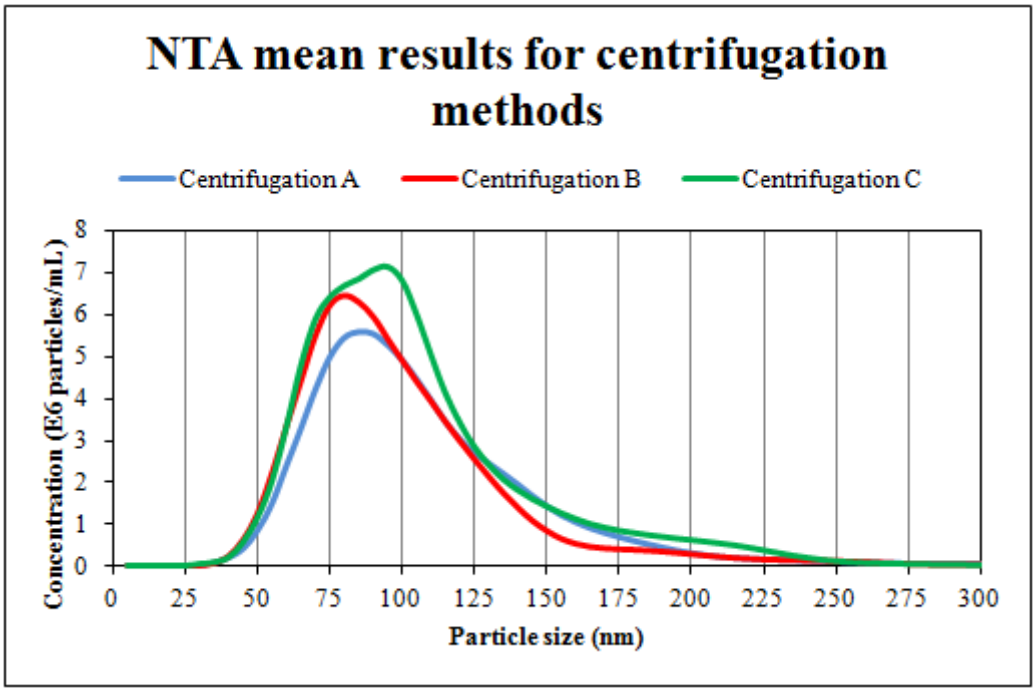


**Figure 31: Illustration of results obtained for the plasma samples from healthy donors in the centrifugation experiment. The x-axis shows particle size in nm, and the y-axis shows concentration of $10^6$ of MPs per mL. The size distributions for the three graphs are approximately the same, though the concentration of MPs seems to differ slightly. See raw data in appendix A.5.**

In figure 31, no major difference between the three results was observed, and the particle size distributions are approximately the same, which was also illustrated by the AUC, which was calculated to be 633.78, 639.49, and 692.19 for centrifugation A, B, and C, respectively. The mean AUC value is thus 655.15, and the standard deviation was calculated to be 32.20. The CV % was calculated to be 4.91 %.

### 7.4.2 Dynamic Light Scattering

Comparison of the three different centrifugation methods obtained by the DLS device is illustrated in figure 32. No major differences are found between the particle size distribution of MPs and relative intensity. Due to the high amount of background noise, the AUC cannot be compared and is therefore not calculated.

## 7.5 Discussion

Comparing different centrifugation methods was conducted in order to investigate the influence of centrifugation on the particle size distribution and MP concentration in plasma samples. The used centrifugation methods in the literature vary widely, and it is therefore complicated to compare results. Healthy plasma samples were obtained from three healthy individuals with no known pathological conditions.

The results obtained from the NTA measurements showed little variation between the three centrifugation methods. The particle size distributions were the same, but the concentration varied some. A variation of ~5 % was observed between the centrifugations, which of the three centrifugation methods tested are used.

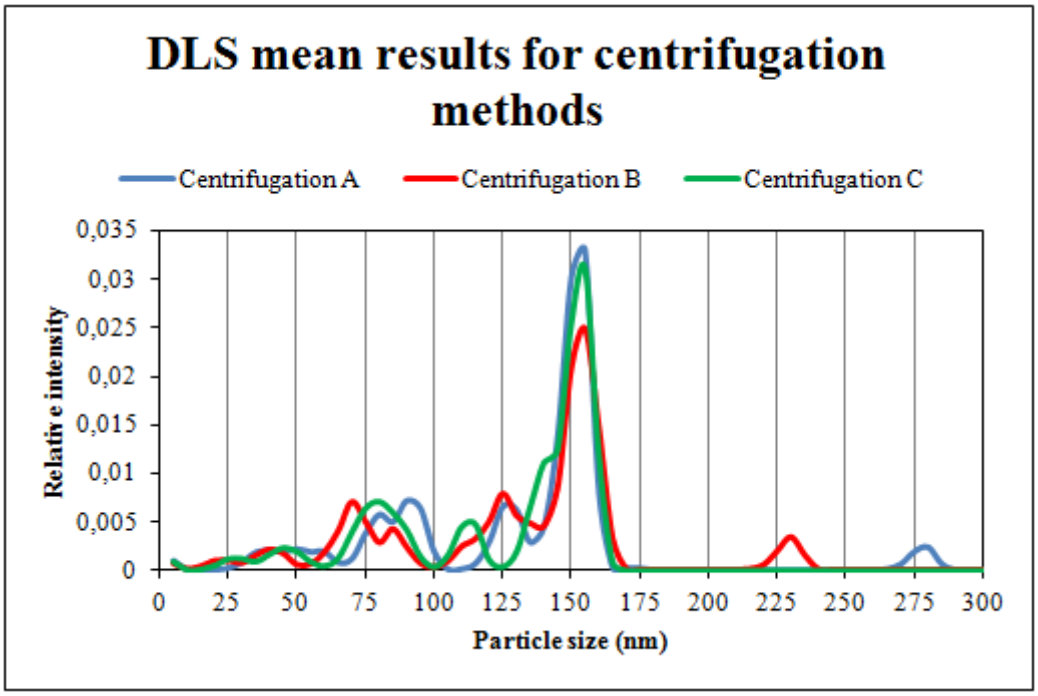


**Figure 32: Illustration of the results obtained for three plasma samples collected from healthy donors in the experiment comparing three different centrifugation methods. The x-axis shows particle size in nm, and the y-axis shows relative intensity of light. Peaks below 0.01 in relative intensity are considered background noise. The three major peaks display the same size distribution. See raw data in appendix A.5.**

Results obtained from the DLS measurements support the results from the NTA measurements. Again, a small variation was found between the three centrifugation methods when comparing the major peaks. Due to the high amount of measured background noise, it was not possible to find the variation between the measurements, but the particle size distributions and measured relative intensity align.

Lacroix and colleagues [Lacroix *et al.*, 2011] have also conducted a similar experiment comparing Centrifugation B and Centrifugation C. As for the result obtained in this study, Centrifugation C also displayed a higher concentration of MPs in the study by Lacroix and colleagues, but Lacroix and colleagues found Centrifugation B to be the best adaptable centrifugation method for routine laboratory testing due to the more complex sample handling with Centrifugation C. The same conclusion is made in the present study due to the simplicity of two successive centrifugations with no high-speed centrifugation needed.

# Part 8: Pilot Studies

# Clinical potential of methods

## 8.1 Aim of Experiment

The aim is to investigate if there is a significant difference in the concentration of MPs in healthy individuals compared to diseases individuals. Furthermore, the clinical potential of the two methods will be evident.

## 8.2 Materials

Blood samples were obtained from one healthy individual, who gave informed consent, and from three anonymous patients admitted to Aalborg Hospital, who suffered from AF, MM, and IHD. The healthy volunteers were not taking any medication that could interfere with the result. The healthy blood sample was obtained in 'Experiment 4' and it was used as a reference value. Patient blood samples were collected in hospital departments of admission by a qualified and certified person. Fasting was not mandatory. Blood samples were drawn from the antecubital vein with a 21-gauge needle and collected in three 9 mL citrate glasses containing 0.109 M citrate (Vacuette®; Greiner Bio-One, Kremsmünster, Austria). The first few millilitres were discarded to avoid artefacts, which can be generated by contact phase activation.
NTA measurements were conducted by the use of a NanoSight LM10-HS device (NanoSight Ltd., Amesbury, United Kingdom), and the used software was NTA 2.1 analytical software (NanoSight Ltd., Amesbury, United Kingdom). DLS measurements were conducted by the use of a prototype of a ThromboLUX device (Light Integra Technology, Vancouver, Canada), and the analysis software were FLEX02-12BD (measurement software) and CorrelatorComms 1.141 (analysis software). DPBS was used as diluents.

## 8.3 Methods

### 8.3.1 Sample Preparation

The blood samples were centrifuged to separate blood cells and plasma with the intention to produce platelet-free-plasma (PFP), according to the protocol in appendix A.2. The blood samples were centrifuged twice at 2,500g for 15 minutes at RT. The supernatant was transferred into a 15 mL centrifugation tube between the centrifugations. Aspiration of plasma was stopped approximately one centimetre above the buffy coat. The resultant platelet-free-plasma (PFP) was transferred to 1.5 mL microtubes, each containing 100 µL of plasma sample. Aspiration was stopped approximately 100 µL above the bottom of the tube. One aliquot was used for the experiment, whereas the remaining aliquots were frozen and used for future experiments. Plasma samples were diluted according to results obtained in 'Experiment 2'.

### 8.3.2 Nanoparticle Tracking Analysis

All experiments with plasma samples were conducted as described in the protocol in appendix A.2. Prior to measurement of plasma samples, the thumbprint was located by the use of a blank sample, and microbeads were measured to check the instrument settings, according to protocol in appendix A.2. The blank sample was injected into the sample chamber by the use of 1 mL sterile syringes (Becton Dickinson, Madrid, Spain) until it reached the tip of the sample chamber output. The thumbprint was located along with the preferred measuring area and the appropriate camera and parameter settings were found, according to protocol in appendix A.2. The first plasma sample was then loaded by injecting the sample with a 1 mL sterile syringe and measured. Each syringe can contain a total of three samples, thus triplicates with the same prepared sample can be tested in triplicates. The sample chamber was washed after each sample by 70 % EtOH. The samples were measured in the 'single shutter and gain mode' for 60 seconds. The temperature of each run was measured by a temperature measuring device specifically developed to the sample chamber. The NTA 2.1 Analytical Software was used for capturing and analysing the data.

### 8.3.3 Dynamic Light Scattering

All experiments with plasma samples were conducted as described in the protocol in appendix A.2. Prior to measurement of plasma samples, the intensity setting were checked using a blank sample and microbeads in the suitable concentrations found in 'Experiment 1'. A total of 40 µL of each dilution was used to each measurement, which was prepared in 1.5 mL microtubes. The blank sample was loaded into the sample holder in a disposable plastic capillary (Drummond Scientific Company, Pennsylvania, USA), according to protocol in appendix A.2. The blank sample was measured, and when a satisfactory intensity was observed, the blank sample was removed from the sample chamber. The microbeads were then measured to verify the intensity. The samples were then measured in triplicates. The samples were measured for 240 seconds, and all experiments were conducted at room temperature. The CorrelatorComms software was used to analyse data obtained by the FLEX02-12BD software.

### 8.3.4 Statistical Analysis

A calculated the AUC for each result was used to describe the results. Mean results were calculated for each sample and dilution.

## 8.4 Results

### 8.4.1 Nanoparticle Tracking Analysis

In order to investigate the potential of NTA to differentiate between healthy control samples and samples from three different disease states were measured. The healthy sample was used as reference sample, and it was compared to the three pathological samples. The AUC for the healthy sample was calculated to be 143.32.

Figure 33 illustrates the AF sample analysed on the NTA device. The concentration of MPs in the AF sample was not found to be higher when comparing to the healthy plasma sample, but the AF sample displays a greater separation of the particle sizes. Four subpopulations of MPs at 65 nm, 84 nm, 112 nm, and 148 nm appeared in the results. The AUC was calculated to be 92.56, thus the MP level was found to be lower in this patient suffering from AF.

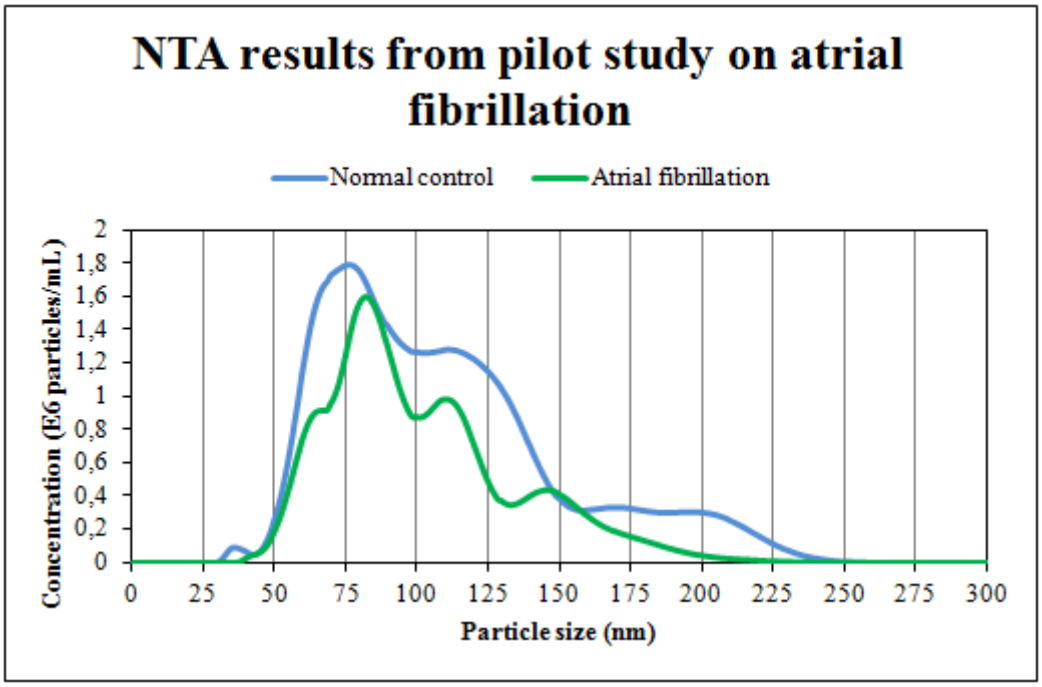


**Figure 33: Illustration of results obtained for the plasma samples from healthy donors in the centrifugation experiment. The x-axis shows particle size in nm, and the y-axis shows concentration of $10^6$ of MPs per mL. The size distributions for the three graphs are approximately the same, though the concentration of MPs seems to differ slightly. See raw data in appendix A.6.**

In figure 34, the result obtained for the IHD sample is illustrated. For this sample a clear increased in concentration of MPs was found. Furthermore, the particle size distribution is narrow with a mode particle size at 82 nm. The AUC was calculated to be 156.73, meaning that there is only a slight increase in MP level in the patient suffering from IHD compared to normal control.

Figure 35 illustrates the result obtained for the MM sample. A higher concentration of MPs was found and two major subpopulations of particle sizes were evident. These subpopulations were found at 94 nm and 124 nm. The AUC was calculated to be 261.80, thus a much higher MP level was observed in this patient.

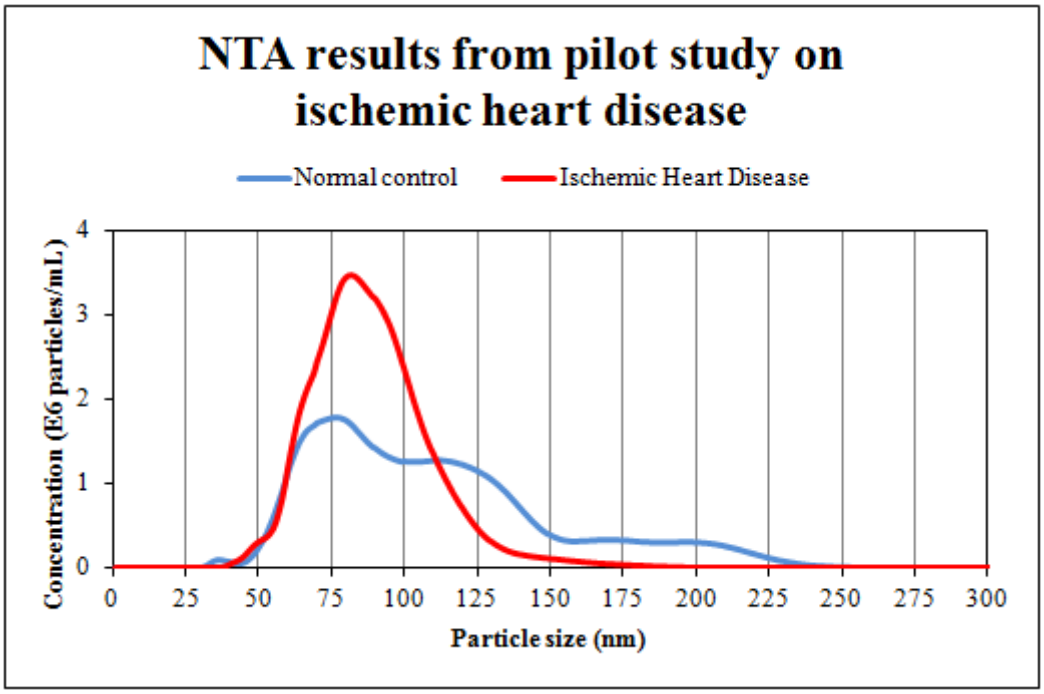


**Figure 34: Illustration of results obtained for the plasma samples from healthy donors in the centrifugation experiment. The x-axis shows particle size in nm, and the y-axis shows concentration of $10^6$ of MPs per mL. The size distributions for the three graphs are approximately the same, though the concentration of MPs seems to differ slightly. See raw data in appendix A.6.**

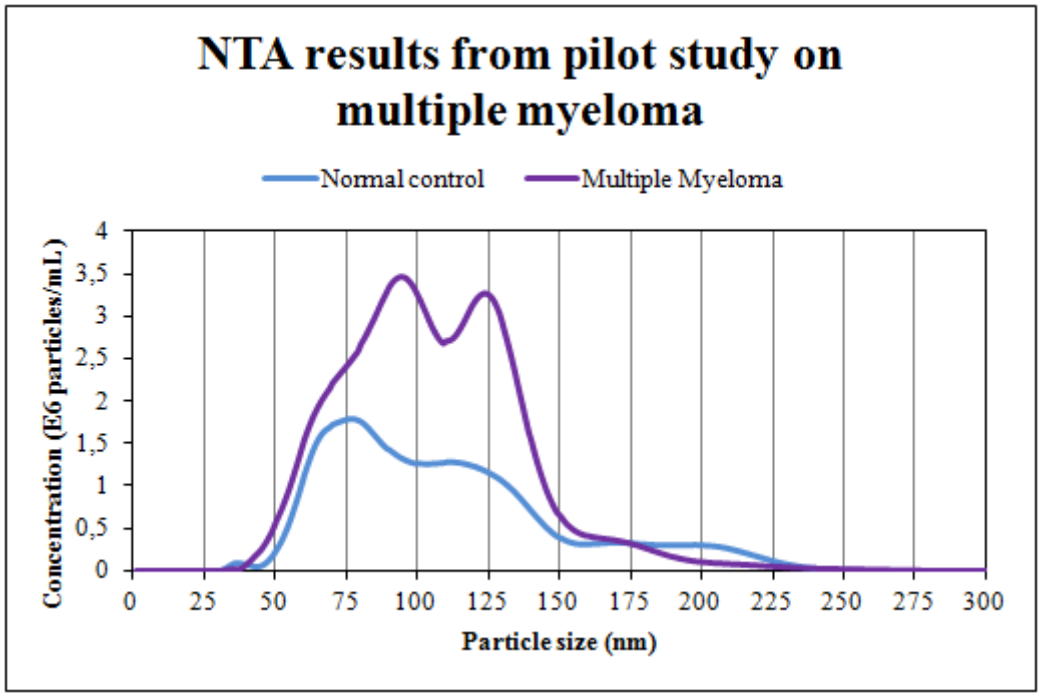


**Figure 35: Illustration of results obtained for the plasma samples from healthy donors in the centrifugation experiment. The x-axis shows particle size in nm, and the y-axis shows concentration of $10^6$ of MPs per mL. The size distributions for the three graphs are approximately the same, though the concentration of MPs seems to differ slightly. See raw data in appendix A.6.**

### 8.4.2 Dynamic Light Scattering

In order to investigate the potential of DLS to differentiate between healthy control samples and pathological samples, samples from three different disease states were measured. The healthy sample was used as reference sample, and it was compared to the three pathological samples.

Figure 36 illustrates the results obtained for the AF sample on the DLS device. The AF sample appears to have a similar level of MPs when compared to the healthy sample.

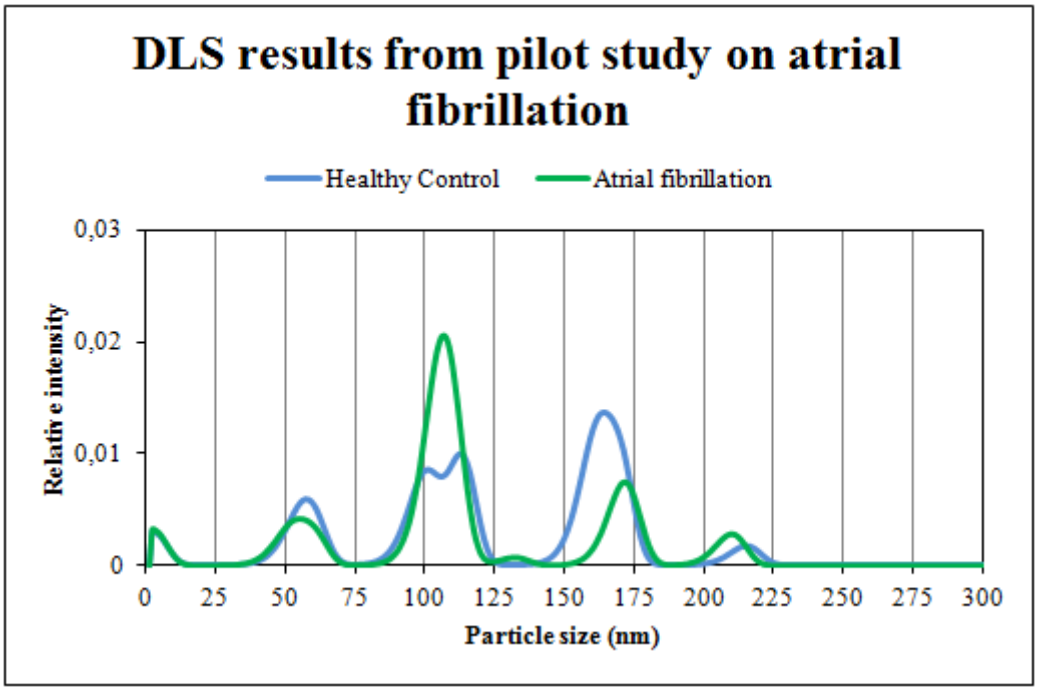


**Figure 36: Illustration of the results obtained for plasma samples collected from a healthy donor and a patient suffering from atrial fibrillation. The x-axis shows particle size in nm, and the y-axis shows relative intensity of light. Peaks below 0.01 in relative intensity are considered background noise. Differences are found in particle size distribution, but only merely in measured relative intensity. See raw data in appendix A.6.**

In figure 37, the result obtained for the IHD sample is illustrated. The height of the peaks appears to be almost equal, and perhaps even higher for the healthy sample compared to the pathological sample.

Figure 38 illustrates the result obtained for the MM sample. A higher intensity was observed at 212, but the remaining peaks displayed a lower relative intensity than the peaks found for the healthy sample.

## 8.5 Discussion

The clinical potential of NTA and DLS was investigated by compared a plasma sample obtained from a healthy individual to three different disease samples. The disease samples were provided by anonymous patients admitted to Aalborg Hospital, and their medical histories have not been available.

NTA proved to be able to differentiate between healthy and some pathological samples, although an increase in MP concentration was only proven for the IHD and MM samples. The DLS results showed increase in the measured relative intensity for one subpopulation of the measured particle sizes in the MM sample, but the majority of the MP sizes observed for all three diseases were not higher in relative intensity, thus no difference between the healthy control and the patient sample was found.

The effects of AF on the MP content have been investigated by Azzam and Zagloul [Azzam & Zagloul, 2009]. Platelet-derived MPs were investigated in peripheral blood collected from 20 valvular AF patients, and an increase was found in these patients when comparing to healthy controls. Azzam and Zagloul [Azzam

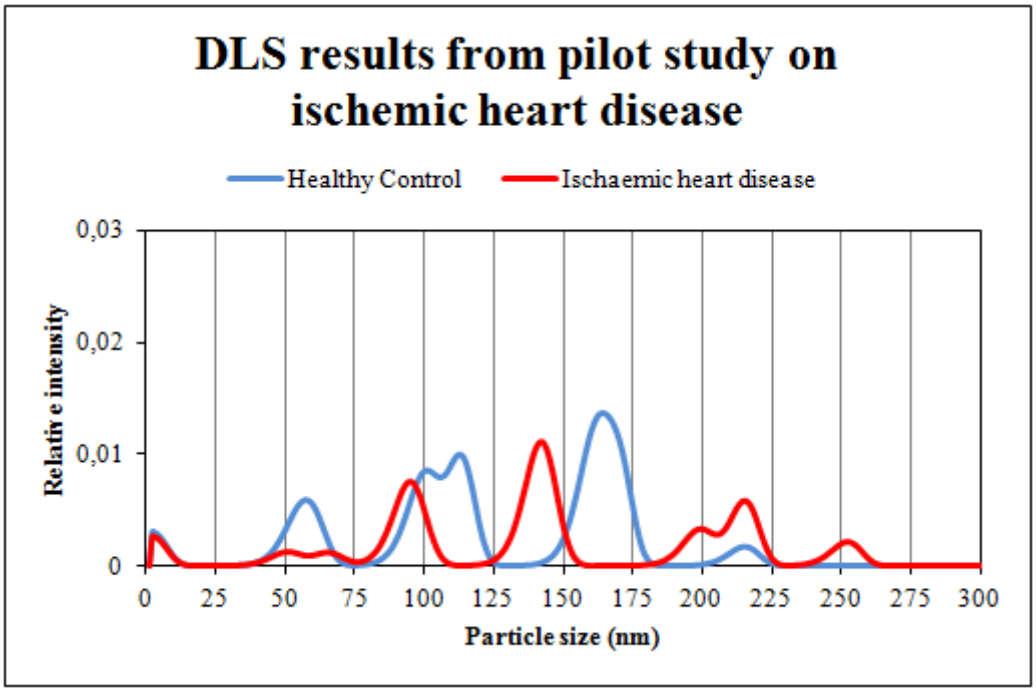


**Figure 37: Illustration of the results obtained for plasma samples collected from a healthy donor and a patient suffering from IHD. The x-axis shows particle size in nm, and the y-axis shows relative intensity of light. Peaks below 0.01 in relative intensity are considered background noise. No difference is observed for the measured relative intensity, but differences in size distributions appear. See raw data in appendix A.6.**

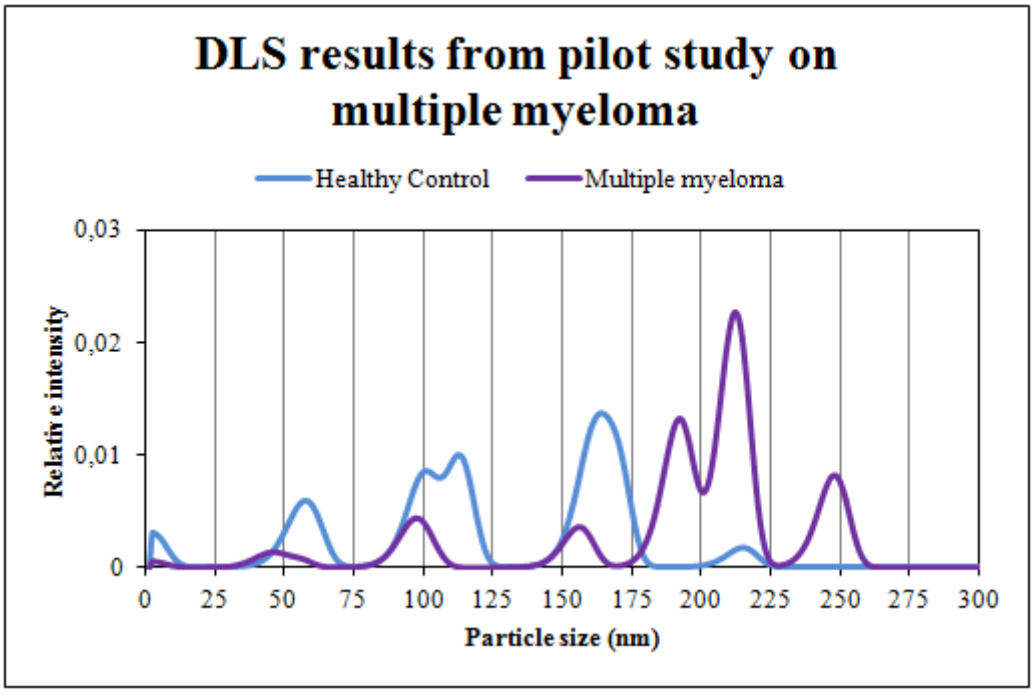


**Figure 38: Illustration of the results obtained for plasma samples collected from a healthy donor and a patient suffering from MM. The x-axis shows particle size in nm, and the y-axis shows relative intensity of light. Peaks below 0.01 in relative intensity are considered background noise. Differences in both particle size distribution and measured relative intensity are observed. See raw data in appendix A.6.**

& Zagloul, 2009] used flow cytometry for their measurement, and the increase in MPs may differ from the results obtained in the present study due to the use of different methods. In addition, a study conducted by Choudhury and colleagues [Choudhury *et al.*, 2007] also observed an increase in platelet-derived MPs in

patients suffering from nonvalvular AF. A total of 70 patients were included in the study along with 46 disease control subjects and 33 healthy control subjects. All of the 70 patients and the 46 disease control subjects were found to have increased platelet-derived MP levels.

The results obtained in the present study are based on one patient and does therefore not provide a general idea about the MP content of AF patients. Further investigations are needed in order to determine whether AF patients actually have a higher or lower concentration of circulating MPs.

The MP involvement in IHD patients have been investigated by Sinning and colleagues [Sinning *et al.*, 2011]. Investigating the MP level in 200 coronary artery disease patients of which 72 patients experienced major adverse cardiovascular and cerebral events, Sinning and colleagues provide evidence of increased levels to be associated with increased risk of cardiovascular mortality when comparing the patients experiencing the events with patients that did not experience the event. Increased MP levels can be used as indicators of the risk of dying in IHD patients.

The results obtained in the present study found the concentration of MPs to be higher in the IHD patient. Although the increased levels of MPs also were found by Sinning and colleagues [Sinning *et al.*, 2011], the preliminary result in the present project is only indicative of a possibility of IHD to have increased concentration of MPs. Further study of patients with IHD is needed to further conclude on the general MP level in these patients.

The involvement of MP in cancer has been studied intensively. The present study showed increased levels of MPs in a patient suffering from MM. Toth and colleagues [Toth *et al.*, 2008] discovered increased levels of endothelial cell-derived MPs in breast cancer patients. Furthermore, increasing levels of leukocyte-derived MPs correlated with increasing tumour size and can therefore be used as indicator of the disease progression. Only few reports on the involvement of MPs in MM could be found. Auwerda and colleagues [Auwerda *et al.*, 2011] investigated the MP-associated TF activity in 122 newly diagnosed MM patients and found levels of MP-associated TF activity to be increased. Furthermore, the elevated levels of MP-associated TF activity were found to decrease in response to chemotherapy. It would be interesting to investigate whether the MPs observed in the present study express TF activity by the use of antibodies specific for TF conjugated with a fluorescent dye.

Both NTA and DLS seem to be capable of differentiating between healthy samples and pathological samples, but due to a limited number of disease samples this needs to be investigated further.

# Part 9: Discussion

## 9.1 Summary Discussion

In the present investigation, an evaluation of two novel detection methods for the characterisation of MPs was conducted. NanoSight LM10-HS is laser-illuminated optical microscope based method, and Thrombo-LUX is a prototype of the well known DLS method. Five experiments were conducted to achieve a thorough evaluation. Experiment 1 aimed to determine the precision and accuracy of the two methods by the use of polystyrene microbeads. Experiment 2 aimed to determine the detection limits of MP concentration of the methods by the use of plasma samples obtained from healthy individuals and one diabetic patient. Experiment 3 aimed to investigate the effects of freezing plasma samples at -80°C on the concentration and particle size distribution of MPs. For this experiment, plasma samples obtained for Experiment 2 were also used. Experiment 4 aimed to investigate the effects of centrifugation on the concentration and particle size distribution three centrifugation methods were compared using plasma samples obtained from another three healthy donors. Finally, Experiment 5 aimed to investigate the clinical potential of the two methods. One healthy individual and three anonymous patients suffering from AF, IHD, and MM were compared. The healthy plasma sample was used as control.

### 9.1.1 Inter-run Variation Experiment

NTA was found to possess the ability to reproduce and measure accurately, although a detection limit of ~50 nm was observed. This is further confirmed by Filipe and colleagues [Filipe *et al.*, 2010]. The detection limit only concerns these microbeads. Studies have proved that the detection limit of NTA depends on the refractive index of the measured particles [Carr *et al.*, 2009]. For example, colloid gold particles have a very high refractive index and can therefore be measured to a small as 10 nm in diameter, whereas biological MPs have low refractive indexes and thus the detection limit of NTA increases when measuring MPs with lower refractive indexes [Carr *et al*, 2009].

DLS was also found to possess these abilities, but due to the prototype, the sizes of MPs observed when raw data was transformed were incorrect, and therefore the particles sizes should not be considered correct in future experiments.

Filipe and colleagues [Filipe *et al.*, 2010] have also compared NTA and DLS, but the DLS device used was a Malvern Zetasizer, which is fully developed and not a prototype as the ThromboLUX device. The results obtained by Filipe and colleagues [Filipe *et al.*, 2010] proved DLS to be an optimal method for detection of monodisperse solution of MPs, whereas the different particle sizes of a polydisperse solution could only be differentiated when the ratio between the small particles and the large particles were 150:1. Thus, DLS is not an optimal method to measure different particle sizes in the same sample.

### 9.1.2 Dilution Experiment

A linear correlation was found between dilutions and the AUC observed in the results from the NTA measurements, which can be used for experiments, where the concentration of MPs is too high to be measured with normal dilutions.

The results obtained with the DLS device showed that the plasma samples should not be diluted in DPBS. For the healthy plasma samples very low relative intensities was observed. The peaks observed were found close to boundary of background noise. Therefore, pure plasma samples should be used when investigating MP concentration and particle size distributions with the use of the DLS device.

### 9.1.3 Fresh-frozen Experiment

Storage of plasma samples is required for the two methods to have a possible clinical potential. Therefore, the influence of freezing on MP concentration and particle size distribution was investigated. Healthy plasma

samples were first measured as fresh samples after being drawn from the donors in the morning. The samples were then frozen at -80°C for 1, 7, 15, and 40 days.
The results obtained with the NTA device showed that freezing does effect the MP concentration of the samples, but the decrease in MP concentration was found to be consistent for all frozen samples. Furthermore, the particle size distribution did not change between the samples even though the concentration changed. This could indicate that the decrease in concentration is not caused by an aggregation of MP during freezing or thawing of the samples. These results support previous investigations of the effect of freezing on MPs [Sokolova *et al.*, 2011].
The DLS results were difficult to interpret and a conclusion was impossible to make based on the results. Only few peaks were displayed above the limit of measured background noise and their particle size distributions were not the same. Therefore, a comparison of the fresh and frozen samples could not be conducted. Furthermore, no literature investigating the effects of freezing of plasma samples containing MPs could be found, thus no comparison could be conducted here.
Lacroix and colleagues [Lacroix *et al.*, 2011] have investigated the effects of freezing at -80°C on the MP count using flow cytometry, a thrombin generation assay, and a procoagulant phospholipid-dependent clotting time assay. It was observed that freezing of plasma samples containing MPs does not influence the analysis of MPs and MP count.
Therefore, it does not appear that freezing and storage of plasma samples at -80°C affect the particle size distribution, but the concentrations of MPs seem to be affected. It is therefore suggested that all plasma samples are frozen prior to investigation on NTA and DLS devices to ensure the same basis for interpretation.

### 9.1.4 Centrifugation Experiment

Centrifugation methods used by different research groups differ greatly, and it is therefore complicated to compare results between groups.
NTA measurements showed little to no variation between the tested centrifugation methods. The particle size distributions were nearly the same, but the MP concentrations differed. The results indicate that for NTA measurements it does not differ which of the three centrifugation methods are chosen prior to analysis. The same was found for the DLS measurements. Again, a small variation was found between the three centrifugation methods when comparing the major peaks.
Lacroix and colleagues [Lacroix *et al.*, 2011] have also conducted a similar experiment comparing centrifugation methods. The results obtained in their study were similar to the results obtained in the present study. Furthermore, Lacroix and colleagues found Centrifugation B to be the best adaptable centrifugation method for routine laboratory testing due to the more complex sample handling with Centrifugation C, and such high-speed centrifugation may not be readily available. The same conclusion is made in the present study due to the simplicity of two successive centrifugations with no ultracentrifugation needed.

### 9.1.5 Pilot Studies

The results obtained from the NTA measurements comparing healthy and diseased samples showed that the AF patient did not have an elevated concentration of microparticles, but several different subpopulations of MPs were observed. Other studies have shown the opposite, thus an increase of MPs was found [Azzam & Zagloul, 2009; Choudhury *et al.*, 2007]. The DLS measurements showed an increased relative intensity of one subpopulation of the measured MPs, but in general no difference between the healthy sample and the patient sample was observed. The IHD displayed a higher concentration of MPs [Sinning *et al.*, 2011]. The cause of the high MP concentration has yet to be determined, and further study of the general MP level in IHD patients needs to be conducted. The MM patient was found to have an increased concentration of MPs when comparing to the healthy plasma sample. Few reports on the MP content in MM patients are found,

and therefore a study including several MM patients should be conducted. A general view of the MP levels in MM patients will be crucial to understand the involvement of MPs in the MM malignancy.
The results obtained in this study was based on one sample from one patient from each disease, which only makes the results preliminary and further studies on the MP concentration and particle size distribution must be conducted in order to confirm or contradict the results previously obtained in this study and by other researchers.
Both NTA and DLS seem to be capable of differentiating between a healthy sample and pathological samples, but this needs to be investigated further.

## 9.2 Conclusion

In conclusion, both NTA and DLS showed relative reproducibility and accuracy for measurement of microbeads and MPs in plasma samples. The most suitable dilution of plasma samples in buffer for measurement on NTA was found to be 2 µL of plasma sample in 1000 µL DPBS for both healthy and diseased plasma samples. Freezing did not affect the particle size distributions of measured MPs, but the concentration of MPs was found to be higher for the fresh sample when measuring the samples with NTA. The DLS results were inconclusive for the fresh-frozen experiment. Centrifugation showed to have little or no effect on the particle size distribution and concentration of MPs in plasma samples for measurements with both methods. The clinical potential of both NTA and DLS was proven when both methods were able to differentiate between healthy plasma samples and pathological plasma samples.
Thus, both methods exhibit relative reproducibility and they can be used as complementary methods for the detection and characterisation of MPs in plasma.

## 9.3 Future Perspectives

An increased focus on MPs has emerged during the last two decades. The physiology of MPs has been established years ago, and the main focus today is the involvement of MPs in disease states.
The results obtained in this study are very preliminary for NTA and DLS. Few healthy donors were investigated, and the displayed MP content differs between each individual. A consensus between the samples and an expected mean AUC value could be obtained if testing several healthy donors. Exclusion criteria for a study of this kind would be necessary to prevent inclusion of outliers, and thus prevention of a higher mean measured particle size. The obtainment of a reference value would improve the ability of detecting persons with increased MP levels. Donors of all ages should be recruited. DLS does not possess the ability to differentiate between different MP types and development of providing this ability to NTA is in progress, and thus for now the methods cannot conclude much about the MP types in the plasma samples. Donors should therefore be pre-evaluated with different screening tests, such as thrombin generation assays and whole blood analysis prior to analysis by NTA. Such a study could be useful in the clinical routine laboratory where individuals with low amounts of MPs quickly could be determined not to be in the area of disease possibility. The few patient samples investigated in the present study does only provide a slightly useful image of what could be expected in patients suffering from the three investigated diseases. Large clinical studies specifically investigating each disease need to be conducted to find the MP concentration and particle size distribution in these diseases.
Furthermore, it would be interesting to investigate if there is a difference between genders. This issue was investigated by Toth and colleagues [Toth *et al.*, 2007], who compared the MP level of men and women. It was found that women had a higher level of several different MP. Furthermore, Toth and colleagues also investigated if this increased amount of MPs dependent on their menstrual cycles. During the luteal phase, women had a higher concentration of MPs when compared to the measured concentration during the follicular phase. This interesting result should be considered when investigating the concentration of MPs, and a

large clinical study with women in their reproductive phase of life could conducted to determine if this difference is consistent.

The DLS method is only a prototype and development of the method is in progress. Especially the difficulties observed when transferring the raw data from the DLS analytical software to Microsoft Excel must be improved. The differences in the measured particle sizes differ to such amounts, that the results seems untrustworthy, and clinical research cannot be conducted on such grounds. A more intense collaboration with the inventors discussing the observed difficulties could enhance the development, and suitable DLS analytical software could thus be developed.

Developments of the NTA device and software are also in progress. The ability to characterise the origin of MPs by the use of fluorescence has been investigated, and Dragovic and colleagues [Dragovic *et al.*, 2011] are the first to describe how MPs can be phenotyped by the use of fluorescent antibodies. By labelling with an antibodies specific for platelet-derived MPs, these can be measured individually with the use of a fluorescence mode in the NTA software. This will lead to measurement of only the labelled MPs and not the total pool of MPs. If one wants to measure the total pool, the 'single shutter and gain mode' can be used, and a comparison of the results will provide a concentration of how many MPs in the sample is derived from platelets. The development of this system is in progress with great potential to replace flow cytometry, which is the major method of choice for phenotyping of MPs.

# References

| | |
|---|---|
| [Abcam®, 2011] | Abcam® Secreted extracellular vesicles pathway card. Available online: http://www.abcam.com/index.html?pageconfig=resource&rid=12745&pid=7 Date: 14-05-2012 |
| [Auwerda *et al.*, 2011] | Auwerda J. J., Yuana Y., Osanto S., de Maat M. P., Sonneveld P., Bertina R. M., Leebeek F. W.: Microparticle-associated tissue factor actitivity and venous thrombosis in multiple myeloma, *Thromb Haemost*, 2011;105(1):14-20 |
| [Azzam & Zagloul, 2009] | Azzam H., Zagloul M.: Elevated platelet microparticle levels in valvular atrial fibrillation, *Hematology*, 2009;14(6):357-60 |
| [Bassé *et al.*, 1994] | Bassé F., Gaffet P., Bienvenüe A.: Correlation between inhibition of cytoskeleton proteolysis and anti-vesiculation effect of calpeptin during A23187-induced activation of human platelets: are vesicles shed by filopod fragmentation?, *Biochim Biophys Acta*, 1994;1190(2):217-24 |
| [Biró *et al.*, 2005] | Biró É., Akkerman J. W. N., Hoek F. J., Gorter G., Pronk L. M., Sturk A., Nieuwland R.: The phospholipid composition and cholesterol content of platelet derived microparticles: a comparison with platelet membrane fractions, *J Thromb Haemost*, 2005;3:2754-63 |
| [Blanchard *et al.*, 2002] | Blanchard N., Lankar D., Faure F., Regnault A., Dumont C., Raposo G., Hivroz C.: TCR activation of human T cells induces the production of exosomes bearing TCR/CD3/ζ complex, *J Immunol*, 2002;168(7):3235-41 |
| [Boulanger *et al.*, 2001] | Boulanger C. M., Scoazec A., Ebrahimian T., Henry P., Mathieu E., Tedgui A., Mallat Z.: Circulating microparticles from patients with myocardial infarction cause endothelial dysfunction, *Circulation*, 2001;104(22):2649-52 |
| [Bucciarelli *et al.*, 2011] | Bucciarelli P., Martinelli I., Artoni A., Passamonti S. M., Previtali E., Merati G., Tripodi A., Mannucci P. M.: Circulating microparticles and risk of venous thromboembolism, *Thromb. Res.* 2011 Sep 9;xxx:xxx-xxx |
| [Burnier *et al.*, 2009] | Burnier L., Fontana P., Kwak B. R., Angelillo-Scherrer A.: Cell-derived microparticles in haemostasis and vascular medicine, *Thromb. Haemost.*, 2009;101:439-451 |
| [Carr *et al.*, 2009] | Carr B., Hole P., Malloy A., Nelson P., Wright M., Smith J.: Applications of nanoparticle tracking analysis in nanoparticle research – a mini-review, E*uropean Journal of Parenteral and Pharmaceutical Sciences*, 2009;14(2):45-50 |
| [Castaman *et al.*, 1996] | Castaman G., Yu-Feng L., Rodeghiero F.: A bleeding disorder characterised by isolated deficiency of platelet microvesicle generation, *Lancet*, 1996;347(9002):700-1 |
| [Castaman *et al.*, 1997] | Castaman G., Yu-Feng, Battistin E., Rodeghiero F.: Characterisation of a novel bleeding disorder with isolated prolonged bleeding time and deficiency of platelet microvesicle generation, *Br J Haemotol*, 1997;96(3):458-63 |
| [Chargaff & West, 1946] | Chargaff E., West R.: The biological significance of the thromboplastic protein of blood, *J Biol Chem.*, 1946;166(1):189-97 |
| [Chirinos *et al.*, 2005] | Chirinos J. A., Heresi G. A., Velasquez H., Jy W., Jimenez J. J., Ahn E., Horstman L. L., Soriano A. O., Zambrano J. P., Ahn Y. S.: Elevation of endothelial microparticles, platelets, and leukocyte activation in patients with venous thromboembolism, *J Am Coll Cardiol*, 2005;45(9):1467-71 |
| [Choudhury *et al.*, 2007] | Choudhury A., Chung I., Blann A. D., Lip G. Y.: Elevated platelet microparticle levels in nonvalvular atrial fibrillation: relationship to p-selectin and antothrombotic therapy, *Chest*, 2007;131(3):809-15 |
| [Coleman *et al.*, 2001] | Coleman M. L., Sahai E. A., Yeo M., Bosch M., Dewar A., Olson M. F.: Membrane blebbing during apoptosis results from caspase-mediated activation of ROCK I, *Nat Cell Biol*, 2001;3(4):339-45 |

| | |
|---|---|
| [Colognato *et al.*, 2008] | Colognato R., Bonelli A., Ponti J., Farina M., Bergamaschi E., Sabbioni E., Migliore L.: Comparative genotoxicity of cobalt nanoparticles and ions on human peripheral leukocytes in vitro, *Mutagenesis*, 2008;23(5):377-82 |
| [Davizon & López, 2009] | Davizon P., López J. A.: Microparticles and thrombotic disease, *Curr Opin Hematol*, 2009;16(5):334-41 |
| [del Conde *et al.*, 2005] | del Conde I., Shrimpton C. N., Thiagarajan P, López J. A.: Tissue-factor-bearing microvesicles arise from lipid raft and fuse with activated platelets to initiate coagulation, *Blood*, 2005;106(5):1604-11 |
| [Dragovic *et al.*, 2011] | Dragovic R. A., Gardiner C., Brooks A. S., Tannetta D. S., Ferguson D. J., Hole P., Carr B., Redman C. W., Harris A. L., Dobson P. J., Harrison P., Sargent I. L.: Sizing and phenotyping of cellular vesicles using Nanoparticle Tracking Analysis, *Nanomedicine*, 2011;7(6):780-78 |
| [Dvorak *et al.*, 1981] | Dvorak H. F., Quay S. C., Orenstein N. S., Dvorak A. M., Hahn P., Bitzer A. M., Carvalho A. C.: Tumor shedding and coagulation, *Science*, 1981;212(4497):923-24 |
| [Falati *et al.*, 2003] | Falati S., Liu Q., Gross P., Merrill-Skoloff G., Chou J., Vandendries E., Celi A., Croce K., Furie B. C., Furie B.: Accumulation of tissue factor into development thrombi in vivo is dependent upon microparticle P-selectin glycoprotein ligand 1 and platelet P-selectin, *J Exp Med*, 2003;197(11):1585-98 |
| [Filipe *et al.*, 2010] | Filipe V., Hawe A., Jiskoot W.: Critical evaluation of Nanoparticle Tracking Analysis (NTA) by NanoSight for the measurement of nanoparticles and protein aggregates, *Pharm Res*, 2010;27(5):796-10 |
| [Flaumenhaft, 2006] | Flaumenhaft R.: Formation and fate of platelet microparticles, 2006;36(2):182-87 |
| [Flaumenhaft *et al.*, 2009] | Flaumenhaft R., Dilks J. R., Richardson J., Alden E., Patel-Hett S. R., Battinelli E., Klement G. L., Sola-Visner M., Italiano J. E. Jr.: Megakaryocyte-derived microparticles: direct visualization and distinction from platelet-derived microparticles, *Blood*, 2009;113(5):1112-21 |
| [Fourcade *et al.*, 1995] | Fourcade O., Simon M. F., Viodé C., Rugani N., Leballe F., Ragab A., Fournié B., Sarda L., Chap H.: Secretory phospholipase $A_2$ generated the novel lipid mediator lysophosphatidic acid in membrane microvesicles shed from activated cells, *Cell*, 1995;80(6):919-27 |
| [Fox *et al.*, 1990] | Fox J. E., Austin C. D., Boyles J. K., Steffen P. K.: Role of the membrane skeleton in preventing the shedding of procoagulant-rich microvesicles from the platelet plasma membrane, *J Cell Biol.*, 1990;111(2):483-93 |
| [Fox *et al.*, 1991] | Fox J. E., Austin C. D., Reynolds C. C., Steffen P. K.: Evidence that agonist-induced activation of calpain causes the shedding of procoagulant-containing microvesicles from the membrane of aggregating platelets, 1991;266(20):13289-95 |
| [Freikman et al., 2008] | Freikman I., Amer J., Cohen J. S., Ringel I., Fibach E.: Oxidative stress causes membrane phospholipid rearrangement and shedding from RBC membranes – An NMR study, Biochim Biophys Acta, 2008;1778(10):2388-94 |
| [Freyssinet, 2003] | Freyssinet J. M.: Cellular microparticles: what are they bad or good for?, *J Thromb Haemost*, 2003;1(7):1655-62 |
| [Furie & Furie, 2006] | Furie B., Furie B. C.: Cancer-associated thrombosis, *Blood Cells Mol Dis*, 2006;36(2):177-81 |
| [Furie & Furie, 2008] | Furie B., Furie B. C.: Mechanisms of thrombus formation, N Engl J Med, 2008;359(9):938-49 |
| [George *et al.*, 1982] | George J. N., Thoi L. L., McManus L. M., Reimann T. A.: Isolation of human platelet membrane microparticles from plasma and serum, *Blood*, 1982;60(4):834-40 |

| | |
|---|---|
| [Ghonaim *et al.*, 2009] | Ghonaim H. M., Li S., Blagbrough I. S.: Very long chain N4,N9-diacyl spermines: non-viral lipopolyamine vectors for efficient plasmid DNA and siRNA delivery, *Pharm Res*, 2009;26(1):19-31 |
| [Gross *et al.*, 2005] | Gross P. L., Furie B. C., Merrill-Skoloff G., Chou J., Furie B.: Leukocyte-versus microparticle-mediated tissue factor transfer during arteriolar thrombus development, *J Leukoc Biol*, 2005;78(6):1318-26 |
| [Habib *et al.*, 2008] | Habib A., Kunzelmann C., Shamseddeen W., Zobairi F., Freyssinet J. M., Taher A.: Elevated levels of circulating procoagulant microparticles in patients with beta-thalassemia, *Haematologica*, 2008;93(6):941-42 |
| [Horstman & Ahn, 1999] | Horstman L. L., Ahn Y. S.: Platelet microparticles: a wide-angle perspective, 1999;30(2):111-42 |
| [Hugel *et al.*, 1999] | Hugel B., Socié G., Vu T., Toti F., Gluckman E., Freyssinet J. M., Scrobohaci M. L.: Elevated levels of circulating procoagulant microparticles in patients with paroxysmal nocturnal haemoglobinuria and aplastic anemia, *Blood*, 1999;93(10):3451-56 |
| [Hugel *et al.*, 2005] | Hugel B., Martínez M. C., Kunzelmann C., Freyssinet J.: Membrane microparticles: Two sides of the coin, *Physiology*, 2005;20:22-27 |
| [Hughes *et al.*, 2000] | Hughes M., Hayward C. P., Warkentin T. E., Horsewood P., Chorneyko K. A., Kelton J. G.: Morphological analysis of microparticle generation in heparin-induced thrombocytopenia, *Blood*, 2000;96(1):188-94 |
| [Jimenez *et al.*, 2001] | Jimenez J. J., Jy W., Mauro L. M., Horstman L. L., Ahn Y. S.: Elevated endothelial microparticles in thrombotic thrombocytopenia purpura: findings from brain and renal microvascular cell culture and patients with active disease, *Br J Haematol*, 2001;112(1):81-90 |
| [Kelton *et al.*, 1992] | Kelton J. G., Warkentin T. E., Hayward C. P., Murphy W. G., Moore J. C.: Calpain activity in patients with thrombotic thrombocytopenic purpura is associated with platelet microparticles, *Blood*, 1992;80(9):2246-51 |
| [Kendall & Kosseva, 2006] | Kendall K., Kosseva M. R.: Nanoparticle aggregation influenced by magnetic fields, *Colloids and Surfaces A: Physicochem Eng Aspects*, 2006;286(1-3):112-116 |
| [Korade & Kenworth, 2008] | Korade Z., Kenworth A. K.: Lipid rafts, cholesterol, and the brain, *Neuropharmacology*, 2008;55(8):1265-73 |
| [Lacroix *et al.*, 2012] | Lacroix R., Judicone C., Poncelet P., Robert S., Arnaud L., Sampol J., Dignat-George F.: Impact of pre-analytical parameters on the measurement of circulating microparticles: towards standardization of protocol, *J Thromb Haemost*, 2012;10(3):437-46 |
| [Leroyer *et al.*, 2008] | Leroyer A. S., Tedqui A., Boulanger C. M.: Microparticles and type 2 diabetes, *Diabetes Metab*, 2008;34(1):27-32 |
| [Mack *et al.*, 2000] | Mack M., Kleinschmidt A., Brühl H., Klier C., Nelson P. J., Cihak J., Plachý J., Stangassinger M., Erfle V., Schlöndorff D.: Transfer of the chemokine receptor CCR5 between cells by membrane-derived microparticles: a mechanism for cellular human immunodeficiency virus 1 infection, *Nat Med*, 2000;6(7):769-75 |
| [Maurer-Spurej *et al.*, 2006] | Maurer-Spurej E., Brown K., Labrie A., Marziali A., Glatter O.: Portable dynamic light scattering instrument and method for the measurement of blood platelet suspensions, *Phys Med Biol*, 2006;51(15):3747-58 |
| [Mause & Weber, 2010] | Mause S. F., Weber C.: Microparticles: protagonists of a novel communication network for intercellular information exchange, *Circ Res*, 2010;107(9):1047-57 |
| [McLaughlin *et al.*, 1993] | McLaughlin P. J., Gooch J. T., Mannherz H. G., Weeds A. G.: Structure of gelsolin segment 1-actin complex and the mechanism of filament severing, *Nature*, 1993;364(6439):685-92 |

| | |
|---|---|
| [Messer *et al.*, 2009] | Messer L., Alsaleh G., Freyssinet J. M., Zobairi F., Leray I., Gottenberg J. E., Sibilia J., Toti-Orfanoudakis F., Wachsmann D.: Microparticle-induced release of B-lymphocyte regulators by rheumatoid synoviocytes, *Arthritis Res Ther*, 2009;11(2):R40 |
| [Miller *et al.*, 2009] | Miller K., Erez R., Segal E., Shabat D., Satchi-Fainaro R.: Targeting bone metastases with a bispecific anticancer and antiangiogenic polymer-alendronate-taxane conjugate, *Angew Chem Int Ed Engl*, 2009;48(16):2949-54 |
| [Miyazaki *et al.*, 1996] | Miyazaki Y., Nomura S., Miyake T., Kagawa H., Kitada C., Taniquichi H., Komiyama Y., Fujimura Y., Ikeda Y., Fukuhara S.: High shear stress can initiate both platelet aggregation and shedding of procoagulant containing microparticles, *Blood*, 1996;88(9):3456-64 |
| [Nassar *et al.*, 2009] | Nasser T., Rom A., Nyska A., Benita S.: Novel double coated nanocapsules for intestinal delivery and enhanced oral bioavailability of tacrolimus, a P-gp substrate drug, *J Control Release*, 2009;133(1):77-84 |
| [Neville *et al.*, 2009] | Neville F., Pchelintsev N. A., Broderick M. J., Gibson T., Millner P. A.: Novel one-pot synthesis and characterisation of bioactive thiol-silicate nanoparticles for biocatalytic and biosensor applications, *Nanotechnology*, 2009;20(5):055612 |
| [Nomura *et al.*, 1995] | Nomura S., Suzuki M., Katsura K., Xie G. L., Miyazaki T., Kido H., Kagawa H., Fukuhara S.: Platelet-derived microparticles may influence the development of atherosclerosis in diabetes mellitus, *Atherosclerosis*, 1995;116(2):235-40 |
| [Perez-Pujol *et al.*, 2007] | Perez-Pujol S., Marker P. H., Key N. S.: Platelet microparticles are heterogeneous and highly dependent on the activation mechanism: studies using a new digital flow cytometer, *Cytometry A*, 2007;71(1):38-45 |
| [Rand *et al.*, 2006] | Rand M. L., Wang H., Bang K. W., Packham M. A., Freedman J.: Rapid clearance of procoagulant platelet-derived microparticles from the circulation of rabbits, *J Thromb Haemost*, 2006;4(7):1621-23 |
| [Reininger *et al.*, 2006] | Reininger A. J., Heijnen H. F., Schumann H., Specht H. M., Schramm W., Ruggeri Z. M.: Mechanisms of platelet adhesion to von Willebrand factor and microparticle formation under high shear stress, *Blood*, 2006;107(9):3537-45 |
| [Rozmyslowicz *et al.*, 2003] | Rozmyslowicz T., Majka M., Kijowski J., Murphy S. L., Conover D. O., Poncz M., Ratajczak J., Gaulton G. N., Ratajczak M. Z.: Platelet- and megakaryocyte-derived microparticles transfer CXCR4 receptor to CXCR4-null cells and make them susceptible to infection by Xa-HIV, *AIDS*, 2003;17(1):33-42 |
| [Sabatier *et al.*, 2002] | Sabatier F., Darmon P., Hugel B., Combes V., Sanmarco M., Velut J. G., Arnoux D., Charpiot P., Freyssinet J. M., Oliver C., Sampol J., Dignat-George F.: Type 1 and type 2 diabetes patients display different patterns of cellular microparticles, *Diabetes*, 2002;51(9):2840-45 |
| [Shet *et al.*, 2003] | Shet A. S., Aras O., Gupta K., Hass M. J., Rausch D. J., Saba N., Koopmeiners L., Key N. S., Hebbel R. P.: Sickle blood contains tissue factor-positive microparticles derived from endothelial cells and monocytes, *Blood*, 2003;102(7):2678-83 |
| [Simak *et al.*, 2004] | Simak J., Holada K., Risitano A. M., Zivny J. H., Young N. S., Vostal J. G.: Elevated circulating endothelial membrane microparticles in paroxysmal nocturnal haemoglobinuria, *Br J Haematol*, 2004;125(6):804-13 |
| [Sims *et al.*, 1989] | Sims P. J., Wiedmer T., Esmon C. T., Weiss H. J., Shattil S. J.: Assembly of the platelet prothrombinase complex is linked to vesiculation of the platelet plasma membrane. Studies in Scott syndrome: an isolated defect in platelet procoagulant activity, *J Biol Chem*, 1989;264(29):17049-57 |
| [Sinning *et al.*, 2011] | Sinning J. M., Losch J., Walenta K., Böhm M., Nickenig G., Werner N.: Circulating CD31+/Annexin V+ microparticles correlate with cardiovascular outcomes, *Eur Heart J*, 2011;32(16):2034-41 |

| | |
|---|---|
| [Sokolova *et al.*, 2011] | Sokolova V., Ludwig A. K., Hornung S., Rotan O., Horn P. A., Epple M., Giebel B.: Characterisation of exosomes derived from human cells by nanoparticle tracking analysis and scanning electron microscopy, *Colliods Surf B Biointerfaces*, 2011;87(1):146-50 |
| [Soltan *et al.*, 2009] | Soltan M. K., Ghonaim H. M., El Sadek M., Kull M. A., El-aziz L. A., Blagbrough I. S.: Design and synthesis of N4,N9-disubstituted spermines for non-viral siRNA delivery – structure-activity releationship studies of siFection efficiency versus toxicity, *Pharm Res*, 2009;26(2):286-95 |
| [Tans *et al.*, 1991] | Tans G., Rosing J., Thomassen M. C., Heeb M. J., Zwaal R. F., Griffin J. H.: Comparison of anticoagulant and procoagulant activities of stimulated platelets and platelet-derived microparticles, *Blood*, 1991;77(12):2641-48 |
| [Tesselaar *et al.*, 2007] | Tesselaar M. E., Romijn F. P., Van Der Linden I. K., Prins F. A., Bertina R. M., Osanto S.: Microparticle-associated tissue factor activity: a link between cancer and thrombosis?, *J Thromb Haemost*, 2007;5(3):520-27 |
| [Tomer *et al.*, 2001] | Tomer A., Harker L. A., Kasey S., Eckman J. R.: Thrombogenesis on sickle cell disease, *J Lab Clin Med*, 2001;137(6):398-07 |
| [Toth *et al.*, 2007] | Toth B., Nikolajek K., Nieuwland R., Lohse P., Pihusch V., Friese K., Thaler C. J.: Gender-specific and menstrual cycle dependent differences in circulating microparticles, *Platelets*, 2007;18(7):515-21 |
| [Toth *et al.*, 2008] | Toth B., Nieuwland R., Liebhardt S., Ditsch N., Steinig K., Stieber P., Rank A., Göhring P., Thaler C. J., Friese K., Bauerfeind I.: Circulating microparticles in breast cancer patients: a comparative analysis with established biomarkers, *Anticancer Res*, 2008;28(2A):1107-12 |
| [Trushkevych *et al.*, 2008] | Trushkevych O., Collings N., Hasan T., Scardaci V., Ferrari A. C., Wilkinson T. D., Crossland W. A., Milne W. I., Geng J., Johnson B. F., Macaulay S.: Characterisation of carbon nanotube-thermotropic nematic liquid crystal composites, *J Phys D*, 2008;41(12):125106 |
| [VanWijk *et al.*, 2003] | VanWijk M. J., VanBavel E., Sturk A., Nieuwland R.: Microparticles in cardiovascular diseases, *Cardiovasc Res*, 2003;59(2):277-87 |
| [Warkentin *et al.*, 1994] | Warkentin T. E., Hayward C. P., Boshkov L. K., Santos A. V., Sheppard J. A., Bode A. P., Kelton J. G.: Sera from patients with heparin-induced thrombocytopenia generate platelet-derived microparticles with procoagulant activity: an explanation for the thrombotic complications of heparin-induced thrombocytopenia, *Blood*, 1994;84(11):3691-99 |
| [Weerheim *et al.*, 2002] | Weerheim A. M., Kolb A. M., Sturk A., Nieuwland R.: Phospholipid composition of cell-derived microparticles determined by one-dimensional high-performance thin-layer chromatography, *Anal Biochem*, 2002;302(2):191-98 |
| [Wiedmer *et al.*, 1990] | Wiedmer T., Shattil S. J., Cunningham M., Sims P. J.: Role of calcium and calpain in complement-induced vesiculation of the platelet plasma membrane and in the exposure of the platelet factor Va receptor, *Biochemistry*, 1990;29(3):623-32 |
| [Wiedmer *et al.*, 1993] | Wiedmer T., Hall S. E., Ortel T. L., Kane W. H., Rosse W. F., Sims P. J.: Complement-induced vesiculation and exposure of membrane prothrombinase sites in platelets of paroxysmal nocturnal hemoglobinuria, *Blood*, 1993;82(4):1192-96 |
| [Willekens *et al.*, 2005] | Willekens F. L., Werre J. M., Kruijt J. K., Roerdinkholder-Stoelwinder B., Groenen-Döpp Y. A., van den Bos A. G., Bosman G. J., van Berkel T. J.: Liver Kupffer cells rapidly remove red blood cell-derived vesicles from the circulation by scavenger receptors, *Blood*, 2005;105(5):2141-45 |
| [Wolf, 1967] | Wolf P.: The nature and significance of platelet products in human plasma, *Br J Haematol*, 1967;13:269-288 |
| [Wu *et al.*, 2006] | Wu Y., Tibrewal N., Birge R. B.: Phosphatidylserine recognition by phagocytosis: a view to a kill, *Trends Cell Biol*, 2006;16(4):189-97 |

| | |
|---|---|
| [Wun *et al.*, 1997] | Wun T., Paglieroni T., Tablin F., Welborn J., Nelson K., Cheung A.: Platelet activation and platelet-erythrocyte aggregates in patients with sickle cell anemia, *J Lab Clin Med*, 1997;129(5):507-16 |
| [Wun *et al.*, 1998] | Wun T., Paglieroni T., Rangaswami A., Franklin P. H., Welborn J., Cheung A., Tablin F.: Platelet activation in patients with sickle cell disease, *Br J Haematol*, 1998;100(4):741-49 |
| [Xu *et al.*, 2010] | Xu Y., Nakane N., Maurer-Spurej E.: Novel test for microparticles in platelet-rich plasma and platelet concentrates using dynamic light scattering, *Transfusion*, 2011;51(2):363-70 |
| [Zhunusayev *et al.*, 2008] | Zhunuspayev D. E., Mun G. A., Hole P., Khutoryanskiy W.: Solvent effects on the formation of nanoparticles and multilayered coatings based on hydrogen-bonded interpolymer complexes of poly(acrylic acid) with homo- and copolymers of N-vinyl pyrrolidone, *Langmuir*, 2008;24(23):13742-47 |
| [Zwaal *et al.*, 1992] | Zwaal R. F., Comfurius P., Bevers E. M.: Platelet procoagulant activity and microvesicle formation. Its putative role in hemostasis and thrombosis, *Biochim Biophys Acta*, 1992;1180(1):1-8 |
| [Zwaal *et al.*, 2004] | Zwaal R. F., Comfurius P., Bevers E. M.: Scott syndrome, a bleeding disorder caused by defective scrambling of membrane phospholipids, *Biochim Biophys Acta*, 2004;1636(2-3):119-28 |

# Abbreviations

## Overview of abbreviations

| | |
|---|---|
| AF | Atrial fibrillation |
| AUC | Area under curve |
| BAFF | B cell-activating factor |
| CI | Confidence interval |
| CV | Coefficient of variation |
| DLS | Dynamic Light Scattering |
| DPBS | Dulbecco's Phosphate Buffered Saline |
| EMCCD | Electron multiplying charged-couple device |
| GPIb | Glycoprotein Ib, also known as CD42 |
| HPTLC | High performance thin-layer chromatography |
| IHD | Ischemic heart disease |
| MM | Multiple myeloma |
| MP | Microparticle |
| MPs | Microparticles |
| NTA | Nanoparticle Tracking Analysis |
| PFP | Platelet-free-plasma |
| PPP | Platelet-poor-plasma |
| PSGL-1 | P-selectin glycoprotein ligand 1, also known as CD162 |
| ROCK1 | Rho-associated kinase 1 |
| RT | Room temperature |
| SD | Standard deviation |
| TF | Tissue factor |
| TNFR1 | Tumour necrosis factor receptor type-1 |
| vWF | von Willebrand factor |

# Appendix

# Overview of Appendix

Appendix A: CD

1. Poster from ISEV congress
2. Protocols
3. Raw data from experiments with microbeads
4. Raw data from dilution and fresh-frozen experiments
5. Raw data from centrifugation experiment
6. Raw data from pilot studies